Doklady Physics, Vol. 47, No. 2, 2002, pp. 102–105. Translated from Doklady Akademii Nauk, Vol. 382, No. 4, 2002, pp. 470–473.

PHYSICS

Energy Dissipation in a Vibrating Structurally Heterogeneous Cavity Filled with a Viscous Liquid

Yu. I. Yalamov and A. A. Gurchenkov

Presented by Academician R.F. Ganiev June 6, 2001

Received July 2, 2001

In this paper, we study vibrations of a viscous liquid filling a cavity made in a vibrating body. The cavity, containing structural elements in the form of radial and ring-shaped ribs, is filled partly with a viscous liquid and partly with a constant-pressure gas. Assuming that the energy dissipation per vibrational period is small compared to the system energy, we derive general equations for perturbed motion of a body containing a liquid in its interior.

The viscosity of liquid components substantially affects the stability of motion of a body filled with a liquid fuel. There exist two mechanisms of energy dissipation, caused by vibrations of the liquid in the cavity. One of them is associated with vortex formation at the cavity walls and the subsequent energy dissipation in a thin near-wall boundary layer (for smooth cavity walls and large Reynolds numbers). The second mechanism includes the separation of intense discrete vortices that dissipate, furthermore, in the entire bulk of the liquid (for a cavity having structural elements with sharp edges). Being essentially nonlinear, the latter effect exceeds the former one by at least two orders of magnitude.

Therefore, additional dissipative forces should be introduced into equations of motion for a solid containing a cavity filled with liquid.

In this paper, an approach is proposed for the first time that makes it possible to simultaneously take into account both mechanisms of energy dissipation. We should especially emphasize that the method of the boundary layer, which was successfully used to allow for the energy dissipation in cavities with smooth walls, is invalid in cavities containing structural elements.

Our approach is similar to the method broadly used by Landau [1]. It is applicable in cavities having structural elements in their volumes, which is especially important for applications.

Here, we consider a class of perturbed motions of a body containing a liquid where both the relative energy dissipation and the generalized coordinates characterizing perturbed motions of the body and of the liquid are small. The cavity shape is supposed to be arbitrary. In the case of a perfect liquid, the system of equations turns into the equations derived in [2]. As particular cases, our results include those presented in [3–5].

Thus, we consider a body with a cavity. The cavity is filled partly with a viscous incompressible liquid having a density ρ and kinematic viscosity ν, and partly with a constant-pressure gas. The cavity contains ribs formed by surfaces orthogonal to its walls.

For unperturbed case, we analyze the translational motion of the liquid-filled body. In the course of this motion, the liquid occupies the volume Q bounded by the surface S of cavity walls and by the planar free surface Σ. The latter is perpendicular to the total-acceleration vector j (the g-load vector), which is caused by the mass forces of unperturbed motion.

The perturbed motion of the body is determined by the vectors of both small displacement $\mathbf{u}(t)$ and small rotation $\mathbf{\Theta}(t)$. The perturbed liquid flow is characterized by the parameters $S_k(t)$, each of them representing the amplitude of the kth tone of vibrations of the liquid at a certain point on its free surface.

We now write out equations for the perturbed motion of a body with a liquid, ignoring terms of higher orders of smallness with respect to the generalized coordinates (see [6]):

$$(m^0 + m)\ddot{\mathbf{u}} + (L^0 + L, \ddot{\mathbf{\Theta}}) + \sum_{k=1}^{\infty} \boldsymbol{\lambda}_k \ddot{S}_k = \mathbf{P} + \delta\mathbf{P},$$

$$(J^0 + J, \ddot{\mathbf{\Theta}}) + (\bar{L}^0 + \bar{L}, \ddot{\mathbf{u}}) - \mathbf{j}(\tilde{L}^0 + \tilde{L}, \mathbf{\Theta}) + \sum_{k=1}^{\infty} \boldsymbol{\lambda}_{0k} \ddot{S}_k = \mathbf{M}_0 + \delta\mathbf{M}_0, \quad (1)$$

$$\mu_k(\ddot{S}_k + \omega_k^2 S_k) + (\boldsymbol{\lambda}_k, \ddot{\mathbf{u}}) + (\boldsymbol{\lambda}_{0k}, \ddot{\mathbf{\Theta}}) = \delta P_k,$$
$$k = 1, 2, \ldots.$$

Moscow Pedagogical University,
ul. Radio 10a, Moscow, 105007 Russia

1028-3358/02/4702-0102$22.00

Here, m^0 and m are the masses of the solid and of the liquid; J^0 and J are the symmetric inertia tensor of the solid and the symmetric tensor for adjoint moments of inertia of the liquid, respectively; L^0 and L are the antisymmetric tensors for static moments of the body and of the liquid; and $\bar{L}^0$ and $\bar{L}$ are the tensors conjugate to L^0 and $\tilde{L}$, respectively. The tensors $\tilde{L}^0$ and $\tilde{L}$ correspond to moments of mass forces acting in the case of an unperturbed motion; the vectors $\boldsymbol{\lambda}_k$ and $\boldsymbol{\lambda}_{0k}$ characterize the inertial coupling of body motions with wave motions of the liquid; and $\delta\mathbf{P}$, $\delta\mathbf{M}_0$, and δP_k represent generalized forces caused by the energy dissipation in the cavity.

For $\delta\mathbf{P} = \delta\mathbf{M}_0 = \delta P_k = 0$, Eqs. (1) turn into equations describing the perturbed motion of a body with a cavity partly filled with a perfect liquid [2]. In what follows, the coefficients entering into the equations of motion for the body filled with a perfect liquid are assumed to be known.

Thus, in order to construct equations of motion for a body having a cavity partly filled with a viscous liquid, we should find the generalized dissipative forces $\delta\mathbf{P}$, $\delta\mathbf{M}_0$, and δP_k.

Let a cavity with smooth walls have m ribs formed by surface elements orthogonal to the cavity surface S. We also assume that the rib height b, which is measured in the direction of the normal to the cavity surface, is small compared to both the characteristic cavity dimension and the minimum distance between the ribs. In addition, the liquid is assumed to flow with large values of the Reynolds number $\mathrm{Re} = \dfrac{vl}{\nu} \gg 1$, where v and l are the characteristic liquid velocity and the characteristic linear cavity size, respectively.

Under these conditions, the energy dissipation occurs not only in a thin layer near the boundaries of the volume occupied by the liquid (the first dissipation mechanism) but also in the entire bulk of the liquid (the second dissipation mechanism). The rate of the energy dissipation per unit volume of the liquid is on the order of $\dfrac{1}{\sqrt{\mathrm{Re}}}$ near the wet cavity surface S and on the order of $\dfrac{1}{\mathrm{Re}}$ near the free surface of the liquid [1].

Below, we restrict our analysis to considering terms on the order of $\dfrac{1}{\sqrt{\mathrm{Re}}}$ in the expressions for dissipative forces and, therefore, ignore the energy dissipation near the free surface of the liquid.

Since the boundary layer is thin $\left(\text{on the order of } \dfrac{1}{\sqrt{\mathrm{Re}}}\right)$, an element of the surface S can be treated as an element of an infinite plane that bounds a half-space occupied by a viscous liquid. This element moves with a velocity equal to the difference between the velocities of the body and of the perturbed flow of the perfect liquid.

A force applied to an element of the surface S, which moves with the velocity $v(r, t)$, can be represented as (see [7]):

$$d\mathbf{F} = -\rho\sqrt{\frac{\nu}{\pi}}\int_0^t \frac{\dot{\mathbf{v}}(\mathbf{r}, \tau)d\tau}{\sqrt{t-\tau}}dS, \tag{2}$$

where $\mathbf{r}$ is the radius vector of a current point of the surface S. Then, the first mechanism leads to an energy-dissipation rate in the cavity equal to

$$\dot{E} = \int_S (\mathbf{v}, d\mathbf{F}) = -\rho\sqrt{\frac{\nu}{\pi}}\int_S \left(\mathbf{v}(\mathbf{r}, t), \int_0^t \frac{\dot{\mathbf{v}}(\mathbf{r}, t)d\tau}{\sqrt{t-\tau}}dS\right). \tag{3}$$

The velocity for the perturbed flow of the perfect liquid $\mathbf{v}^0$ is presented in the form (see [2])

$$\mathbf{v}^0 = \dot{\mathbf{u}} + \sum_{j=1}^{3} \dot{\Theta}_j \nabla\Psi_j + \sum_{k=1}^{\infty} \dot{S}_k \nabla\varphi_k. \tag{4}$$

Here, $\Theta_j = (\boldsymbol{\Theta}, \mathbf{e}_j)$ are the components of the vector $\boldsymbol{\Theta}$ in the body's coordinate system $Ox_1x_2x_3$, $\mathbf{e}_j$ are the basis vectors of this coordinate system, and $\Psi_j(x_1, x_2, x_3)$ and $\varphi_k(x_1, x_2, x_3)$ are the solutions to boundary value problems dependent only on the cavity configuration. Therefore, the relative velocity $\mathbf{v}$ can be expressed as

$$\begin{aligned}\mathbf{v} &= \dot{\mathbf{u}} + \dot{\Theta} \times \mathbf{r} - \mathbf{v}^0 \\ &= -\sum_{j=1}^{3} \dot{\Theta}_j(\nabla\Psi_j + \mathbf{r} \times \mathbf{e}_j) - \sum_{k=1}^{\infty} \dot{S}_k \nabla\varphi_k.\end{aligned} \tag{5}$$

In addition, a linear rib element can be treated as an element of an infinitely long plate, which is perpendicular to the boundary of the half-space occupied by the liquid vibrating along this boundary. At the same time, the vibration velocity is equal to the normal component of the relative perfect-liquid velocity at points corresponding to the midline of the rib element under consideration in the case when the rib is absent.

The relative-velocity component normal to the rib can be written as

$$v_\nu = (\mathbf{v}, \boldsymbol{\nu}) = -\sum_{j=1}^{3}\dot{\Theta}_j\left\{\frac{\partial\Psi_j}{\partial\nu} - (\mathbf{r}\times\boldsymbol{\nu})_j\right\} - \sum_{k=1}^{\infty}\dot{S}_k\frac{\partial\varphi_k}{\partial\nu}, \tag{6}$$

where $\mathbf{r}(\Gamma)$ is the radius vector of points belonging to the rib midline, Γ is the length of the midline arch, and the vector $\boldsymbol{\nu}$ of the outer normal to the rib surface forms an acute angle with the direction of the relative velocity of the liquid. The subscript j corresponds to the jth vector component.

The semiempirical approach used in [2] was based on a drag force applied to a linear rib element, which can be represented in the form

$$d\mathbf{F} = \rho c b^{3/2}\omega v_\nu \boldsymbol{\nu} d\Gamma, \tag{7}$$

where the coefficient c depends on the vibration amplitude.

Expression (7) is rather convenient in analysis of steady-state harmonic vibrations. However, in studying transient processes, additional hypotheses are necessary to construct a dynamic scheme based on formula (7).

In this paper, we propose another expression free from the above-mentioned disadvantages (see [8]):

$$d\mathbf{F} = \rho c_x b^{3/2}\int_0^t \frac{\dot{v}_\nu d\tau}{\sqrt{t-\tau}}\boldsymbol{\nu} d\Gamma. \tag{8}$$

The coefficient c_x in (8) is such that the energy dissipation per vibrational period is identical for both resistance laws (7) and (8).

It is easy to show that in the harmonic-vibration mode, expressions (7) and (8) coincide with each other. However, since relation (8) is not associated with the amplitude and frequency of a harmonic process, it is applicable for analyzing transients.

The second dissipation mechanism leads to the following expression for the energy-dissipation rate in the cavity:

$$\dot{E} = \sum_{l=1}^{m}\int_{\Gamma_l}(\mathbf{v}, d\mathbf{F}), \tag{9}$$

where m is the number of ribs and Γ_l is the contour formed by the rib midline.

Thus, the relation for the total rate of the energy dissipation in a cavity with allowance for both these dissipation mechanisms takes the form

$$\dot{E} = -\rho\sqrt{\frac{\nu}{\pi}}\int_S\left(\mathbf{v}(\mathbf{r}, t), \int_0^t\frac{\dot{\mathbf{v}}(\mathbf{r}, \tau)d\tau}{\sqrt{t-\tau}}\right)dS + \rho c_x b^{3/2}\sum_{l=1}^{m}\int_{\Gamma_l}\left(\mathbf{v}(\mathbf{r}, t), \int_0^t\frac{\dot{v}_\nu(\tau)d\tau}{\sqrt{t-\tau}}\boldsymbol{\nu}\right)d\Gamma. \tag{10}$$

The first term in formula (10) is associated with the energy dissipation at smooth walls, while the second one takes into account the presence of ribs in the cavity. Substituting expressions (5) and (6) for the relative velocity of the liquid into relation (10), we arrive at

$$\dot{E} = -\left(B, \int_0^t\frac{\ddot{\boldsymbol{\Theta}}(\tau)d\tau}{\sqrt{t-\tau}}\right), \dot{\boldsymbol{\Theta}} - \sum_{k=1}^{\infty}\left(\boldsymbol{\beta}'_{0k}, \int_0^t\frac{\ddot{S}_k(\tau)d\tau}{\sqrt{t-\tau}}\right), \dot{\boldsymbol{\Theta}} - \sum_{k=1}^{\infty}\left(\beta_{0k}, \int_0^t\frac{\ddot{\boldsymbol{\Theta}}(\tau)d\tau}{\sqrt{t-\tau}}\right)\dot{S}_k - \sum_{k=1}^{\infty}\left(\sum_{n=1}^{\infty}\beta_{kn}\int_0^t\frac{\ddot{S}_k(\tau)d\tau}{\sqrt{t-\tau}}\right)\dot{S}_k. \tag{11}$$

Here, B is the tensor with the elements $\beta^{0'}_{ij}$, $\boldsymbol{\beta}'_{0k}$ are the vectors with the components β'_{0kj}, and β'_{kn} are the scalars. In addition,

$$\beta^{0'}_{ij} = \beta^{0'}_{ji} = \rho\sqrt{\frac{\nu}{\pi}}\int_S(\mathbf{r}\times e_j + \nabla\Psi_j), (\mathbf{r}\times e_i + \nabla\Psi_i)dS + \rho c_x\sum_{l=1}^{m}b_l^{3/2}\int_{\Gamma_l}\left[\frac{\partial\Psi_j}{\partial\nu} - (\mathbf{r}\times\boldsymbol{\nu})_j\right], \left[\frac{\partial\Psi_j}{\partial\nu} - (\mathbf{r}\times\boldsymbol{\nu})_i\right]d\Gamma,$$

$$\boldsymbol{\beta}'_{0kj} = \rho\sqrt{\frac{\nu}{\pi}}\int_S(\mathbf{r}\times\mathbf{e}_j + \nabla\Psi_j), \nabla\varphi_k dS + \rho c_x\sum_{l=1}^{m}b_l^{3/2}\int_{\Gamma_l}\left[\frac{\partial\Psi_j}{\partial\nu} - (\mathbf{r}\times\boldsymbol{\nu})_j\right], \nabla\varphi_k d\Gamma, \tag{12}$$

$$\beta'_{kn} = \beta'_{nk} = \rho\sqrt{\frac{\nu}{\pi}}\int_S(\nabla\varphi_n, \nabla\varphi_k)dS + \rho c_x\sum_{l=1}^{m}b_l^{3/2}\int_{\Gamma_l}\left(\frac{\partial\varphi_n}{\partial\nu}\frac{\partial\varphi_k}{\partial\nu}\right)d\Gamma,$$

$$j = 1, 2, 3, \quad n, k = 1, 2, \ldots, \quad l = 1, 2, \ldots, m.$$

In each of formulas (12), the first term takes into account the effect of the boundary layer, while the second term is associated with vortex formation at the rib edges. The second term dominates at finite vibrational amplitudes of both body and liquid, while the first term

manifests itself either at vanishing amplitudes or in the case of the absence of ribs.

On the other hand, the energy-dissipation rate is determined by the expression

$$\dot{E} = (\delta\mathbf{P}, \dot{\mathbf{u}}) + (\delta\mathbf{M}_0, \dot{\boldsymbol{\Theta}}) + \sum_{k=1}^{\infty} \delta P_k \dot{S}_k. \qquad (13)$$

Being compared, relations (11) and (13) yield

$$\delta\mathbf{P} \equiv 0,$$

$$\delta\mathbf{M}_0 = -\left(B, \int_0^t \frac{\ddot{\boldsymbol{\Theta}}(\tau)d\tau}{\sqrt{t-\tau}}\right), \dot{\boldsymbol{\Theta}} - \sum_{k=1}^{\infty}\left(\beta'_{0k}, \int_0^t \frac{\ddot{S}_k(\tau)d\tau}{\sqrt{t-\tau}}\right), \qquad (14)$$

$$\delta P_k = -\left(\beta'_{0k}, \int_0^t \frac{\ddot{\boldsymbol{\Theta}}(\tau)d\tau}{\sqrt{t-\tau}}\right) - \sum_{n=1}^{\infty} \beta_{kn} \int_0^t \frac{\ddot{S}_n(\tau)d\tau}{\sqrt{t-\tau}}.$$

At large values of the Reynolds number, the relations derived are quite sufficient to construct equations for perturbed motion of a body with a cavity partly filled with a viscous liquid.

REFERENCES

1. L. D. Landau and E. M. Lifshitz, *Mechanics of Continua* (Pergamon Press, Oxford, 1960; Gostekhizdat, Moscow, 1955).
2. G. N. Mikishev and B. I. Rabinovich, *Dynamics of a Solid with Cavities Partially Filled with a Liquid* (Mashinostroenie, Moscow, 1968).
3. F. L. Chernous'ko, Prikl. Mat. Mekh. **30**, 977 (1966).
4. B. I. Rabinovich, Prikl. Mat. Mekh. **20**, 39 (1956).
5. G. N. Mikishev and N. Ya. Dorozhkin, Izv. Akad. Nauk SSSR, Mekh. Zhidk. Gaza, No. 1, 84 (1967).
6. B. I. Rabinovich and V. M. Rogovoĭ, Kosm. Issled. **8**, 315 (1970).
7. N. A. Slezkin, *Dynamics of Viscous Incompressible Liquid* (Gostekhteorizdat, Moscow, 1955).
8. V. T. Desyatov, *Experimental Study of the Rotary-Motion Stability for Bodies Filled with a Liquid. Dynamics of Spacecrafts and Study of Extraterrestrial Space* (Mashinostroenie, Moscow, 1986).

Translated by Yu. Verevochkin

Doklady Physics, Vol. 47, No. 2, 2002, pp. 106–108. Translated from Doklady Akademii Nauk, Vol. 382, No. 5, 2002, pp. 612–614.

PHYSICS

On the Theory of the Ductile–Brittle Transition (Cold Brittleness)

Ya. S. Semenov

Presented by Academician V.V. Osiko October 9, 2001

Received May 21, 2001

It is known [1–4] that the ductile–brittle transition (DBT) depends on temperature, chemical composition, stressed state, and loading rate. Moreover, it was established [4, 5] that the DBT can be attributed to a unified mechanism consisting in the disturbance of the electron-structure order responsible for the chemical bond. This is either the restoration or the destruction of the directed component of the chemical bond at the DBT critical temperatures T_{cr} or the so-called "crystallization" of valence electrons. The simplest kind of this phenomenon in the presence of a uniform compensating nuclear field is Wigner crystallization [6, 7].

As was indicated in [5], a decrease in the thermal vibrations or a change in an alloying element leads to the appearance of directed chemical bonds, i.e., to the crystallization of the electron structure at T_{cr} of DBT. In this case, we can use the formalism of the second-order phase transition as, e.g., in [6–8].

Let the system of electrons be described by the following Hamiltonian in the x representation:

$$H = \int dx\, a^{s*}(x)\left\{\frac{\hat{p}^2}{2m} + U(x) - \mu\right\}a^s(x) + \frac{1}{2}\int dxdy\nu(x-y)a^{s*}(x)a^{s'*}(y)a^{s'}(y)a^s(x), \quad (1)$$

where $a^{s*}(x)$ and $a^s(x)$ are, respectively, the creation and annihilation operators for particles with spin $s = \pm\frac{1}{2}$, $\nu(x, y)$ is the s-independent potential of interaction between two particles, $U(x) = U(x + R)$ is the periodic field of the crystal lattice $\{R\}$, $\frac{\hat{p}^2}{2m}$ is the kinetic energy operator ($h = 1$), and μ is the chemical potential. We integrate over the entire volume of the system, take the cyclic boundary conditions, and sum with respect to the repeating superscripts s' and s.

The operators $a^{s*}(x)$ and $a^s(x)$ are expressed in terms of the secondary-quantization operators with the Wannier functions $W_n(x - R)$ of electrons. We obtain

$$a^{s*}(x) = \sum_{R,n} a_n^{s*}(R)W_n^*(x-R), \qquad a^s(x) = \sum_{R,n} a_n^s(R)W_n(x-R). \quad (2)$$

The Wannier functions $W_n(x - R)$ are defined in terms of the Bloch functions as

$$W_n(x-R) = \frac{1}{\sqrt{N}}\sum_k u_{k,n}(x)e^{ik,R}, \quad (2a)$$

where the summation with respect to k is performed over the first Brillouin zone of the lattice $\{R\}$ and N is the number of lattice cites in the cell volume V. The Bloch functions $u_{k,n}(x)$ are associated with the nth zone and are the solutions of the Schrödinger equation

$$\left[\frac{\hat{p}^2}{2m} + U(x)\right]u_{k,n}(x) = L_n^0(k)u_{k,n}(x) \quad (3)$$

with the eigenvalues $L_n^0(k)$.

Including the valence angle and taking into account that the energy gaps between zones are somewhat broadened due to thermal vibrations and are higher than the corresponding characteristic interaction energies, we write the Hamiltonian in the new representation as:

$$H = \sum_{n,R_1,R_2} L_n(R_1-R_2)a_n^{s*}(R_1)a_n^s(R_2) + \frac{1}{2}\sum_{n;\,R_1,R_2,R_3,R_4} \nu_n(R_1R_2R_3R_4)a_n^{s*}(R_1) \times a_n^{s*}(R_2)a_n^s(R_3)a_n^s(R_4), \quad (4)$$

where

Institute of Physics and Technology for Problems of the North, Siberian Division, Russian Academy of Sciences, ul. Oktyabr'skaya 1, Yakutsk, 677891 Russia

1028-3358/02/4702-0106$22.00

$$L_n(R_1 - R_2) = \sum_k (L_n^0(k) - \mu)e^{ik(R_1 - R_2)},$$
$$\nu(R_1R_2R_3R_4) = \int dxdy\nu(x-y) \tag{5}$$
$$\times W_n^*(x - R_1)W_n^*(y - R_2)W_n(y - R_3)W_n(x - R_4).$$

We introduce the Green's function

$$G_n(RR'; t - t') = -2\pi i\theta(t - t')\langle [a_n^s(R, t), \bar{a}_n^s(R', t')]_+\rangle, \tag{6}$$

where $a_n^s(R, t)$ and $\bar{a}_n^s(R', t')$ are the operators in the Heisenberg representation; $\theta(t - t')$ is the unit step function; $[\cdot,\cdot]_+$ is the anticommutator; the angular brackets mean averaging over the grand canonical ensemble with Hamiltonian (4) and the parameter $\beta = \frac{1}{T}$, where T is the absolute temperature in the energy units; and the summation is performed with respect to the superscript s. It is evident that this Green's function satisfies the equation

$$\sum_{R_1}\{G_n^{(0)-1}(R - R_1; E) - \hat{M}(R, R_1; E)\} \times G_n(R_1, R'; E) = 2, \tag{7}$$

where $G_n^{(0)-1}(R - R_1; E) = E\delta_{RR_1} - L_n(R - R_1)$ is the inverse unperturbed Green's function, and $\hat{M}$ is the mass operator [E is the parameter of the Fourier transform with respect to time $(t - t')$].

The analysis of solutions according to [8–10] leads to the first density matrix

$$\rho(R, R') \equiv \langle a^{s*}(R)a^s(R')\rangle = \frac{i}{2\pi}\int_{-\infty}^{+\infty}\frac{G(R, R'; E + i\varepsilon) - G(R, R'; E - i\varepsilon)}{e^{\beta E} + 1}dE. \tag{8}$$

Further, it is possible to determine the density $n(x)$ of "true" particles by using Eq. (2a). In a certain limit, the mass operator $M(R, R'; E)$ can be expressed as a functional of $\rho(R, R'; E)$. In this case, after the transformations according to [8–10], we obtain the nonlinear equation

$$G^{(0)-1}(p)G_0(p) + G_1(p)\sum_{\{k_s\}}\alpha(k_s)G^{(0)-1} \times \left(p + \frac{k_s}{2}\right)e^{ik_s, X} - M_0(p)G_0(p)$$
$$-\sum_{\{k_s\}}M_1(p, k_s)G_0\left(p - \frac{k_s}{2}\right)\alpha(k_s)e^{ik_s, X} - \sum_{\{k_s\}}\sum_{\{k_s'\}}M_1\left(p - \frac{k_s}{2}, k_s\right)G_1\left(p + \frac{k_3'}{2}\right)\alpha(k_s)\alpha(k_s')e^{i(k_s + k_s'), X} = 2, \tag{9}$$

which can be solved as a set of the finite-difference equations determining $G_0(p)$ and $G_1(p)$.

Then, using (8) and changing $G_0(p)$, $G_1(p)$ to $\eta_0^{(1)}(p)$, $\eta_1^{(1)}(p)$, we obtain the set of equations

$$\eta_0^{(1)}(p) = \hat{\psi}_1\{\eta_0^{(1)}(p), \eta_1^{(1)}(p)\},$$
$$\eta_1^{(1)}(p) = \hat{\psi}_2\{\eta_0^{(1)}(p), \eta_1^{(1)}(p)\}, \tag{10}$$

where ψ_1 and ψ_2 are the nonlinear integral operators.

From the physical reasons for $T \longrightarrow \infty$, the solution of Eq. (7) is the spatially uniform; i.e.,

$$\rho(R, R') = \rho^0(R, R') = \eta_0^{(1)}(R - R'). \tag{11}$$

For the set of equations (7) at $T > T_{cr}$, we have $\eta_0^{(1)} \equiv 0$, $\eta_0^{(1)} \equiv \eta_0^{(0)}(R - R')$; i.e., T_{cr} is the phase-transition point or the stability-loss point for the spatially homogeneous solution.

However, T_{cr} can be determined by the branch method following [9]. This method is based on the fact that, at $T < T_{cr}$ and $T \longrightarrow T_{cr}$, the functions

$$\delta n_0(p) = \eta_0^{(1)}(p) - \eta_0^{(0)}(p), \quad \delta\eta_1(p) = \eta_1^{(1)}(p) \tag{12}$$

tend to zero but remain infinitesimal. Taking the variations of Eq. (10) with allowance for Eq. (12), we obtain

$$\delta\eta_0(p) = \hat{A}_1\{\delta\eta_0(p), \delta\eta_1(p)\},$$
$$\delta\eta_1(p) = \hat{A}_2\{\delta\eta_0(p), \delta\eta_1(p)\}, \tag{13}$$

where $\hat{A}_1$ and $\hat{A}_2$ are the linear integral operators depending on $\beta = \frac{1}{T}$ and μ.

The least positive eigenvalue β_{cr} of set (13) determines the highest T_{cr} phase-transition temperature depending on the particle density through μ. If a band is filled, the corresponding particle density is $n(R) \equiv 2$ and the redistribution of particles between the quantum states is impossible; therefore, the crystallization of the electron structure does not occur.

Thus, the crystallization of the electron structure responsible for the chemical bond is possible only for atoms with unfilled electron shells, and the above theory correctly describes the DBT mechanism. For binary

iron alloys, this phenomenon takes place when impurities have unfilled *np*, *nd*, and *pf* electron shells [4, 5]. In order to reduce T_{cr} of the DBT for iron alloys, it is necessary to alloy the iron matrix with elements that have unfilled *np*, *nd*, and *pf* electron shells and larger angles and lengths of chemical bonds.

REFERENCES

1. A. A. Presnyakov, *Cold Shortness* (Nauka, Alma-Ata, 1972).
2. V. I. Trefilov, Yu. V. Mil'man, and S. A. Firstov, *The Physical Foundations of Refractory Metals Strength* (Naukova Dumka, Kiev, 1975).
3. *Proceedings of NATO Advanced Research Inst. on Atomistics of Fracture May 23–31, 1981, Calcatoggio, Corsica, France*, Ed. by R. M. Latunision and J. R. Pickens (Plenum Press in coop. with NATO Sci. Affairs Div. Cop., 1983; Mir, Moscow, 1987).
4. V. P. Larionov and Ya. S. Semenov, *The Physical Foundations of Visco Brittle Transition in Low-Alloy Steels* (Nauka, Novosibirsk, 1992).
5. V. P. Larionov and Ya. S. Semenov, Dokl. Akad. Nauk **335**, 52 (1994).
6. E. P. Wigner, Trans. Faraday Soc. **34**, 678 (1938).
7. G. L. Krasko, Fiz. Tverd. Tela (Leningrad) **7**, 936 (1965) [Sov. Phys. Solid State **7**, 751 (1965)].
8. A. G. Khachaturyan, *The Theory of Phase Transformations and the Structure of Solid Solutions* (Nauka, Moscow, 1974).
9. A. G. Khachaturyan, Fiz. Tverd. Tela (Leningrad) **5**, 26 (1963) [Sov. Phys. Solid State **5**, 16 (1963)].
10. S. V. Tyablikov, *Methods in the Quantum Theory of Magnetism* (Nauka, Moscow, 1965; Plenum Press, New York, 1967).

Translated by V. Bukhanov

Doklady Physics, Vol. 47, No. 2, 2002, pp. 109–113. Translated from Doklady Akademii Nauk, Vol. 382, No. 5, 2002, pp. 615–620.

PHYSICS

Exchange Symmetry in the Feynman Path-Integral Formalism for Many-Electron Systems with Spin

S. V. Shevkunov

Presented by Academician V.V. Osiko September 18, 2001

Received August 15, 2001

The problem of explicit inclusion of the spin-dependent permutation symmetry in the Feynman path-integral method is solved for many-electron systems. As an example, the Monte Carlo numerical calculations for near-degenerate hydrogen plasma are presented. The new method is promising in systematic computations for systems of quantum particles at finite temperatures, with an accuracy similar to that for systems of classical particles.

1. INTRODUCTION

Over the few decades since the publication of the pioneering Metropolis paper [1], a special research field, the computer simulation of materials at the atomic level, was formed in theoretical physics. Over the last two decades, the rapid development of computer technologies created a basis for the transformation of computer simulation methods into an independent field, intermediate between pure theory and experiment. Until the mid-1960s, computer simulation methods were used only for classical-mechanics systems. In the early 1960s, Feynman proposed an alternative formulation of quantum mechanics in terms of path integrals [2]. In this formalism, the motion of a quantum particle is described by virtual paths. The evolution-operator kernel is expressed as a sum of complex amplitudes for all paths. The partition function is obtained from the quantum evolution operator by the formal change of time to imaginary reciprocal temperature. Each quantum particle corresponds to its own closed path. A problem in such a form can be solved by the Monte Carlo method. Feynman paths are approximated by broken lines whose vertex coordinates are stored in the computer memory. The integration reduces to random walks in the path space with the weight function dependent upon the action calculated for the path corresponding to the imaginary time [3]. Fosdick and Jordan [4, 5] were the first who numerically implemented these concepts for the simplest system of two interacting helium atoms. In Russia, the first attempts to apply the path integral method to the computer simulation of electron systems were undertaken in [6–9].

Among problems seriously impeding the systematic application of the path integral method to the study of many-particle quantum systems at finite temperatures, the description of the permutation symmetry is most difficult. In terms of the path integrals, the symmetrization over permutations requires integration over the coupled Feynman paths, and each kind of coupling corresponds to its own positive or negative weight factor. Although the Hamiltonian of the system of nonrelativistic particles does not affect spin variables, the system energy depends strongly on the spin state via the type of coordinate permutation symmetry. In the system of identical fermions, the wave function changes sign upon the *simultaneous* permutation of the spin and coordinate variables of an electron pair. In spin or coordinate variables taken separately, the wave function can be neither symmetric nor antisymmetric. The specific permutation symmetry in the spin variables necessarily leads to definite (complementary to it) permutation symmetry in the coordinate variables. The partition function is the trace of the statistical operator calculated in the representation of the *complete* set of wave functions. The complete set of linearly independent wave functions can be constructed based on the Young symmetry operators [10].

Until recently, in path-integral computer simulation, either the spin of particles was ignored, the exchange symmetry was approximately taken into account by combining determinants formed by one-particle functions [7, 8], or else the exchange was neglected altogether. Note that spinless fermions do not exist, and the disregard of spin can be hardly considered as an approximation since it is difficult to check the corresponding error, which can even exceed the result. This statement is illustrated by the well-known orthostate and parastate of hydrogen molecules. An explicit procedure of including spin and exchange symmetry in the path-integral description of the systems of interacting electrons was first formulated in [11, 12]. This algorithm provides numerical simulation for systems

St. Petersburg State Technical University,
ul. Politekhnicheskaya 29, St. Petersburg, 195251 Russia

1028-3358/02/4702-0109$22.00

including up to about ten electrons. For a larger number of particles, the calculation becomes virtually impracticable, because the computer time needed for calculation of the control tables for the combinatorial coefficients increases faster than $N!$ The path-integral method was used to simulate an electron pair in a microcavity in the context of the problem of electrides [13], a hydrogen molecule in a state close to the ground state [14], and the thermally excited states of a hydrogen atom and lithium and beryllium ions in a dense plasma [15].

In this paper, we present the results of the path-integral simulations for a many-electron system at finite temperature with the exact inclusion of the exchange and spin of electrons. For the first time, the Monte Carlo method as an exact statistical-mechanics method was applied to systems with spin, and the limitations on the number of particles in the description of exchange was removed.

2. THE PROBLEM OF A LARGE NUMBER OF PARTICLES IN THE DESCRIPTION OF EXCHANGE IN SYSTEMS WITH SPIN

The impossibility of directly calculating the control tables for the combinatorial coefficients was solved by including the calculations of combinatorial coefficients to the Markov random walk procedure. The space of random walks was extended. In the new method, a microscopic state is defined by the coordinates of vertices of the paths, the structure of their couplings, and a limited random sample of permutations used to calculate the combinatorial weight of the given microscopic state. As a whole, the calculation procedure remains in principle exact, although the sample of permutations is limited.

The Young operator corresponding to the eigenvalue $S(S+1)$ of the spin-squared operator can be represented as the product of the operators of pair symmetrization $(1 + \hat{n}_{ij})$ and antisymmetrization $(1 - \hat{n}_{ij})$ over the numbers of arguments

$$\hat{J}(S) = (1-\hat{n}_a)(1-\hat{n}_b)\ldots(1+\hat{n}_\nu)(1+\hat{n}_w). \quad (1)$$

Upon removing the parentheses, product (1) takes the form

$$\hat{J}(S) = \sum_n \alpha_s(n)\hat{N}_n. \quad (2)$$

The summation in Eq. (2) is performed over all $N!$ permutations of arguments over numbers $\hat{N}_n$. Combinatorial weights $\alpha(n)$ take one of three values: +1, –1, and 0. If the permutation operator in sum (2) is representable in the form

$$\hat{N}_n = \hat{N}_k\hat{N}_l\hat{N}_m, \quad (3)$$

where $\hat{N}_k$ and $\hat{N}_l$ are the permutation operators for arguments in the first and second columns of the Young diagram, respectively, and $\hat{N}_m$ is the operator of the permutations of the diagram lines, then we have $\alpha_s(n) = (-1)^{c(k)+c(l)}$, where $c(k)$ and $c(l)$ are the parities of permutations $\hat{N}_k$ and $\hat{N}_l$. If the operator N_n cannot be represented in form (3), it does not appear in the symmetry operator $\hat{J}(S)$ and its combinatorial weight in sum (2) is $\alpha_s(n) = 0$. It was shown in [12] that the partition function for N identical fermions with a spin of 1/2 is written as

$$Z = \frac{1}{N!}\sum_S (2S+1)\sum_n {}^S(-1)^{c(l)+c(k)}\int d^N r \times \langle\{\mathbf{r}_i\}|\exp(-\beta\hat{H})|\hat{N}_n\{\mathbf{r}_i\}\rangle = \frac{1}{N!}\sum_S (2S+1) \times \sum_n \alpha_s(n)\int d^N r\langle\{\mathbf{r}_i\}|\exp(-\beta\hat{H})|\hat{N}_n\{\mathbf{r}_i\}\rangle, \quad (4)$$

where $\beta \equiv \frac{1}{k_B T}$ is the inverse temperature, k_B is the Boltzmann constant, $\hat{H}$ is the Hamiltonian, and subscript S means that the summation is performed only over the permutation operators appearing in the Young operator $\hat{J}(S)$. Each $\hat{N}_n$ permutation generates a certain diagram of coupled virtual numbered paths. Subsets of diagrams differing only in the enumeration of vertices form classes. They can be combined with the common factor

$$\omega_s(\{\nu_i\}) = \sum_n {}^{\{\nu_i\}}\alpha_s(n), \quad (5)$$

and the summation over all permutations $N!$ can be replaced by the summation over the classes specified by the generic graph $\hat{\Pi}_{\{\nu_i\}}$, where multidimensional index $\{\nu_i\} = \{\nu_1, \nu_2, \ldots, \nu_N\}$ determines the diagram structure and ν_i is the number of cycles formed by i connected paths. The superscript $\{\nu_i\}$ in the summation symbol in Eq. (5) denotes that the summation is performed only over those n for which operators $\hat{N}_n$ belong to the class with the generic graph $\hat{\Pi}_{\{\nu_i\}}$

$$Z = \frac{1}{N!}\sum_{\{\nu_i\}}\omega(\{\nu_i\})\int d^N r \times \langle\{\mathbf{r}_i\}|\exp(-\beta\hat{H})|\hat{\Pi}_{\{\nu_i\}}\{\mathbf{r}_i\}\rangle, \quad (6)$$

where

$$\omega(\{\nu_i\}) = \sum_S (2S+1)\omega_s(\{\nu_i\}).$$

In principle, Eq. (6) provides the basis for a Markov random process for the numerical calculations of equi-

librium expectation values. However, the implementation of this program in practice turns out to be possible only for a relatively small number of particles. Indeed, according to Eq. (5), the calculation of the control table for the combinatorial weights $\omega_s(\{\nu_i\})$ implies sorting all permutations contained in the Young symmetry operator, and the number of the necessary operations increases faster than $N!$ To solve this problem, the combinatorial coefficients $\omega(\{\nu_i\})$ are calculated by the substantial-sample method. Thus, the calculation of the integral in Eq. (6) is united with the calculation of the combinatorial coefficients into the unified Markov random process. It is advantageous to divide the averaging over permutations into segments so that there are no transitions between classes within each segment and the repeated calculation of matrix elements in integral (6) is not required. In each segment, a random equiprobable sampling from the set of all permutations $\hat{N}_n$ is performed, verifying the conditions that they belong both to a given class $\{\nu_i\}$ and to the Young operator $\hat{J}(S)$. A permutation is assigned by the combinatorial factor $\alpha_{s,\{\nu_i\}}(n) = \alpha_s(n)$ if both conditions are satisfied and by the factor $\alpha_{s,\{\nu_i\}}(n) = 0$ if at least one condition is violated. At each step of the random process, we have the following unbiased estimate for the combinatorial factor $\omega_s(\{\nu_i\})$:

$$\tilde{\omega}_s(\{\nu_i\}, \{n_k\}, l) = \frac{N!}{l}\sum_{k=1}^{l}\alpha_{s,\{\nu_i\}}(n_k), \qquad (7)$$

where l is the size of the sample $\{n_k\}$. It is of fundamental importance that the approximate character of $\omega_s(\{\nu_i\})$ estimate (7) found with a finite sample $\{n_k\}$ in a *single* step of the Markov process does not imply an approximate character of the whole calculation procedure if this procedure is based on the combinatorial weights $\tilde{\omega}_s(\{\nu_i\}, \{n_k\}, l)$ instead of $\omega_s(\{\nu_i\})$. Indeed, Eq. (5) can be rewritten in the form

$$\begin{aligned}\omega_s(\{\nu_i\}) &= \frac{1}{l(N!)^{l-1}}\sum_{\{n_k\}}\sum_{k=1}^{l}{}^{\{\nu_i\}}\alpha_s(n_k)\\ &= \frac{1}{l(N!)^{l-1}}\sum_{\{n_k\}}\sum_{k=1}^{l}\alpha_{s,\{\nu_i\}}(n_k) \qquad (8)\\ &= \frac{1}{(N!)^{2l-1}}\sum_{\{n_k\}}\tilde{\omega}_s(\{\nu_i\}, \{n_k\}, l),\end{aligned}$$

where $\{n_k\} = n_1, n_2, \ldots, n_l$ is a sample of l numbers from the unbroken series of integers from 1 to $N!$ and where the numbers in the series $\{n_k\}$ may repeat. The summation over $\{n_k\}$ in Eq. (8) means the summation over all possible samples. Substituting Eq. (8) into Eq. (6) and expressing the matrix element in the integrand as a product of high-temperature matrix elements, for which the explicit expressions are known [2], we find the partition function in the form

$$\begin{aligned}Z = \frac{1}{N!^{3l-1}}&\sum_{\{\nu_i\}}\sum_{\{n_k\}}\sum_{S}(2S+1)\tilde{\omega}_s(\{\nu_i\}, \{n_k\}, l)\\ &\times\int d^N r(1)d^N r(2)\ldots d^N r(M)\\ &\times\left\langle\{\mathbf{r}_i(M)\}\left|\exp\left(-\frac{\beta\hat{H}}{M}\right)\right|\{\mathbf{r}_i(1)\}\right\rangle\\ &\times\left\langle\{\mathbf{r}_i(1)\}\left|\exp\left(-\frac{\beta\hat{H}}{M}\right)\right|\{\mathbf{r}_i(2)\}\right\rangle\ldots\\ &\ldots\left\langle\{\mathbf{r}_i(M-1)\}\left|\exp\left(-\frac{\beta\hat{H}}{M}\right)\right|\hat{\Pi}_{\{\nu_i\}}\{\mathbf{r}_i(M)\}\right\rangle,\end{aligned} \qquad (9)$$

which is exact although written in terms of the coefficients $\tilde{\omega}_s(\{\nu_i\}, \{n_k\}, l)$ determined with limited samples. The partition function in form (9) allows us to remove the exchange-imposed limitations on the number of particles and to construct the Markov random process for systems including hundreds and thousands of particles.

3. NUMERICAL RESULTS FOR HYDROGEN PLASMA

In this section, we present the numerical results obtained by the Monte Carlo path-integral method for hydrogen plasma with a density $\rho = 6.96 \times 10^{20}$ cm^{-3} and temperature $T = 37\,130$ K. The exchange effects are significant under these conditions, since the thermal de Broglie wavelength for electrons, $\Lambda = \frac{h}{\sqrt{2\pi m k_B T}} = 3.9 \times 10^{-8}$ cm, is comparable to the mean distance between neighboring particles, $\rho^{-3} = 11.3 \times 10^{-8}$ cm. Periodic boundary conditions are imposed on the system. The unit cell with an edge length of 52.38×10^{-8} cm corresponding to this periodicity holds 100 electrons described as quantum particles and 100 protons described as classical particles. The Feynman path of each electron is represented by a broken line consisting of $M = 320$ sections. The Coulomb interactions of each particle with the others are calculated by the nearest image method [6]. For the prelimit approximation of the action in the Feynman paths, the nonsingular-potential method is used [15]. The Markov process consists of steps corresponding to the displacement of one of the M vertices of the path, translation and rotation of the path as a whole, and connection and disconnection of two paths. The calculations involve 900 million steps. The first 320 million of these were used to thermalize the system, and the rest were used to calculate the equi-

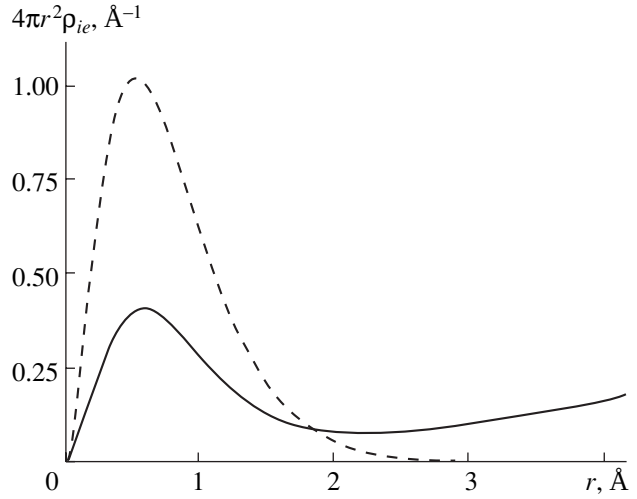

Fig. 1. The radial distribution of the electron density near a proton. The solid curve is the Monte Carlo path-integral calculation for the hydrogen plasma with the temperature T = 37130 K and total density $\rho = 0.696 \times 10^{21}$ cm^{-3}; the dashed curve corresponds to the ground state of the hydrogen atom.

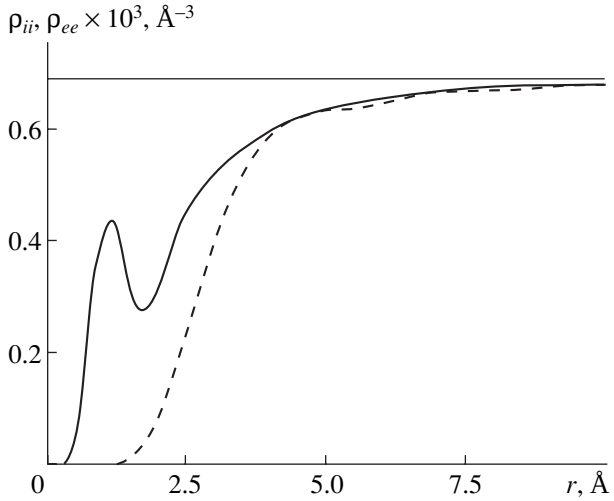

Fig. 2. The pair correlation functions for the hydrogen plasma calculated under the same conditions as in Fig. 1. The solid and dashed lines are ρ_{ii} and ρ_{ee}, respectively. The straight horizontal line corresponds to the total density.

librium expectation values. At the stage of calculating the expectation values, about 3000 connections and disconnections took place. The size of the random sample for calculation of combinatorial coefficients at a single step was l = 10. At the thermalization stage, the procedure of the subsequent multiplication of path vertices was applied and accelerated the process by one to two orders of magnitude.

Microstructural characteristics of plasma in the form of the pair correlation function are represented in Figs. 1–3. The ion–electron correlation function $\rho_{ie}(r)$ has the meaning of the density of the probability of finding an electron at a distance r from a proton. In the coordinate representation with allowance for the degeneracy with respect of the eigenvalues of the spin projection operator, we have

$$\rho_{ie}(r) = \frac{\sum_S (2S+1)\int d\mathbf{r}_1 d\mathbf{r}_2 \ldots d\mathbf{r}_N d\mathbf{R}_1 \ldots d\mathbf{R}_N \left\langle \{\mathbf{r}_i\}, \{\mathbf{R}_i\}, S \left\| \frac{1}{N}\sum_{k,n} \delta(r - |\mathbf{x}_k - \mathbf{X}_n|) \exp(-\beta\hat{H}) \right\| \{\mathbf{r}_i\}, \{\mathbf{R}_i\}, S \right\rangle}{4\pi r^2 \sum_S (2S+1)\int d\mathbf{r}_1 d\mathbf{r}_2 \ldots d\mathbf{r}_N d\mathbf{R}_1 \ldots d\mathbf{R}_N \left\langle \{\mathbf{r}_i\}, \{\mathbf{R}_i\}, S \left\| \exp(-\beta\hat{H}) \right\| \{\mathbf{r}_i\}, \{\mathbf{R}_i\}, S \right\rangle}, \quad (10)$$

where $\{\mathbf{x}_i\} \equiv \mathbf{x}_1, \mathbf{x}_2, \ldots, \mathbf{x}_N$ and $\{\mathbf{X}_i\}$ are the spatial variables for electrons and protons, respectively, $\{\mathbf{r}_i\}$ and $\{\mathbf{R}_i\}$ are the eigenvalues of coordinate operator, and $\delta(r)$ is the one-dimensional Dirac delta function. The matrix elements in Eq. (10) are calculated in the representation of wave functions symmetrized over the permutations according to the eigenvalue of the spin-S operator squared of the system. The electron–electron, $\rho_{ee}(r)$, and ion–ion, $\rho_{ii}(r)$, correlation functions can be written similar to Eq. (10) with the replacement of $|\mathbf{x}_k - \mathbf{X}_n|$ by $|\mathbf{x}_k - \mathbf{x}_n|$ and $|\mathbf{X}_k - \mathbf{X}_n|$, respectively, and the summation under the condition $n \neq k$. The function $\rho_{ie}(r)$ (Fig. 1), as well as $\rho_{ii}(r)$ and $\rho_{ee}(r)$ (Fig. 2), was numerically calculated by the path-integral method.

The mean-force potential

$$W_{ee}(r) \equiv -k_B T \ln\left(\frac{\rho_{ee}(r)}{\rho}\right), \quad (11)$$

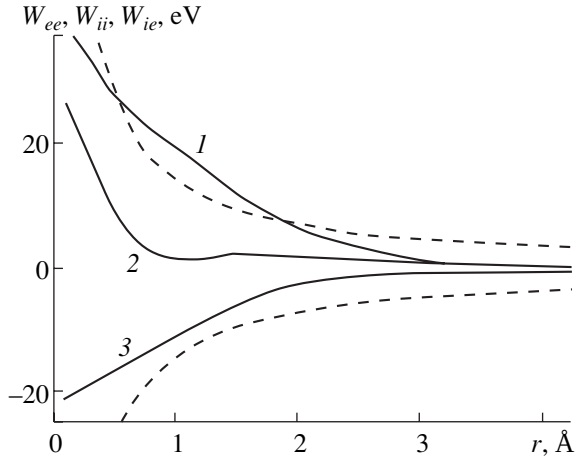

Fig. 3. The mean-force potentials in the hydrogen plasma, (*1*) W_{ee}, (*2*) W_{ii}, and (*3*) W_{ie} under the same conditions as in Fig. 1. The dashed curves correspond to the interaction of two elementary charged particles in vacuum.

where ρ is the particle density, describes interaction between two particles with inclusion of indirect interactions via the other particles in the system. Deviation of $W_{ee}(r)$ from the interaction energy $\frac{e^2}{r}$ of two pointlike charged particles is caused by quantum effects and interactions with the other particles. Apparently, the quantum effects manifest themselves at interparticle distances smaller than the thermal de Broglie wavelength, whereas the shielding of interaction by other particles of the medium becomes more pronounced with increasing r. The curves shown in Fig. 3 demonstrate that the mean-force potentials for all three types of interactions satisfy the condition $W_{ee}(r)$, $W_{ii}(r)$, $W_{ie}(r) \ll k_B T$ at $r > 4$ Å. The interparticle interaction is considerably shielded at these distances. The reduction of the Coulomb interaction is of a collective origin. The curve shown in Fig. 4 demonstrates that the number of electrons spaced from the proton at distances smaller than $r = 4$ Å is as low as 0.66. The electron nearest to the proton cannot shield the field of the proton to the extent suggested by the data presented in Fig. 3. The charge of other electrons plays a significant role in this region.

The higher the plasma density, the more conventional the degree of ionization. To a first approximation, the probability of ionization can be estimated from the area under the peak in Fig. 1. Figure 4 demonstrates that the degree of ionization under these conditions is $\Delta N_b = 0.45$.

The quantum-mechanical uncertainty in the coordinate leads to smoothing of the plots for mean-force potentials at small distances. The effect is clearly pronounced at distances $r < 2$ Å (Fig. 3). At a distance of 1 Å, the potentials $W_{ee}(r)$ and $W_{ie}(r)$ differ from the interaction energies of the classical pointlike charges by 5 and 3 eV, respectively. The quantum effects at these distances lead to strengthening the interelectron repulsion and to weakening the attraction between electrons and protons. At distances $r < 0.5$ Å, the effect has the same sign for both curves and is rapidly enhanced with a decrease in r. The $W_{ii}(r)$ curve at distances $r <$ 0.5 Å has a steeper slope, since heavy protons behave as classical particles and the quantum-mechanical uncertainty in their positions has no effect here. The effect is enhanced due to a small dip at a distance of about 1 Å. This dip corresponds to the formation of the bound state involving two hydrogen atoms. This bound state is manifested as a peak in the $\rho_{ii}(r)$ curve (Fig. 2).

The calculated correlation functions demonstrate the clearly pronounced quantum character of the particle motion at distances where the electrostatic interaction is not shielded. The interactions at these distances are primarily responsible for the thermal properties of the dense plasma. At larger distances, where the particle motion is nearly classical, the interactions are significantly shielded. In spite of the relatively high temperature, the calculation of deviating the characteristics of the dense hydrogen plasma from those of the ideal plasma requires the fundamental inclusion of the quantum effects.

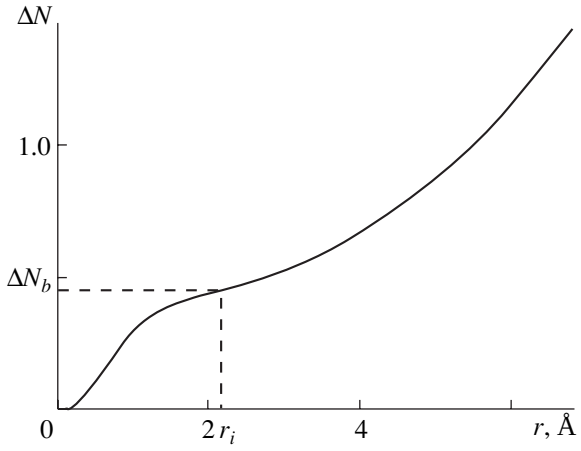

Fig. 4. The average number of electrons spaced from the proton at distances smaller than r as calculated for the hydrogen plasma under the same conditions as in Fig. 1. The distance r_i corresponds to the dip in the curve shown in Fig. 1.

REFERENCES

1. N. Metropolis, A. W. Rosenbluth, M. N. Rosenbluth, and H. A. Teller, J. Chem. Phys. **21**, 1087 (1953).
2. R. P. Feynman and A. R. Hibbs, *Quantum Mechanics and Path Integrals* (McGraw-Hill, New York, 1965; Mir, Moscow, 1968).
3. V. M. Zamalin, G. E. Norman, and V. S. Filinov, *Monte Carlo Method in Statistical Thermodynamics* (Nauka, Moscow, 1977).
4. L. D. Fosdick and H. F. Jordan, Phys. Rev. **143**, 58 (1966).
5. H. F. Jordan and L. D. Fosdick, Phys. Rev. **171**, 128 (1968).
6. V. M. Zamalin and G. E. Norman, Zh. Vychisl. Mat. Mat. Fiz. **13**, 408 (1973).
7. V. S. Filinov, Teplofiz. Vys. Temp. **11**, 871 (1973); **13**, 251 (1975); **13**, 1146 (1975); **14**, 245 (1976).
8. V. S. Filinov, Phys. Lett. A **54A**, 259 (1975).
9. V. S. Filinov and G. E. Norman, Phys. Lett. A **55A**, 219 (1975).
10. H. Weyl, *The Theory of Groups and Quantum Mechanics* (Dover, New York, 1931; Nauka, Moscow, 1983).
11. S. V. Shevkunov (Available from VINITI, Moscow, No. 6370-B87, 1987).
12. S. V. Shevkunov, Zh. Éksp. Teor. Fiz. **118**, 36 (2000) [JETP **91**, 31 (2000)].
13. S. V. Shevkunov and P. N. Vorontsov-Velyaminov, Mol. Simul. **7**, 249 (1991).
14. S. V. Shevkunov, Dokl. Akad. Nauk **369**, 43 (1999) [Dokl. Phys. **44**, 730 (1999)].
15. S. V. Shevkunov, Teplofiz. Vys. Temp. **29**, 45 (1991).

Translated by K. Kugel

Doklady Physics, Vol. 47, No. 2, 2002, pp. 114–118. Translated from Doklady Akademii Nauk, Vol. 382, No. 6, 2002, pp. 754–758.

PHYSICS

Laser Annealing of Colloidal Media for Holographic Recording

I. V. Bogdan*, Yu. N. Vygovskiĭ, Yu. S. Zagaĭnova***, A. N. Malov***, S. N. Malov*, V. Yu. Molotsilo***, A. A. Petrov***, and N. O. Reĭngand******

Presented by Academician Yu.N. Denisyuk August 31, 2001

Received September 4, 2001

Holograms recorded in photosensitive layers with a thickness of several millimeters have a number of attractive specific properties. Thus they can be widely used in the development of modern elements for optical information processors, in systems of optical memories with multiplex information storage, in devices for interfiber connection in optical telecommunication networks, etc. [1]. However, known recording media turn out to be unsuitable for obtaining such holograms, since, as a rule, a change in the layer-thickness structure occurs in processing these media, caused, e.g., by shrinkage of photoemulsions.

At the same time, the new recording media desired can be obtained on the basis of colloidal emulsion systems of self-developing dichromatic gelatin (SDDG) [2]. However, in the process of synthesizing the superthick (more than 0.5 mm) layers, the problem of their drying arises, which takes a long time (more than 3 days), followed by the jellification or ripening of the colloidal medium. This problem appears at the last stage of the phototechnological process and cannot be solved by traditional methods of blowing hot air or by alcoholic dehydration, which lead to the appearance of a strong gradient of optical properties over the thickness of the layer. In phototechnological production, ultrasonic and acoustic treatment as well as microwave heating [3] have been used already for a long time. However, their application makes an accurate energy dosage of ultrasonic or microwave treatment upon the object difficult. In addition, the processing of colloidal layers by microwave radiation often results in their exfoliation from the substrate and in an uncontrollable change in the conformational state of gelatin macromolecules.

In this paper, the holographic characteristics of SDDG are considered in the case of synthesizing emulsion with the use of a high-power IR radiation of the 1.06-μm wavelength. The radiation provides laser annealing (drying) and gelatination of colloidal layers of millimeter thickness, as well as the possibility of controlling the properties of the material when annealing by IR laser radiation.

CONTROLLING THE GELATIN-LAYER STRUCTURE

Gelatin as a polymeric system passes through a sequence of various aggregate states in the preparation of a dichromatic-gelatin layer. A diluted solution of gelatin in water is the initial state. In this state, macromolecules are in the condition of a Gaussian coil or a globule. In the forming process, as a result of the interaction of chain macromolecules after the solution has been poured onto the substrate, gel formation occurs. This gel can manifest properties of either a liquid crystal (if the molecules are hard-chained) or a concentrated solution with equal volumetric fractions of solvent and polymer [2].

Evaporation of the solvent (water) from the poured emulsion is accompanied by the process of returning macromolecules into the native state of the collagen-like three-strand spiral structure deformed to a certain extent by conditions of the film formation. In the process of gelatination under both the action of forces from the substrate side and drying conditions, the unwrapping of macromolecules into linear structures occurs with a simultaneous twisting of segments into spiral pieces. Such a spontaneous return into the native spiral state in the process of gelatination occurs statistically and locally due to the interaction of macromolecular segments. In turn, this provides the presence of well developed short-range order in the gelatin emulsion, without the long-range order inherent in collagens [4].

* *Irkutsk Branch of Laser Physics Institute, Siberian Division, Russian Academy of Sciences, Irkutsk Office, P/O Box 4038, Irkutsk, 664003 Russia*

** *Media Company, Novoslobodskaya ul. 36/1, Bld. 1, 103055 Russia*

*** *Irkutsk State University, bul'v. Gagarina 20, Irkutsk, 664003 Russia*

**** *Institute for Mechanical Engineering Problems, Russian Academy of Sciences, V.O., Bol'shoi pr. 61, St. Petersburg, 199178 Russia*

1028-3358/02/4702-0114$22.00

STRUCTURE OF WATER AND THE ACTION OF INFRARED RADIATION

An SDDG system contains a very large amount of water. Therefore, this system can be treated as an almost-water solution, for which the role of the quasi-crystalline structure of the entire liquid is essential [5]. Connection into a unified three-dimensional network and the collective character of molecular motion in water are confirmed by studies in the field of molecular dynamics [6]. Under the action of IR radiation, the structure energy increases, hydrogen bonds are weakened, vibration amplitudes rise, and the concentration of defects produced by translations of molecules from crystal-lattice sites into a neighboring potential well is enhanced. Water molecules form a collective module, and, therefore, an association of five molecules is considered as a particle more or less reflecting actual properties of water [5]. Interaction of water with dissolved species results in the formation of an aquacomplex, i.e., an association of a species molecule with several molecules of water. Water molecules entering into the complex composition, in turn, are connected with neighboring water molecules; i.e., the aquacomplexes can be considered as segments of the hydrogen-bond network in water [5, 6].

We can affect the structure of the SDDG-emulsion throughout the entire bulk of the layer using laser IR radiation. In this case, the molecular reconstruction mechanism by the action of the electromagnetic field of IR radiation is determined by the loss of the coordination stability of vibrations for a fraction of molecules. It is, naturally, impossible to specify a certain radiation wavelength optimal for such an annealing, due to the complicated composition of the emulsion. Therefore, based on known data concerning the water-absorption spectra, we used the carbon-dioxide laser radiation with a wavelength of about 1 μm. In addition, the radiation of the nearest IR range passes through a glass substrate so that undesirable effects of the IR-radiation interference are absent in the layer bulk.

The energy action of IR-radiation upon the SDDG-layer should satisfy the following requirements:

(i) the absence of either parasitic illumination or photosensitivity loss in the system;

(ii) the elimination of gelatin thermal destruction;

(iii) the minimization of noticeable heating of the system, which could result in both the unwrapping of spiral macromolecular regions and a drop of the photosensitivity [4].

Thus, the energy pumping should be very selective in order to change only the ternary and quaternary structures of gelatin, i.e., the disposition and elongation of its molecules. Therefore, it is worthwhile to use laser radiation with low photon energies, which is not absorbed by proteins and individual water molecules.

The action of the electromagnetic field upon the water solution of gelatin macromolecules results in a violation of the equilibrium state of the system. After ceasing irradiation, dielectric relaxation occurs. Being subjected to the action of the electromagnetic field of IR radiation, water molecules begin to reconstruct themselves in accordance with the Le Chatelier principle. In this case, the absorption frequency of 1000 cm^{-1} (the wavelength of 1 μm) can be interpreted as a sum of two frequencies: 200 cm^{-1} (the frequency of individual rotary oscillations) and ~800 cm^{-1} (the libration frequency of water molecules within the collective module, or aquacomplex) [5].

EXPERIMENTAL METHOD

Synthesizing SDDG layers. Samples were prepared in accordance with the following method. Gelatin was dissolved in water for 1 h (1 g of gelatin per 5 ml of distilled water) at 50°C. Then, after the glycerin had been added (0.8 ml per 5 ml of water), the solution was held at 40°C for 2 h. Ammonium bichromate in the needed concentration (20% with respect to the dry-gelatin mass, or 0.2 g per 5 ml of water), ammonium for attaining pH = 9.0, and methylene blue dye (MB) in the form of a solution (10 mg of MB per 100 ml of water) was added to the solution obtained. The emulsion solution prepared was poured into a transparent cuvette with side walls of a necessary height (from 0.5 to 3 mm) and covered by a cover glass. Then, this solution was gelatinated for 24 h at 25°C. As a result, a layer with the desired thickness was obtained.

Technique of laser annealing. After holding poured-on emulsion layers for a day, a primary quasi-crystalline SDDG structure was formed [4]. Then the plates were subjected to the action of laser IR radiation with a wavelength of 1 μm.

Measurement of holographic characteristics. The results of laser annealing were determined according to changes in the diffraction efficiency (DE) of holograms recorded in similar annealed test layers due to the interference of two plane waves of helium–neon laser radiation (λ = 633 nm). The spatial frequency of the diffraction grating being recorded was about 500 lines per 1 mm. The power of two beams incident onto a plate was 6 mW. Diffraction efficiency was measured as a ratio of the intensities for the diffracted and incident beams.

The experimental data on the diffraction efficiency variation as a function of annealing parameters are shown in Figs. 1–4.

Thus, under the action of the electromagnetic field of IR radiation, a pulsed perturbation of the water structure occurs (in the first approximation) at the level of collective modules, since the individual water molecules and protein molecules do not absorb radiation with a wavelength of about 1 μm [7]. The reconstruction of the quasi-crystalline water structure results in a change in the water–gelatin interaction. Gelatin macromolecules stir under the action of this field and change their conformation ternary and quaternary states in

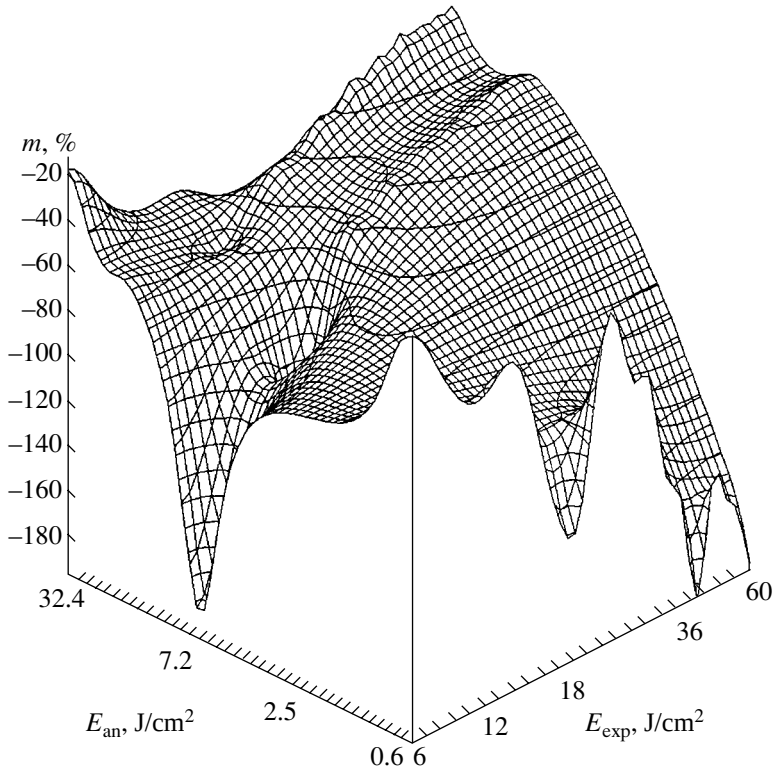

Fig. 1. Diffraction efficiency (DE) of a test holographic grating recorded in a SDDG layer by the helium–neon laser radiation as a function of the laser annealing energy and exposure time under the action of pulsed laser IR radiation of a 5-ms duration. Maximum DE are: 9.8% (without annealing) and 8.8% (with annealing). Here, and in Figs. 2–4, E_{an} is the total energy for the sequence of annealing pulses; E_{exp} is the exposure energy for a test grating in the case of helium–neon laser radiation; $m = [(DE_{an} - DE_0)/D_{an}] \times 100\%$, where DE_{an} is the diffraction efficiency for the test grating recorded by the annealed SDDG; and DE_0 is the diffraction efficiency for the test grating recorded by the unannealed SDDG.

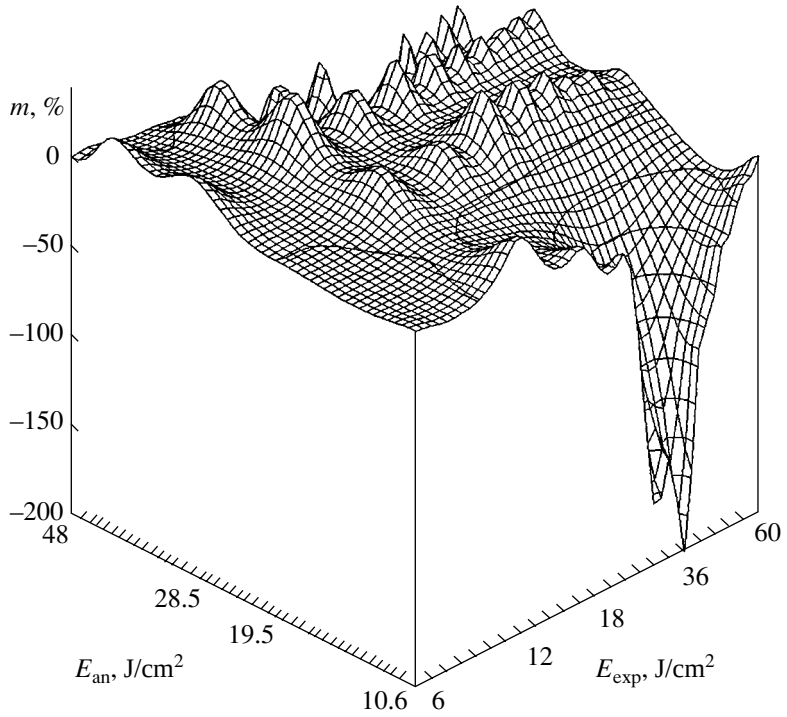

Fig. 2. Diffraction efficiency (DE) of a test holographic grating recorded in the SDDG layer by helium–neon laser radiation as a function of the laser annealing energy and exposure time under the 4-pulse action of laser IR radiation for the 4-ms pulse duration. Maximum values of the DE are 3% (without annealing) and 3.8% (with annealing).

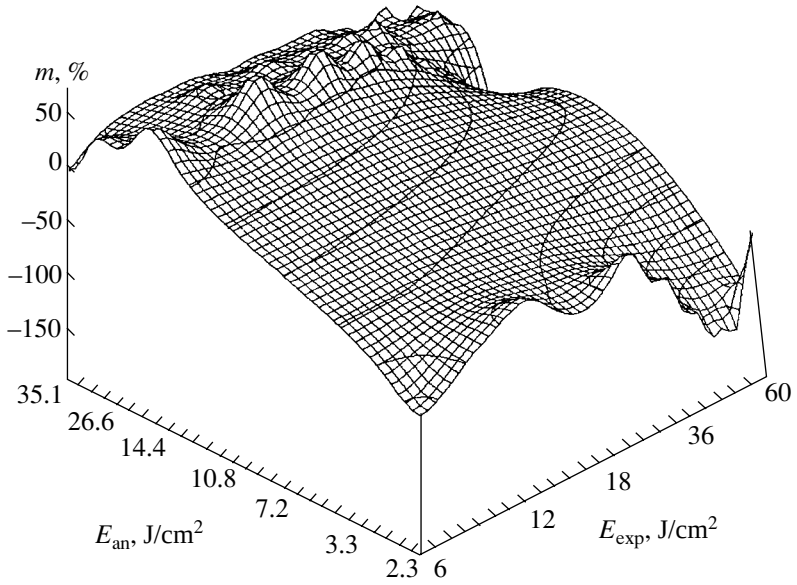

Fig. 3. Diffraction efficiency (DE) of test holographic grating, which is recorded in the SDDG layer by helium–neon laser radiation as a function of the laser annealing energy and exposure time under the 8-pulse action of laser IR radiation for a 2-ms pulse duration. Maximum DE values are 1.4% (without annealing) and 4.2% (with annealing).

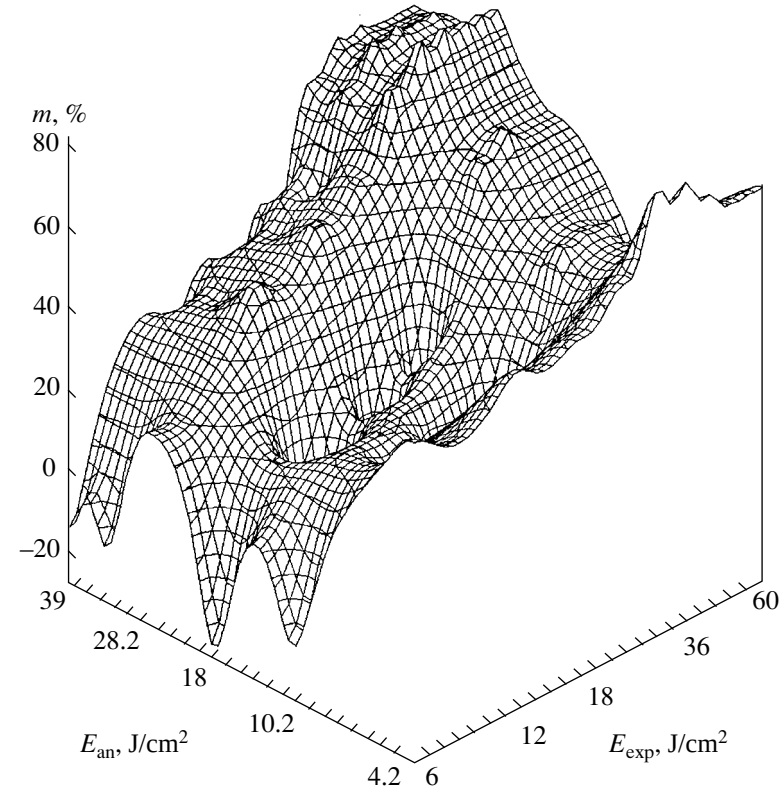

Fig. 4. Diffraction efficiency (DE) of test holographic grating recorded in the SDDG layer by helium–neon laser radiation as a function of the laser annealing energy and exposure time under the 6-pulse action of laser IR radiation for a 3-ms pulse duration. Maximum DE values are 1.3% (without annealing) and 3.7% (with annealing).

order to attain a minimum energy in the new quasicrystalline structure. In this case, the spiral segments are not destroyed; i.e., the photosensitive properties of the entire SDDG system can remain unchanged.

A pulse-periodic regime of irradiation in the case of laser annealing is more favorable, since it allows estimating the exact energy of action on the layer structure. Pulse-periodic irradiation is, to some extent, similar to

a sharp shaking-up of the system, and the necessary package of macromolecules is attained at the expense of relaxation processes.

Thus, in this paper, the possibility of the improvement of SDDG properties under the action of laser IR radiation is experimentally confirmed. In addition to the reduction of the time for synthesizing the layer, the application of laser annealing for structuring the SDDG results in an increase in the diffraction efficiency and improves the uniformity of properties throughout the entire bulk of the system, which is very important for the 1- to 5-mm-thick layers. Laser annealing, as a whole, serves as an additional parameter of controlling the technological process. Optimal regimes of laser annealing are revealed, as well as the emulsion compositions that make it possible to increase the photosensitivity by recording holograms using the radiation of a helium–neon laser with a wavelength of 0.63 μm and reduce the time of emulsion ripening by several times (from three days to 2–3 h).

ACKNOWLEDGMENTS

This work was supported by the Russian Foundation for Basic Research, project 01-02-17141 (performed under the name "Theoretical and experimental studies of recording holographic structures in bulk phase media with the self-development effect") and by the European Office of Aerospace Research and Development, USA, project no. 2057P (performed under the name "New aspects of holographic technologies and their applications on the basis of dynamic and nondynamic recording media").

REFERENCES

1. Yu. N. Denisyuk and N. M. Ganzherli, Zh. Tekh. Fiz. **63**, 81 (1993) [Tech. Phys. **38**, 98 (1993)].
2. Yu. N. Vygovskiĭ, P. A. Draboturin, A. G. Konop, *et al.*, Komp'yut. Optika, No. 18, 133 (1998).
3. A. N. Didenko and B. V. Zverev, *Microwave Power Engineering* (Nauka, Moscow, 2000).
4. Yu. N. Vigovsky, S. P. Konop, A. N. Malov, and S. N. Malov, Laser Phys. **8**, 901 (1998).
5. V. I. Yashkichev, *Water, Its Molecular Motion, Structure, Interphase Processes, and Response to External Actions* (Agar, Moscow, 1996).
6. *Method of Molecular Dynamics in Physical Chemistry*, Ed. by Yu. K. Tovbin (Nauka, Moscow, 1996).

Translated by T. Galkina

Doklady Physics, Vol. 47, No. 2, 2002, pp. 119–120. Translated from Doklady Akademii Nauk, Vol. 382, No. 6, 2002, pp. 759–760.

PHYSICS

On the Localizability of Gravitational Energy

Academician A. A. Logunov and M. A. Mestvirishvili

Received October 30, 2001

In the general relativity theory (GRT), the covariant law for the density of the energy–momentum tensor T_μ^ν of a medium in a Riemannian space has a form

$$\nabla_\nu T_\mu^\nu \equiv \partial_\nu T_\mu^\nu - \frac{1}{2}T^{\sigma\lambda}\partial_\mu g_{\sigma\lambda}, \quad T^{\sigma\lambda} = -2\frac{\delta L_M}{\delta g_{\sigma\lambda}}. \quad (1)$$

This equation immediately follows from the Gilbert–Einstein equations. The law of energy–momentum conservation for both matter and the gravitational field in the GRT has a noncovariant form

$$\partial_\nu(T_\mu^\nu + \tau_\mu^\nu) = 0. \quad (2)$$

This is a way that leads to the appearance of the gravitational-field pseudotensor τ_μ^ν in the GRT, which is not a covariant quantity. It is impossible, in principle, to write out in the GRT an equation for the conservation of the energy–momentum of both matter and the gravitational-field in the general covariant form. As a result, the concept has arisen based on the GRT that localizing the gravitational energy is impossible.

In the relativistic gravitational theory (RGT), the gravitational field is treated as a physical tensor field $\Phi^{\mu\nu}$ with spins 2 and 0 that develops in a Minkowski space. In the RGT, the conserved density of the energy–momentum tensor for all material fields, including the gravitational field, is the source of the gravitational field. This approach provides rigorous fulfillment of the laws of conservation for both the energy–momentum and angular momentum. In this case, due to the action of the gravitational field, an effective Riemannian space arises that has the field origin. In the RGT, the density of the Lagrangian has the form

$$L = L_g(\tilde{\gamma}^{\mu\nu}, \tilde{\Phi}^{\sigma\lambda}) + L_M(\tilde{g}^{\sigma\lambda}, \tilde{\Phi}_A). \quad (3)$$

Here,

$$L_g = \frac{1}{16\pi}\tilde{g}^{\mu\nu}(G_{\mu\nu}^\lambda G_{\lambda\sigma}^\sigma - G_{\mu\sigma}^\lambda G_{\nu\lambda}^\sigma) - \frac{m^2}{2}\left(\frac{1}{2}\gamma_{\mu\nu}\tilde{g}^{\mu\nu} - \sqrt{-g} - \sqrt{-\gamma}\right), \quad (4)$$

$$G_{\mu\nu}^\lambda = \frac{1}{2}g^{\lambda\sigma}(D_\mu g_{\nu\sigma} + D_\nu g_{\mu\sigma} - D_\sigma g_{\mu\nu}), \quad (5)$$

$\tilde{\gamma}^{\mu\nu} = \sqrt{-\gamma}\gamma^{\mu\nu}$, $\tilde{\Phi}^{\sigma\lambda} = \sqrt{-\gamma}\Phi^{\sigma\lambda}$, $\tilde{g}^{\sigma\lambda} = \sqrt{-g}g^{\sigma\lambda}$, and Φ_A are the matter fields. We imply as matter all material fields excluding the gravitational field.

The metric-tensor density $\tilde{g}^{\sigma\lambda}$ of an effective Riemannian space is connected with the density $\tilde{\Phi}^{\sigma\lambda}$ of the gravitational-field tensor by the relation

$$\tilde{g}^{\sigma\lambda} = \tilde{\gamma}^{\sigma\lambda} + \tilde{\Phi}^{\sigma\lambda}. \quad (6)$$

The equation for the gravitational field can be written out in the form [1]

$$-J^{\sigma\lambda} + m^2\tilde{\Phi}^{\sigma\lambda} = 16\pi\sqrt{\frac{g}{\gamma}}(T^{\sigma\lambda} + t_g^{\sigma\lambda}), \quad (7)$$

where $t_g^{\sigma\lambda}$ is the density of the energy–momentum tensor for the gravitational field. Thus,

$$J^{\sigma\lambda} = -D_\mu D_\nu \times(\gamma^{\mu\nu}\tilde{g}^{\sigma\lambda} + \gamma^{\sigma\lambda}\tilde{g}^{\mu\nu} - \gamma^{\nu\sigma}\tilde{g}^{\lambda\mu} - \gamma^{\mu\lambda}\tilde{g}^{\sigma\nu}). \quad (8)$$

It is easy to see that the identity

$$D_\lambda J^{\sigma\lambda} = 0 \quad (9)$$

takes place. Equations (7) for the gravitational field can be represented as

$$\sqrt{-g}\left(R^{\mu\nu} - \frac{1}{2}g^{\mu\nu}R\right) + \frac{m^2}{2}\left[\tilde{g}^{\mu\nu} + \left(\tilde{g}^{\mu\alpha}g^{\nu\beta} - \frac{1}{2}\tilde{g}^{\mu\nu}g^{\alpha\beta}\right)\gamma_{\alpha\beta}\right] = 8\pi T^{\mu\nu}. \quad (10)$$

Here, m is the graviton mass and $\gamma_{\alpha\beta}$ is the metric tensor

State Center of the Russian Federation, Institute of High Energy Physics, Protvino, Moscow oblast, 142284 Russia

1028-3358/02/4702-0119$22.00

of a Minkowski space. From Eq. (10), we obtain

$$m^2\gamma_{\nu\lambda}D_\sigma\tilde{\Phi}^{\sigma\lambda} = 16\pi\nabla_\mu T^\mu_\nu. \quad (11)$$

According to Eq. (7), we have

$$m^2\tilde{\Phi}^{\sigma\lambda} = J^{\sigma\lambda} + 16\pi\sqrt{\frac{g}{\gamma}}(T^{\sigma\lambda} + t_g^{\sigma\lambda}). \quad (12)$$

Substituting relation (12) into Eq. (11), we arrive at

$$D_\sigma\left[\sqrt{\frac{g}{\gamma}}(T^{\sigma\lambda} + t_g^{\sigma\lambda})\right] = \gamma^{\nu\lambda}\nabla_\mu T^\mu_\nu. \quad (13)$$

On the basis of the general structure for the Lagrangian L_M of the medium, we can find the strong identity [2, 3]

$$\nabla_\mu T^\mu_\nu = -D_\sigma\left(\frac{\delta L_M}{\delta\Phi_A}F^{B;\,\sigma}_{A;\,\nu}\Phi_B\right) - \frac{\delta L_M}{\delta\Phi_A}D_\nu\Phi_A, \quad (14)$$

which holds independent of the equations of motion. In the case when the equations of motion for the medium

$$\frac{\sigma L_M}{\delta\Phi_A} = 0 \quad (15)$$

are valid, the equality

$$\nabla_\mu T^\mu_\nu = 0 \quad (16)$$

takes place. Therefore, in accordance with Eq. (13), the covariant law of conservation for the energy–momentum of matter and of the gravitational field taken together can be written in the form

$$D_\sigma[\sqrt{-g}(T^{\sigma\lambda} + t_g^{\sigma\lambda})] = 0. \quad (17)$$

Thus, in the GRT, covariant law (1) leads to the noncovariant law of conservation (2) for the energy–momentum of both matter and the gravitational field, as well as to the introduction of a certain noncovariant quantity, namely, the pseudotensor τ^ν_μ of the gravitational field. At the same time, according to the GRT, covariant law (1) combined with the gravitational equations in the form (10) or (7) leads exactly to the covariant law of conservation for the energy–momentum of both matter and the gravitational field taken together in form (17). In expression (17), the gravitational component $\sqrt{-g}t_g^{\sigma\lambda}$ additively enters into expression (17) under the sign of the covariant derivative in a Minkowski space. At the same time, in (16), this component disappears as it participates in the formation of an effective Riemannian space. Therefore, under the sign of the covariant derivative in a Riemannian space, only the density of the tensor for the energy–momentum of matter in this space is present. The field approach to gravitation, which is realized in the RGT, results in another (compared to the GRT) system of gravitational equations. This approach also preserves the fundamental principles, namely, the laws of conservation for both the energy–momentum and the angular momentum. This is the reason why, according to the RGT, the gravitational energy is localized, as well as all other forms of energy. In the GRT, the problem is still discussed [4] as to whether the gravitational waves carry energy. According to the RGT, gravitational radiation must exist, and gravitational waves must carry energy.

In conclusion, we note that an effective Riemannian space that arises due to the action of the gravitational field has only a simple topology as far as the gravitational field develops in a Minkowski space.

REFERENCES

1. A. A. Logunov, *Theory of Gravitation* (Nauka, Moscow, 2001).
2. V. I. Denisov and A. A. Logunov, in *Achievements of Science and Engineering. Modern Problems of Mathematics* (VINITI, Moscow, 1982), Vol. 21, p. 89.
3. A. A. Logunov and M. A. Mestvirishvili, *Relativistic Theory of Gravitation* (Mir, Moscow, 1989; Nauka, Moscow, 1989).
4. F. I. Cooperstock, Ann. Phys. **282**, 115 (2000).

Translated by G. Merzon

Doklady Physics, Vol. 47, No. 2, 2002, pp. 121–123. Translated from Doklady Akademii Nauk, Vol. 382, No. 4, 2002, pp. 474–477.

TECHNICAL PHYSICS

A New Mathematical Model for a Thin Electric Dipole

S. B. Klyuev*, I. V. Matveev, V. A. Neganov**, and E. I. Nefedov***

Presented by Academician O.M. Belotserkovskiĭ April 24, 2001

Received June 21, 2001

1. THE ESSENCE OF THE PROBLEM

The design parameters of thin electric dipoles are generally calculated by solving the Pocklington and Harrington integro-differential equations, which may be combined with the Hallen integral equation [1–4]. The most popular approach is based on the moment method and its modifications defined by specific choices of basis functions. In our view, the main disadvantage of this approach lies in the fact that solutions to the integral equations are sought by replacing the original singular kernels written in implicit form with regular (Fredholm) ones. This leads to ill-posed problems for Fredholm integral equations of the first kind [5]. Both the mathematical verification and physical validation of the resulting solutions remain issues open to discussion. In [6], a new class of basis functions was proposed for solving equations of this type. These functions were called the eigenfunctions of an integro-differential operator. However, the use of such functions substantially complicates the algorithm of the numerical solution.

In this paper, we continue the analysis presented in [7, 8] and based on the mathematical theory of singular integral equations (SIEs). This was employed for analyzing superhigh-frequency and extremely high-frequency strip-slotted waveguides [9, 10] to derive an SIE for the longitudinal derivative of the dipole surface-current density.

2. STATEMENT OF THE PROBLEM AND THE SINGULAR INTEGRAL EQUATION

We consider a thin-cut conductor with a total length $2L$ and radius a excited in its gap by means of a high-frequency oscillator (see Fig. 1). The governing equations are derived here for the conventional model of a thin electric dipole ($a \ll L, \lambda$). In this model, both the longitudinal current density η_z^e and the equivalent magnetic current density in the gap are represented by a filamentary current $I_z(z) = 2\pi a \eta_z^e(z)$, which is assumed to be continuous in the gap region and to vanish at the dipole's ends. End currents are ignored. The electric field component E_z induced by the filamentary current is zero on the entire cylinder surface ($\rho = a, z \in [-L, L]$) besides the gap region $2b$, where it is identified with the extraneous electric field $E^{\text{ext}}(z)$.

When the radiation emitted by the dipole is independent of the angle φ, the physical model adopted here is described by the Pocklington equation [1–4]

$$\left(\frac{d^2}{dz^2} + \gamma^2\right)\int_{-L}^{L} \frac{I_z(z')}{4\pi R} e^{i\gamma R} dz = -i\omega\varepsilon_0\varepsilon E^{\text{ext}}, \qquad (1)$$

where $R = \sqrt{(z-z')^2 + a^2}$, $\gamma^2 = k^2\varepsilon\mu$ ($k = \dfrac{\omega}{c}$ is the wave number), ε is the relative permittivity of the ambient

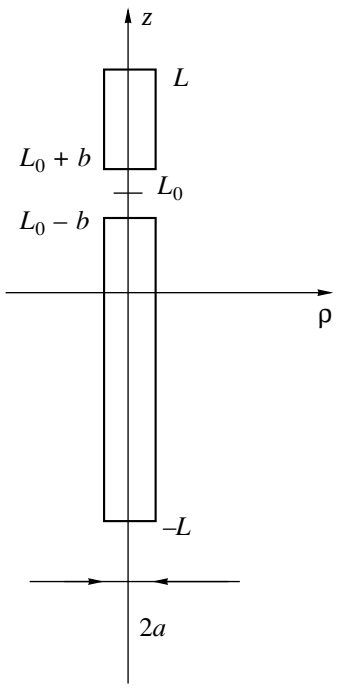

Fig. 1.

* *Institute of Radio Engineering and Electronics, Russian Academy of Sciences (Fryazino Branch), pl. Vvedenskogo 1, Fryazino, Moscow oblast, 141120 Russia*

** *Volga State Academy of Telecommunications and Informatics, ul. L. Tolstogo 23, Samara, 443010 Russia*

1028-3358/02/4702-0121$22.00

medium, μ is its relative permeability, and ε_0 is the free-space permittivity.

Using a well-known representation of the Green's function in Eq. (1) (see [11]),

$$\frac{e^{-i\gamma R}}{4\pi R} = \frac{1}{4\pi}\int_0^\infty \frac{e^{-\sqrt{h^2-\gamma^2}|z-z'|}}{\sqrt{h^2-\gamma^2}} J_0^2(ha)h\,dh, \quad (2)$$

where $J_0(x)$ is the zeroth-order Bessel function of the first kind, we obtain the following integral equation:

$$\int_{-L}^{L} I_z(z')G_1(z,z')dz' = -4\pi i\omega\varepsilon_0\varepsilon E^{\text{ext}}(z) \quad (3)$$

with

$$G_1(z,z') = \int_0^\infty \frac{e^{-\sqrt{h^2-\gamma^2}|z-z'|}}{\sqrt{h^2-\gamma^2}} J_0^2(ha)h^3\,dh. \quad (4)$$

Relation (3) is an inhomogeneous integral equation of the first kind.

It is evident that the integrand in the expression for the kernel $G_1(z, z')$, which is contained in Eq. (3), linearly increases with h as $h \longrightarrow \infty$, and the integral in expression (4) is divergent. In order to eliminate the singularity in kernel (4), we turn from the function $I_z(z)$ to its derivative $I_z' = \dfrac{dI_z}{dz}$ in Eq. (3). Since the current I_z vanishes at the dipole ends [$I_z(L) = I_z(-L) = 0$], we can write

$$\int_{-L}^{L} I_z(z')e^{-\sqrt{h^2-\gamma^2}|z-z'|}dz' = \frac{1}{\sqrt{h^2-\gamma^2}}\int_{-L}^{L} I_z'(z')\,\text{sgn}(z-z')e^{-\sqrt{h^2-\gamma^2}|z-z'|}dz'. \quad (5)$$

Using (5), we rewrite Eq. (3) as

$$\int_{-L}^{L} I_z'(z')G(z,z')dz' = -4\pi i\omega\varepsilon_0\varepsilon E^{\text{ext}}(z), \quad (6)$$

where

$$G(z,z') = \text{sgn}(z-z')\int_0^\infty g(h)J_0^2(ha)dh,$$
$$g(h) = \frac{h^3 e^{-\sqrt{h^2-\gamma^2}|z-z'|}}{h^2-\gamma^2}. \quad (7)$$

Taking the limit of the function $g(h)$ as $h \longrightarrow \infty$,

$$\lim_{h\to\infty} g(h) = he^{-h|z-z'|},$$

we consider the asymptotic form of the kernel:

$$G_\infty(z,z') = \text{sgn}(z-z')\int_0^\infty e^{-h|z-z'|}J_0^2(ha)h\,dh. \quad (8)$$

Using the representation

$$G_\infty(z,z') = \frac{1}{\pi a(z-z')} + \alpha(z,z'), \quad (9)$$

where

$$\alpha(z,z') = \frac{kE(k)-1}{\pi a(z-z')}, \quad k = \left[\left(\frac{z-z'}{2a}\right)^2 + 1\right]^{-\frac{1}{2}},$$

and $E(k)$ is the complete elliptic integral of the second kind, we rewrite Eq. (6) as the following SIE:

$$\frac{1}{\pi a}\int_{-L}^{L}\frac{I_z'(z')}{z-z'}dz' + \int_{-L}^{L} I_z'(z')K_1(z,z')dz' = -\frac{2\pi i\gamma}{bZ_c}U(z). \quad (10)$$

Here,

$$K_1(z,z') = \alpha(z,z') + \text{sgn}(z-z') \times \int_0^\infty \left\{\frac{h^2 e^{-\sqrt{h^2-\gamma^2}|z-z'|}}{h^2-\gamma^2} - e^{-h|z-z'|}\right\}J_0^2(ha)h\,dh, \quad (11)$$

$U(z) = 2bE^{\text{ext}}(z)$ is the voltage over the dipole gap, and $Z_c = \sqrt{\dfrac{\mu_0\mu}{\varepsilon_0\varepsilon}}$ is the characteristic ambient impedance.

Relation (10) is an SIE of the first kind for the longitudinal derivative of the dipole current. Here, $K_1(z, z')$ is a regular kernel, because $k \longrightarrow 1$, $E(k) \longrightarrow 1$, $\alpha(z, z') \longrightarrow \eta\ln|z-z'|(z-z')$, and $\lim\limits_{z\to z'}\alpha(z,z') \longrightarrow 0$ as $z \longrightarrow z'$ (η is a constant factor).

3. SOLUTION OF THE SINGULAR INTEGRAL EQUATION

To solve the SIE, we turn to the dimensionless variables t and t' defined by setting $z = Lt$ and $z' = Lt'$ and rewrite Eq. (10) in the form ($t \in [-1, 1]$):

$$\frac{1}{\pi}\int_{-1}^{1}\frac{I_z'(t')}{t-t'}dt' + \int_{-1}^{1} I_z'(t')K(t,t')dt' = -\frac{2\pi i\gamma a}{bZ_c}U(t), \quad (12)$$

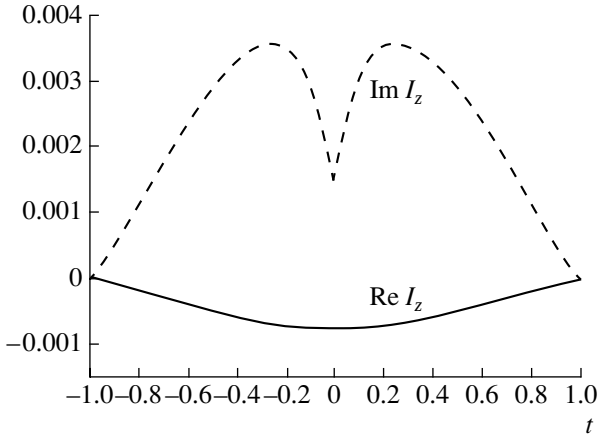

Fig. 2.

where

$$K(t, t') = \frac{[kE(m) - 1]}{\pi(t - t')} + \operatorname{sgn}(t - t') \times \delta \int_0^\infty \left\{ \frac{\beta^2 e^{-\delta\sqrt{\beta^2 - (\gamma a)^2}|t - t'|}}{\beta^2 - (\gamma a)^2} - e^{-\delta\beta|t - t'|} \right\} J_0^2(\beta)\beta d\beta, \quad (13)$$

$$m = \left[\frac{\delta^2 (t - t')^2}{4} + 1 \right]^{-1/2}, \quad \delta = \frac{L}{a}.$$

We solve Eq. (12) using the inversion formula for the Cauchy integral [4]. As a result, we have

$$I_z'(t') + \int_{-1}^{1} I_z'(t') S(t, t') dt' = f(t), \quad (14)$$

where

$$S(t, t') = -\frac{1}{\pi\sqrt{1 - t^2}} \int_{-1}^{1} \frac{\sqrt{1 - \tau^2}}{(\tau - t)} K(\tau, t) d\tau,$$

$$f(t) = \frac{4i\gamma a}{Z_c \sqrt{1 - t^2}} \int_{(L_0 - b)/L}^{(L_0 + b)/L} \frac{E^{\text{ext}}(\tau)}{\tau - t} d\tau + \frac{a_0}{\sqrt{1 - t^2}},$$

and a_0 is an unknown constant determined by setting I_z to zero at the dipole's ends, i.e., by the condition

$$\int_{-1}^{1} I_z'(\tau) d\tau = 0.$$

According to this relation, the total charge accumulated on the dipole must also vanish. Equation (14) is an inhomogeneous Fredholm integral equation of the second kind, and its numerical solution is easy to find. Equation (14) has been analyzed numerically by the method of mechanical quadratures [12].

Figure 2 shows typical distributions for the real and imaginary parts of the dipole current, $\operatorname{Re}\{I_z(t)\}$ and $\operatorname{Im}\{I_z(t)\}$, calculated for $\frac{b}{L} = \frac{1}{100}$, $\frac{a}{\lambda} = \frac{1}{40}$, and $\frac{b}{\lambda} = \frac{1}{4}$. The solid and dashed curves represent $\operatorname{Re}\{I_z(t)\}$ and $\operatorname{Im}\{I_z(t)\}$, respectively. The results obtained in the present study are in good agreement with those reported in [6, 7].

CONCLUSIONS

The proposed approach, based on the mathematical formalism of the SIE theory, was used to derive a new singular integral equation with the intent to calculate the design parameters of a thin electric dipole. The SIE derived here makes it possible to analyze the performance of a thin electric dipole within the framework of a well-posed problem. In particular, the SIE can be solved without dealing with any manifestation of relative convergence of the type encountered in analyses of Fredholm equations of the first kind [4, 5], which include the known Hallen equation. The new SIE can serve as a basis for obtaining approximate analytical expressions for dipole currents. The method developed above provides an efficient tool for calculating the input conductance and input impedances of dipole antennas.

REFERENCES

1. *Computing Methods in Electrodynamics*, Ed. by R. Mitra (Pergamon Press, Oxford, 1973; Mir, Moscow, 1977).
2. D. M. Sazonov, *Antennas and Microwave Devices* (Vysshaya Shkola, Moscow, 1988).
3. G. A. Erokhin, O. V. Chernyshev, N. D. Kozyrev, and V. G. Kocherzhevskiĭ, *Antenna-Feeder Devices and Propagation of Radio Waves* (Radio i Svyaz', Moscow, 1996).
4. V. A. Neganov, S. B. Raevskii, and G. P. Yarovoi, in *Linear Macroscopic Electrodynamics*, Ed. by V. A. Neganov (Radio i Svyaz', Moscow, 2000), Vol. 1.
5. A. N. Tikhonov and V. Ya. Arsenin, *Solution of Ill-Posed Problems* (Nauka, Moscow, 1986).
6. S. I. Éminov, Radiotekh. Electron. **38**, 2160 (1993).
7. V. A. Neganov and I. V. Matveev, Izv. Vyssh. Uchebn. Zaved., Radiofiz. **43**, 335 (2000).
8. V. A. Neganov, I. V. Matveev, and S. V. Medvedev, Pis'ma Zh. Tekh. Fiz. **26**, 86 (2000) [Tech. Phys. Lett. **26**, 535 (2000)].
9. V. A. Neganov, E. I. Nefedov, and G. P. Yarovoĭ, *Strip-Slotted Structures for Super-High and Extremely High Frequencies* (Nauka, Moscow, 1996).
10. V. N. Gridin *et al.*, *Principles for the Design of Microelectronic Devices* (Sov. Radio, Moscow, 1977).
11. V. A. Neganov, E. I. Nefedov, and G. P. Yarovoĭ, *Modern Design Methods for Transmission Lines and Cavities of Super-High and Extremely High Frequencies* (Pedagogika-Press, Moscow, 1998).
12. G. T. Markov and A. F. Chaplin, *Excitation of Electromagnetic Waves* (Énergiya, Moscow, 1967).
13. V. V. Panasyuk, M. P. Savruk, and Z. T. Nazarchuk, *Method of Singular Integral Equations in Two-Dimension Diffraction Problems* (Naukova Dumka, Kiev, 1984).

Translated by A. Betev

Doklady Physics, Vol. 47, No. 2, 2002, pp. 124–127. Translated from Doklady Akademii Nauk, Vol. 382, No. 5, 2002, pp. 621–624.

TECHNICAL PHYSICS

Enhancement of the Magnetoelastic and Magnetoelectric Interaction in Antiferroelectric Antiferromagnets

I. R. Kyzyrgulov and M. Kh. Kharrasov

Presented by Academician V.P. Maslov November 6, 2001

Received July 28, 2000

In recent years, the interest in studies of ferroelectric magnets, i.e., crystals with the perovskite structure, has grown considerably. These crystals demonstrate the coexistence of magnetic and ferroelectric long-range order [1–3]. Most of all, this interest is caused by the fact that such crystals are very promising materials for applications in modern electronics [4].

In this paper, we analyze the possibility of enhancing parameters of the magneto-elastic and magnetoelectric coupling in antiferromagnetic structures with the orthorhombic symmetry (the D_{2h} spatial group) by the exchange interaction.

The system under investigation is described by the Hamiltonian

$$H = H_M + H_U + H_F + H_{MU} + H_{MF} + H_{FU}, \qquad (1)$$

which allows for the energies of magnetic (M), elastic (U), and ferroelectric (F) system parts and their interaction energies. In the Hamiltonian of the magnetic subsystem placed into an external magnetic field, energies of uniform and nonuniform exchange interactions and relativistic interactions are taken into account. The elastic subsystem is considered in the harmonic approximation, and the Hamiltonian of the ferroelectric subsystem allows for the inverse dielectric susceptibility and correlation properties. The magnetoelectric energy is natural and relativistic.

Hamiltonian (1) is written in the representation of the approximate secondary quantization. To this aim, the magnetic moments $\mathbf{M}^\alpha$ of sublattices and the vector of elastic displacements $\mathbf{u}$ are expressed in terms of the Holstein–Primakoff operators a_α^+ and a_α and of the phonon creation and annihilation operators b_{ks}^+, b_{ks}, respectively (see, e.g., [5]). We also represent the deviation of the polarization vector from the equilibrium value in the form

$$\mathbf{P}^\alpha = \sqrt{\frac{\lambda}{8\pi V}}\sum_{k\delta}\frac{\mathbf{e}_k^\delta}{\sqrt{\varepsilon_{k\delta\alpha}^f}}(d_{k\delta\alpha}e^{ikx} + d_{k\delta\alpha}^+ e^{-ikx}),$$

where $\mathbf{e}_k^\delta$ is the unit vector of the ferroelectric polarization, $\varepsilon_{k\delta\alpha}^f$ is the energy of ferroelectric excitations, and δ is the polarization index of a transverse vibration.

Furthermore, for the diagonalization of the Hamiltonian of the magnetic and ferroelectric subsystems, we employ the Bogolyubov canonical transformations

$$a_{k\alpha} = u_{k\alpha\gamma}c_{k\gamma} + v_{k\alpha\gamma}^* c_{-k\gamma}^+, \quad a_\alpha = V^{-1/2}\sum_k a_{k\alpha}e^{ikr},$$

$$d_{k\delta\alpha} = U_{k\delta\alpha\gamma}D_{k\delta\gamma} + V_{k\delta\alpha\gamma}^* D_{-k\delta\gamma}^+.$$

Thus, we can write out Hamiltonian (1) in the form

$$H = \sum_{k\gamma}\varepsilon_{k\gamma}^M c_{k\gamma}^+ c_{k\gamma} + \sum_{ks}\varepsilon_{ks}^U b_{ks}^+ b_{ks} + \sum_{k\delta\alpha}E_{k\delta\alpha}D_{k\delta\alpha}^+ D_{k\delta\alpha}$$

$$+\left\{\sum_{ks\gamma}\Psi_{k\gamma s}^{MU}c_{k\gamma}[b_{-ks} - b_{ks}^+] + \sum_{k\delta\alpha\gamma}\Psi_{k\delta\alpha\gamma}^{MF}c_{k\gamma}\right.$$

$$\left.\times[D_{-k\delta\alpha} - D_{k\delta\alpha}^+] + \sum_{k\delta\alpha s}\Psi_{k\delta\alpha s}^{FU}D_{k\delta\alpha}[b_{-ks} - b_{ks}^+] + \text{H.c.}\right\},$$

where $\varepsilon_{k\gamma}^M$ ($\gamma = 1, 2$), ε_{ks}^U ($s = 1, t_1, t_2$), $E_{k\delta\alpha}$ ($\delta = 1, 2$; $\alpha = 1, 2$) are energies of the corresponding branches of spin waves, elastic waves, and ferroelectric waves. Parameters of the magnetoelastic and magnetoelectric interactions are determined by the expressions

$$\Psi_{k\gamma s}^{MU} = i\sqrt{\frac{\mu M_0}{2\rho\varepsilon_{ks}^U}}(b_{imn} + 2M_0 b_{ijmn}^{\alpha\beta}e_{3j}^\alpha)Q_{ik}^{\beta\gamma}e_{km}^s k_n, \quad (2)$$

$$Q_{ik}^{\beta\gamma} = e_{\perp i}^\beta u_{k\alpha\gamma} + e_{\perp i}^{\beta *} v_{k\alpha\gamma}.$$

Bashkortostan State University, Ufa, ul. Frunze 32, 450074 Russia

1028-3358/02/4702-0124$22.00

Here, the first and second terms describe, respectively, the piezomagnetic effect and the magnetostriction; $\mathbf{e}_{\mathbf{k}}^{s}$ is the unit vector of the phonon polarization; and e_{3i}^{α}, $e_{\perp i}^{\alpha}$ are the transformation coefficients for the M_i^{α} operators with respect to the proper representation

$$e_{3i}^{\alpha} = \frac{M_{0i}^{\alpha}}{M_0}, \quad e_{\perp i}^{\alpha} = \frac{1}{\sqrt{2}}(e_{1i}^{\alpha} + ie_{2i}^{\alpha}), \quad e_1^{\alpha} \perp_s (M_0^{\alpha}, H_0),$$

$$e_2^{\alpha} = [e_3^{\alpha}, e_1^{\alpha}],$$

$$\Psi_{k\delta\alpha\gamma}^{MF} = -\sqrt{\frac{\lambda\mu M_0}{8\pi\varepsilon_{k\delta\alpha}^{f}}} \tag{3}$$

$$\times (a_{im} + 2M_0 a_{ijm}^{\chi\beta} e_{3j}^{\chi}) e_{ki}^{\delta} Q_{mk}^{\beta\gamma} (U_{k\delta\nu\alpha} - V_{k\delta\nu\alpha}),$$

where the first and second terms describe, respectively, the linear magnetoelectric effect and the magnetic anisotropy induced by the vector **P**.

The parameter of the electroelastic coupling has a simple form:

$$\Psi_{k\delta\alpha s}^{FU} = i\sqrt{\frac{\lambda}{8\pi\rho\varepsilon_{k\delta\alpha}^{f}\varepsilon_{ks}^{U}}} \tag{4}$$

$$\times (w_{ijm} e_{ki}^{\delta} e_{kj}^{s} k_m + i\nu_{ijmn} e_{ki}^{\delta} e_{km}^{s} k_j k_n)(U_{k\delta\nu\alpha} - V_{k\delta\nu\alpha}),$$

where w_{ijm} is the tensor of piezoelectric constants and ν_{ijmn} is the tensor describing the coupling of inhomogeneities for the polarization and deformation.

To find the eigenfrequencies of coupled ferroelectric magnetoelastic waves, we use the equations of motion for the secondary-quantized operators. Within the accuracy to the terms quadratic over coupling coefficients, we derive the following dispersion equation:

$$\prod_{s\delta\alpha\gamma} (\omega^2 - \varepsilon_{k\gamma}^{M^2})(\omega^2 - \varepsilon_{ks}^{U^2})(\omega^2 - E_{k\delta\alpha}^2)$$

$$- 4\sum_{\gamma s} \left|\Psi_{k\gamma s}^{MU}\right|^2 \varepsilon_{k\gamma}^{M} \varepsilon_{ks}^{U}$$

$$\times \prod_{s' \neq s,\, \gamma' \neq \gamma} (\omega^2 - E_{k\delta\alpha}^2)(\omega^2 - \varepsilon_{k\gamma'}^{M^2})(\omega^2 - \varepsilon_{ks'}^{U^2})$$

$$- 4\sum_{\gamma\delta\alpha} \left|\Psi_{k\delta\alpha\gamma}^{MF}\right|^2 \varepsilon_{k\gamma}^{M} E_{k\delta\alpha} \prod_{\gamma' = \gamma,\, (\delta', \alpha') \neq (\delta, \alpha)} (\omega^2 - \varepsilon_{k\gamma'}^{M^2})$$

$$\times (\omega^2 - \varepsilon_{ks}^{U^2})(\omega^2 - E_{k\delta'\alpha'}^2) - 4\sum_{\delta\alpha s} \left|\Psi_{k\delta\alpha s}^{FU}\right|^2 \varepsilon_{ks}^{U} E_{k\delta\alpha}$$

$$\times \prod_{s' \neq s,\, (\delta', \alpha') \neq (\delta, \alpha)} (\omega^2 - \varepsilon_{k\gamma}^{M^2})(\omega^2 - \varepsilon_{ks'}^{U^2})(\omega^2 - E_{k\delta'\alpha'}^2) = 0.$$

We now consider the interaction of spin and elastic waves for crystals of orthorhombic symmetry in an external magnetic field. For simplicity, the piezomagnetic effect is ignored. Depending on the direction of the wave vector k, we find according to (2) for certain particular cases [here and below, we omit zero (in our approximation) coupling coefficients].

1a. The case $k \parallel Z$:

$$\Psi_{k11}^{MU} = \eta_1 (u_{k11} - v_{k11})$$

$$\times \sin 2\theta (b_{xxzz}^{11} - b_{xxzz}^{12} - b_{zzzz}^{11} - b_{zzzz}^{12}) k_z,$$

$$\Psi_{k2t_1}^{MU} = \eta_{t_1} (u_{k22} - v_{k22})(b_{xzxz}^{11} \cos 2\theta + b_{xzxz}^{12}) k_z,$$

$$\Psi_{k2t_2}^{MU} = i\eta_{t_2} (u_{k22} + v_{k22}) \cos\theta (b_{yzyz}^{11} + b_{yzyz}^{12}) k_z,$$

where

$$\eta_s \equiv 4\sqrt{\frac{2\mu M_0^3}{\rho\varepsilon_{ks}^{U}}}, \quad \cos\theta = \frac{H_0}{H_\delta}, \quad \sin\theta = \left(1 - \frac{H_0^2}{H_\delta^2}\right)^{1/2},$$

$$\cos 2\theta = 2\frac{H_0^2}{H_\delta^2} - 1, \quad H_\delta = 2\delta M_0.$$

The exchange interaction enhances by a factor of $\sqrt{\delta}$ the coupling of the second spin branch with the first transverse phonon branch.

2a. The case $k \parallel Y$:

$$\Psi_{k11}^{MU} = \eta_1 (u_{k11} - v_{k11})$$

$$\times \sin 2\theta (b_{xxyy}^{11} - b_{xxyy}^{12} - b_{zzyy}^{11} - b_{zzyy}^{12}) k_y,$$

$$\Psi_{k1t_2}^{MU} = i\eta_{t_2} (u_{k11} + v_{k11}) \sin\theta (b_{xyxy}^{11} - b_{xyxy}^{12}) k_y,$$

$$\Psi_{k2t_1}^{MU} = i\eta_{t_1} (u_{k22} + v_{k22}) \cos\theta (b_{zyzy}^{11} + b_{zyzy}^{12}) k_y.$$

Here, the coefficient for the coupling of the first spin branch with the second transverse phonon branch is enhanced due to the exchange interaction.

3a. The case $k \parallel X$:

$$\Psi_{k11}^{MU} = \eta_1 (u_{k11} - v_{k11})$$

$$\times \sin 2\theta (b_{xxxx}^{11} - b_{xxxx}^{12} - b_{zzxx}^{11} - b_{zzxx}^{12}) k_x,$$

$$\Psi_{k1t_1}^{MU} = i\eta_{t_1} (u_{k11} + v_{k11}) \sin\theta (b_{yxyx}^{11} - b_{yxyx}^{12}) k_x,$$

$$\Psi_{k2t_2}^{MU} = \eta_{t_2} (u_{k22} - v_{k22})(b_{zxzx}^{11} \cos 2\theta + b_{zxzx}^{12}) k_x.$$

In this case, the couplings of the first and second spin branches with the t_1 and t_2 transverse phonon branches, respectively, are enhanced by the exchange interaction.

We now consider the magnetoelectric interaction (3). This interaction is different depending on the direction of the k vector with respect to the magnetizations and polarizations of sublattices for various magnetic and ferroelectric waves. For simplicity, we ignore the linear magnetoelectric effect.

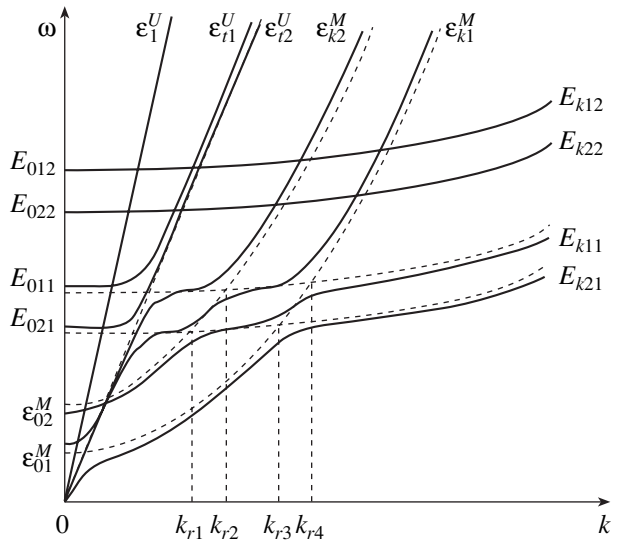

Coupled ferroelectric magnetoelastic waves.

1b. The case $k \parallel Z$:

$$\Psi_{k111}^{MF} = \phi_1(a_{xxy}^{11} - a_{xxy}^{12}) \times \sin\theta(u_{k11} + v_{k11})[U_{k111} - V_{k111}],$$

$$\Psi_{k211}^{MF} = \phi_2(a_{yxy}^{11} - a_{yxy}^{12}) \times \sin\theta(u_{k11} + v_{k11})[U_{k211} - V_{k211}],$$

$$\Psi_{k112}^{MF} = \phi_1[(a_{xzy}^{11} + a_{xzy}^{12})(u_{k22} + v_{k22})\cos\theta + i(a_{xxz}^{11}\cos 2\theta + a_{xxz}^{12})(u_{k22} - v_{k22})][U_{k111} - V_{k111}],$$

$$\Psi_{k212}^{MF} = \phi_2[(a_{yzy}^{11} + a_{yzy}^{12}(u_{k22} + v_{k22})\cos\theta + i(a_{yxz}^{11}\cos 2\theta + a_{yxz}^{12})(u_{k22} - v_{k22})][U_{k211} - V_{k211}],$$

$$\phi_\delta \equiv \sqrt{\frac{\lambda\mu M_0^3}{2\pi\varepsilon_{k\delta 1}^f}}.$$

The coupling of the spin branches with the first and second ferroelectric branches is enhanced by a factor of $\sqrt{\delta}$ due to the exchange interaction.

2b. The case $k \parallel Y$:

$$\Psi_{k111}^{MF} = \phi_1(a_{zxy}^{11} - a_{zxy}^{12}) \times \sin\theta(u_{k11} + v_{k11})[U_{k111} - V_{k111}],$$

$$\Psi_{k211}^{MF} = \phi_2(a_{xxy}^{11} - a_{xxy}^{12}) \times \sin\theta(u_{k11} + v_{k11})[U_{k211} - V_{k211}],$$

$$\Psi_{k112}^{MF} = \phi_1[(a_{zzy}^{11} + a_{zzy}^{12})(u_{k22} + v_{k22})\cos\theta + i(a_{zxz}^{11}\cos 2\theta + a_{zxz}^{12})(u_{k22} - v_{k22})][U_{k111} - V_{k111}],$$

$$\Psi_{k212}^{MF} = \phi_2[(a_{xzy}^{11} + a_{xzy}^{12})(u_{k22} + v_{k22})\cos\theta + i(a_{xxz}^{11}\cos 2\theta + a_{xxz}^{12})(u_{k22} - v_{k22})][U_{k211} - V_{k211}].$$

The coupling of spin branches with the first and the second ferroelectric branches is enhanced by a factor of $\sqrt{\delta}$ due to the exchange interaction.

3b. The case $k \parallel X$:

$$\Psi_{k111}^{MF} = \phi_1(a_{yxy}^{11} - a_{yxy}^{12}) \times \sin\theta(u_{k11} + v_{k11})[U_{k111} - V_{k111}],$$

$$\Psi_{k211}^{MF} = \phi_2(a_{zxy}^{11} - a_{zxy}^{12}) \times \sin\theta(u_{k11} + v_{k11})[U_{k211} - V_{k211}],$$

$$\Psi_{k112}^{MF} = \phi_1[(a_{yzy}^{11} + a_{yzy}^{12})(u_{k22} + v_{k22})\cos\theta + i(a_{yxz}^{11}\cos 2\theta + a_{yxz}^{12})(u_{k22} - v_{k22})][U_{k111} - V_{k111}],$$

$$\Psi_{k212}^{MF} = \phi_2[(a_{zzy}^{11} + a_{zzy}^{12}(u_{k22} + v_{k22})\cos\theta + i(a_{zxz}^{11}\cos 2\theta + a_{zxz}^{12})(u_{k22} - v_{k22})][U_{k211} - V_{k211}].$$

The coupling of spin branches with the first and the second ferroelectric branches is enhanced by a factor of $\sqrt{\delta}$ due to the exchange interaction.

Thus, the study of the magnetoelectric interaction in the antiferroelectric antiferromagnets with orthorhombic symmetry shows that the interactions of individual branches of spin waves and ferroelectric waves in the antiferroelectric antiferromagnets can be enhanced by the parameter of the exchange interaction that results in the increase in the corresponding coupling coefficient by a factor of $\sqrt{\delta}$.

The general pattern of the spectrum of coupled ferroelectric magnetoelastic waves for the case of the propagation of a wave along the *Y*-axis in the absence of an external magnetic field is presented in the figure. The dependences for the frequencies of noninteracting magnetic and ferroelectric waves and coupled ferroelectric magnetoelastic waves on the wave vector are shown by dashed and solid lines, respectively. As is clearly seen from the figure, in various regions the coupled ferroelectric magnetoelastic wave corresponds to eigenmodes of various subsystems. Therefore, moving along a subsystem, it is possible to obtain spin waves, sonic waves, ferroelectric waves, etc.

Estimates of the interaction parameters show that $\frac{\Psi_{k1t_2}^{MU}}{\varepsilon_{k1}^M} \approx 10^{-2}$ and $\frac{\Psi_{k\perp 211}^{MF}}{\varepsilon_{k1}^M} \approx 10^{-1}$; i.e., a gap in the spectrum of spin waves, which is caused by the magnetoelectric interaction due to a significant dielectric con-

stant exceeds by more than an order of magnitude the gap determined by the magnetoelastic energy.

Another important conclusion consists in the fact that only the coupling of the lower acoustic branch of spin vibrations with ferroelectric and elastic modes can be enhanced by the exchange interaction.

REFERENCES

1. L. D. Landau and E. M. Lifshitz, *Electrodynamics of Continuum* (Pergamon Press, Oxford, 1982; Nauka, Moscow, 1982).
2. V. A. Bokov, I. E. Myl'nikova, and G. A. Smolenskiĭ, Zh. Éksp. Teor. Fiz. **41**, 643 (1962) [Sov. Phys. JETP **14**, 462 (1962)].
3. Yu. E. Roginskaya, Yu. N. Venevtsev, and G. S. Zhdanov, Zh. Éksp. Teor. Fiz. **44**, 1418 (1963) [Sov. Phys. JETP **17**, 955 (1963)].
4. V. I. Il'ichev, M. A. Sadovnikov, and A. V. Stefanovich, *High-Temperature Superconductivity of Ceramic Systems* (Moscow, 1992).
5. N. N. Bogolyubov, Jr., and B. I. Sadovnikov, *Certain Problems of Statistical Mechanics* (Nauka, Moscow, 1975).

Translated by T. Galkina

Doklady Physics, Vol. 47, No. 2, 2002, pp. 128–131. Translated from Doklady Akademii Nauk, Vol. 382, No. 6, 2002, pp. 761–764.

TECHNICAL PHYSICS

The Energy of Debonding a Nanometer-Size Coating from a Rigid Substrate

S. L. Bazhenov*, V. G. Myagkov, V. S. Zhigalov**, and A. L. Volynskiĭ*****

Presented by Academician N.F. Bakaev May 30, 2001

Received June 5, 2001

In this study, the shape of an elastic coating upon its debonding from a substrate is theoretically determined. On the basis of this solution, we develop a method of determining the debonding energy (fracture toughness) of the coating. The energies of debonding a carbon film from a glass and a cobalt film from a raw mica were measured. The debonding toughness is close to the energy of the breaking of atomic bonds. This fact made it possible to conclude that the debonding of films of nanometer thickness differs fundamentally from the fracture of macroscopic samples.

Recently, the mechanical behavior of two-layer composites composed of a substrate and a thin coating of nanometer thickness have been vigorously studied. Coatings can be used for various purposes, for example, as a shielding layer, for imparting special optical properties, and for storing information. Unfortunately, due to an insufficient adhesion bond, a coating can debond from the substrate. The coating usually either does not debond at all or debonds altogether. In [1], an unusual debonding mechanism involving the progressive intergrowth of sinusoidal-shaped debondings was found.

The fracture including the adhesion requires the expenditure of energy on forming a new surface. In samples of macroscopic and microscopic sizes, the typical fracture energy is from hundreds to several thousands of joules per square meter. The fracture energy is the sum of two components, the energy of the breaking of intermolecular bonds and the energy spent on plastically deforming the material near the fracture plane [2]. In metals and polymers, the energy of plastic deformation is three–five orders of magnitude higher than the energy of the breaking of chemical bonds. For this reason, the bond-breaking contribution is considered as negligible. The fracture energy decreases with the thickness of samples [3]; however, these data were available only for films of thickness from tens of micrometers to several centimeters. For the samples with a thickness of several nanometers, the fracture energy could not be previously measured. This study is devoted to solving this problem.

We studied two composites. The first was a glass plate 0.5 mm thick covered by a carbon layer 60 nm thick, and the second was a mica plate covered by a cobalt–carbon layer 160 nm thick. The cobalt-to-carbon mass ratio was 80 : 20. The surface of composites was studied by a Nanoscope-2 atomic-force microscope (Digital Instruments, Santa Barbara, Calif.) in the contact-force mode. The electron-microscope investigations were carried out on a Hitachi S-520 scanning electron microscope.

Figure 1 shows the image of the glass/carbon composite obtained by the atomic-force microscope. The single sinusoidal-shape debonding, similar to those described in [1], can be observed at the surface. The profile of the surface along the dashed line is shown in the upper part of the figure. The width and height of this debonding are approximately 1.5 and 0.1 μm, respectively.

Figure 2 shows the similar image of the mica surface covered by a Co–C layer. In this case, the debonding is larger and its width is approximately equal to 8 μm.

Upon bending, the coating length increases. This behavior indicates that, upon debonding and bending, the coating film was biaxially compressed. As a result of bending, the compressive stress decreases. In this case, the bending is accompanied by the adhesion fracture of the coating/substrate interface, in contrast to the classical case of the loss of stability of a compressed elastic rod.

Below, we solved the problem of the debonding of a thin elastic coating under conditions of uniaxial compression along the X-axis in Fig. 3. We seek a coating shape upon the loss of stability (bending). The deformation of the debonded coating is described by the equations for bending an elastic beam. The beam ends are considered as fixed, and the bending is assumed to be small. The latter condition is satisfied if the debonding height of $2A$ is small compared to its length L (Fig. 3).

* *Institute of Synthetic Polymeric Materials, Russian Academy of Sciences, Profsoyuznaya ul. 70, Moscow, 117393 Russia*

** *Kirenskiĭ Institute of Physics, Siberian Division, Russian Academy of Sciences, Akademgorodok, Krasnoyarsk, 660036 Russia*

*** *Moscow State University, Vorob'evy gory, Moscow, 119899 Russia*

1028-3358/02/4702-0128$22.00

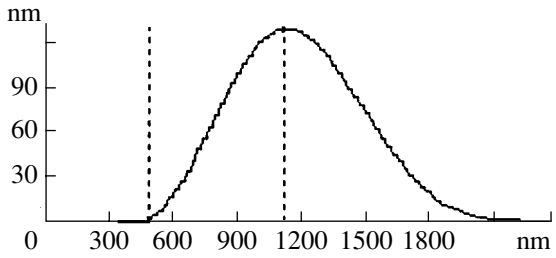

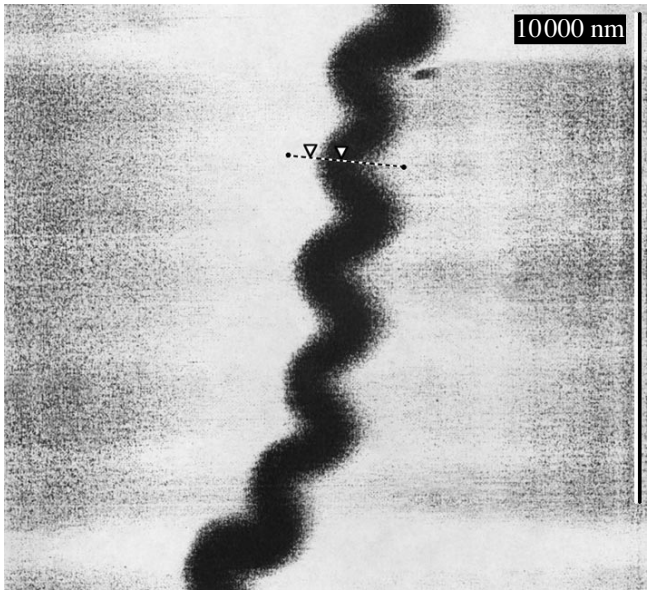

Fig. 1. (Lower part) The coating surface image obtained by an atomic-force microscope and (upper part) the corresponding profile for the glass/carbon composite. Here and in Fig. 2, the surface profile corresponds to the dashed line. The coating thickness is 60 nm.

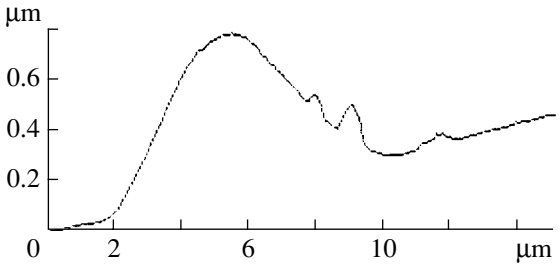

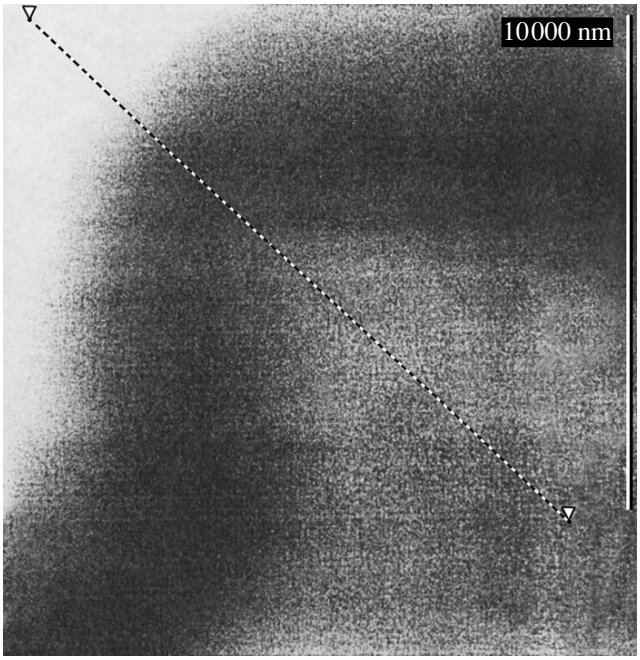

Fig. 2. Surface of mica covered by a 160-nm-thick Co–C layer.

It is assumed that the debonding begins with the appearance of a small defect (a debonding crack). Then, the coating loses its stability (bends) under the action of the compressive force. The bending of the rod leads to a decrease in the compression energy and an increase in the bending energy. If the sum of the energies of compression and bending decreases, the coating bends.

Upon the loss of stability, tensile stresses appear at the crack tip between the substrate and the coating and tend to separate the coating from the substrate. The original crack can spontaneously grow if an elastic-energy decrease caused by the crack growth exceeds the energy of forming a new surface. When the crack attains a certain length, the compressive stress in the coating reduces so that a decrease in the compression energy ceases to compensate the expenditure of energy on debonding with the further increase in length. As a consequence, the crack comes to rest.

We choose the coordinate axes so that the plane $Y = 0$ coincides with the coating plane and denote the coordinates of the two ends of the crack as $x_1 = 0$ and $x_2 = L$ (L is the length of the debonding crack). The bending of an elastic beam is described by the differential equation [4, 5]

$$IE\frac{d^4y}{dx^4} - F\frac{d^2y}{dx^2} = 0, \quad (1)$$

where $y(x)$ is the displacement of the beam elements

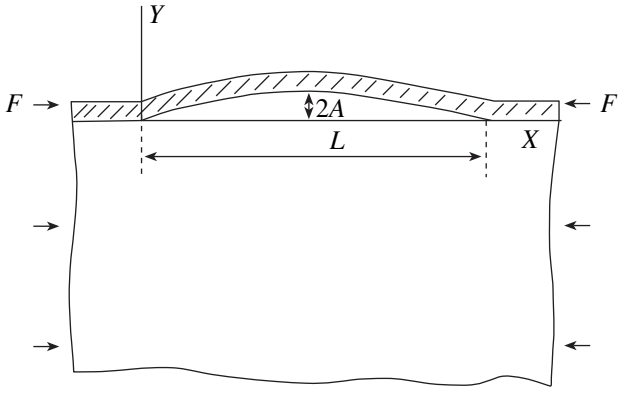

Fig. 3. Scheme of debonding.

(coating) from the plane $Y = 0$ as a result of bending, $I = wh^3/12$ is the moment of inertia of the beam at bending, w is the beam width along the third coordinate Z, h is the thickness of the coating, E is its elastic modulus, and F is the compressive force. For the beam with fixed ends, the boundary conditions have the form

$$y = 0, \quad \frac{dy}{dx} = 0, \text{ for } x = 0 \text{ and } x = L.$$

The solution of Eq. (1) with allowance for these boundary conditions has the form

$$y = A(1 - \cos kx), \tag{2}$$

where A is the half maximum debonding height and $k = 2\pi/L$. Substituting solution (2) into Eq. (1), we determine the compressive force for the coating:

$$F = \frac{4\pi^2 IE}{L^2}. \tag{3}$$

Equation (3) describes the compressive force for the loss of stability of the rod with the fixed ends. The energy of elastic strain for a bent beam is the sum of energies of compression and bending. The energy of compression is equal to

$$W_c = \frac{\sigma^2}{2E} SL,$$

where $\sigma = F/S$ is the compressive stress, $\sigma^2/2E$ is the density of elastic energy, and $S = wh$ is the cross section of the debonded coating. On the basis of Eq. (3), we obtain

$$W_c = \frac{8\pi^4 I^2 E}{L^3 S}. \tag{4}$$

The bending energy for an elastic beam is found by integrating

$$W_b = \frac{EI}{2}\int_0^L \left(\frac{d^2y}{dx^2}\right)^2 dx,$$

and, with allowance for Eq. (2), we obtain

$$W_b = \frac{4\pi^4 A^2 EI}{L^3}. \tag{5}$$

The constant A is determined as follows. In the initial state, the coating is compressed. A length of a small element of the debonded bent coating is equal to

$$dL = \sqrt{1 + y'^2}\,dx.$$

Integrating this relation with allowance for Eq. (2) under the assumption that the debonding amplitude is $A \ll L$, $\sqrt{1 + y'^2} \approx 1 + y'^2/2$, we obtain

$$L_1 = L + \frac{A^2 k^2 L}{4}. \tag{6}$$

The compressive strain of the beam upon its bending decreases by the value $(L_1 - L)/L = A^2k^2/4$. The strain upon the bending is $\varepsilon = \varepsilon_0 - A^2k^2/4$, where ε_0 is the strain before the bending. With allowance for Eq. (3), we obtain

$$A = \sqrt{\frac{\varepsilon_0 L^2}{\pi^2} - \frac{4I}{S}}. \tag{7}$$

It should be noted that $4I/S = h^2/3$, and the second term under the radical sign in Eq. (7) can be neglected if the debonding height $2A$ is much larger than the debonding thickness. Now, we analyze the solution obtained. In order that the debonding lose its stability, the compressive force must exceed the critical value determined by Eq. (3). This condition results in the inequality

$$L_0 > \sqrt{\frac{\pi^2 h^2}{3\varepsilon_0}}, \tag{8}$$

where L_0 is the original length of the debonding defect. Thus, the initial defect must be relatively large in order for the coating to be bent.

We consider the behavior of debonding upon a loss of stability. The strain energy of the bent coating is equal to the sum of energies of compression and bending. Furthermore, the total energy of the system involves the energy of forming a new surface,

$$W = \frac{4\pi^2 \varepsilon_0 EI}{L} - \frac{8\pi^4 EI^2}{SL^3} + G_{Ic} wL, \tag{9}$$

where G_{Ic} is the energy (toughness) of adhesion fracture spent on the formation of 1-m^2 debonding. The debonding grows spontaneously if the total energy decreases with increasing its length L and $\frac{dW}{dL} < 0$. Differentiating Eq. (9), we obtain

$$-\frac{\pi^2 \varepsilon_0 Eh^3}{3L^2} + \frac{\pi^4 Eh^5}{6L^4} + G_{Ic} < 0. \tag{10}$$

The crack comes to rest when this inequality goes over into the equality. With allowance for Eq. (7), we obtain

$$G_{Ic} = \frac{\pi^4 Eh^3 A^2}{3L^4}\left(1 - \frac{h^2}{6A^2}\right). \tag{11}$$

We pass to the analysis of experimental data on the basis of the above theory. It should be noted that the exact value of the elastic modulus of the deposited carbon film is unknown. Assuming that the modulus is

within 200–400 GPa [6] and using the values L = 2.13 μm and A = 0.09 μm (Fig. 1), we obtain the fracture toughness G_{Ic} = 1.7–3.4 J/m^2. This value corresponds to the energy 2.8–3.0 J/m^2 of the brittle fracture of glass [7]. A similar calculation for the composite based on mica for L = 9.2 μm, A = 0.31 μm (Fig. 2), h = 160 nm, and the cobalt elastic modulus E = 209 GPa gives G_{Ic} = 0.36 J/m^2.

For the loss of coating stability, inequalities (8) and (10) must be satisfied. Neglecting the second term in inequality (10), we obtain

$$\frac{\pi^2 h^2}{3\varepsilon_0} < L^2 < \frac{\pi^2 \varepsilon_0 E h^3}{3G_{Ic}}. \quad (12)$$

Double inequality (12) physically means that too short debondings do not lose stability, whereas too long debondings do not grow. This inequality can be satisfied only when the left-hand side of Eq. (12) is less than the right-hand side:

$$G_{Ic} < \varepsilon_0^2 E h. \quad (13)$$

Otherwise, inequality (12) cannot be satisfied for any length of the initial debonding. Inequality (13) provides the important conclusion that there is a critical coating thickness below which its debonding is impossible. The critical coating thickness for the carbon/glass composite is estimated as 30 nm.

Thus, in this study, we pioneered in measuring the debonding energy for a nanometer-thick film. The values obtained for fracture toughness are close to the energy of the breaking of atomic bonds. Consequently, the contribution of the plastic-strain energy of materials can be neglected and the debonding of a nanometer-thick coating differs fundamentally from the adhesion fracture of two plates of macroscopic sizes.

ACKNOWLEDGMENTS

This work was supported by the Russian Foundation for Basic Research (project no. 00-03-33151) and, in part, by the Krasnoyarsk Regional Science Foundation (project no. N10F089C).

REFERENCES

1. V. G. Myagkov, V. S. Zhigalov, and V. A. Seredkin, Dokl. Akad. Nauk **366**, 472 (1999) [Dokl. Phys. **44**, 334 (1999)].
2. G. R. Irwin, in *Handbuch der Physik*, Ed. by H. P. J. Wijn (Springer, Berlin, 1958; Mir, Moscow, 1972), Vol. 6, pp. 551–590.
3. A. A. Berlin, L. I. Manevich, N. S. Grineva, *et al.*, Dokl. Akad. Nauk SSSR **268**, 1426 (1983).
4. L. D. Landau and E. M. Lifshitz, *Theory of Elasticity* (Nauka, Moscow, 1965; Pergamon Press, Oxford, 1986, 3rd ed.).
5. V. V. Bolotin, Mekh. Kompoz. Mater., No. 2, 239 (1984).
6. J. R. Diefendorf, in *Carbon Fibres and Their Composites* (Springer, Berlin, 1985), pp. 46–61.
7. K. J. Fillips, in *Fracture. An Advanced Treatise*, Ed. by H. Liebowits (Academic, New York, 1968; Mir, Moscow, 1976), Vol. 7, Part 1.

Translated by V. Bukhanov

Doklady Physics, Vol. 47, No. 2, 2002, pp. 132–135. Translated from Doklady Akademii Nauk, Vol. 382, No. 4, 2002, pp. 478–481.

MECHANICS

On the Motion of a Body with a Rigid Shell and Variable Mass Geometry in a Perfect Fluid

Academician V. V. Kozlov and S. M. Ramodanov

Received August 28, 2001

1. MOTION OF A VARIABLE BODY

We consider the problem of a body with a rigid shell moving in an infinite volume of a homogeneous perfect fluid. The fluid motion and the fluid in itself are assumed, respectively to be nonrotational and quiescent at infinity. However, in contrast to the classical formulation of the problem on the body motion, we consider that the mass geometry of the body can vary under the action of internal forces according to a law known *a priory*. For example, a material point moves inside a case in accordance with a given law.

We assume that the body and the fluid were immobile at the initial time moment. It is of interest whether or not it is possible to displace the body's case from the given position to an arbitrary preassigned position by means of an appropriate variation of body-mass geometry (under the action of internal forces). At first glance, this seems to be impossible, because the center of mass for the body–fluid system is at rest. However, this argument cannot be taken into account. Firstly, the center of mass of an infinite volume of fluid is uncertain; secondly, we are interested only in the displacement of the body's case but not of the fluid.

We formulate our principal result for a body whose boundary has three mutually orthogonal planes of symmetry. It turns out that, if not all the associated masses of the body (depending only on the body shape) are equal, a driving force can be produced inside its case due to the displacements of points. Moreover, the body can be displaced from an arbitrary position to another arbitrary position in the case of an appropriate control of the mass geometry. We note that the property of the total body controllability is lost if all the associated masses coincide.

The problem under consideration is a particular case of a more general problem on the motion of a deformable body in a fluid, which is of a substantial importance in studying the mechanism of swimming fish and also the cavitation phenomenon. The first results in this field were obtained by Taylor [1] and Lighthill [2]. They considered motion in a viscous fluid. The body–fluid energy exchange takes place because of the vortex separation from sharp edges of the body and also due to an inertial action of the fluid onto the body. In [3], the model problem on dynamics of a deformable plate in a fluid was considered. The proper motion of the plate represents a running wave. An estimate of the effect of wave parameters on the value of a driving-force was made. A qualitative explanation of the mechanism for the motion of fish on the basis of a model of motion in a solid channel was given in [4].

In this connection, the question arises as to whether the motion of the body is possible at the expense of deforming its own boundary in a perfect fluid performing a nonrotational motion. The positive solution to this problem is given in [5]. A similar problem was also considered in [6]. The approach used in [5] was repeated in [7]. In [8], the possibility of producing a driving force was shown for the case when a variable plate of infinite length moves in a perfect nonrotational fluid. This problem was considered most rigorously in [9]. It is assumed that just as after the deformation (without the fluid), the center-of-mass position and that of the principal axes are invariable. The force and the moment acting from the fluid onto the body can be found using the generalized Lagally theorem [10].

In our study, we investigate a more complicated problem on the possibility of the gradual motion of a body with a rigid boundary in a perfect fluid without vortices.

2. THEOREM OF CONTROLLABILITY

Thus, we consider the motion of a body with three orthogonal planes of symmetry. Inside the body, a material point of mass m can move (under the action of internal forces). We relate to the body a mobile reference system $O\xi\eta\zeta$ so that the kinetic energy of the body–fluid system can be represented in the form

$$T' = \frac{(A\mathbf{v}, \mathbf{v})}{2} + \frac{(C\omega, \omega)}{2}.$$

Here, $\mathbf{v}$ is the velocity of the point O, ω is the angular velocity of the body with respect to the mobile axes,

Moscow State University,
Vorob'evy gory, Moscow, 119899 Russia

1028-3358/02/4702-0132$22.00

$A = \mathrm{diag}(a_1, a_2, a_3)$, and $C = \mathrm{diag}(c_1, c_2, c_3)$; all the constants a_k and c_k are positive.

The motion of the point with mass m is assigned by the certain known functions $\xi(t)$, $\eta(t)$, and $\zeta(t)$. The components of the absolute velocity of this point in the mobile axes $\xi\eta\zeta$ have the form

$$u_1 = v_1 + \dot{\xi} - \omega_3\eta + \omega_2\zeta,$$
$$u_2 = v_2 + \dot{\eta} + \omega_3\xi - \omega_1\zeta,$$
$$u_3 = v_3 + \dot{\zeta} + \omega_1\eta - \omega_2\xi.$$

Here, v_1, v_2, $v_3(\omega_1, \omega_2, \omega_3)$ are the components of the vector $v(\omega)$.

The total kinetic energy of a variable body is

$$T = T' + \frac{m(u_1^2 + u_2^2 + u_3^2)}{2}.$$

The theorems on the variation of the momentum and the angular momentum with respect to the mobile axes yield the generalized Kirchhoff equations

$$\left(\frac{\partial T}{\partial \omega}\right)^{\cdot} + \left[\omega, \frac{\partial T}{\partial \omega}\right] + \left[v, \frac{\partial T}{\partial v}\right] = 0,$$
$$\left(\frac{\partial T}{\partial v}\right)^{\cdot} + \left[\omega, \frac{\partial T}{\partial v}\right] = 0. \qquad (2.1)$$

According to [9], this type of equation also describes the motion of a body with a variable boundary. In [5–7], equations (2.1) were not used explicitly.

Equations (2.1) need to be supplemented by kinematic relations. Let θ, φ, and ψ be the Euler angles defining the orientation of a mobile trihedron $(\xi\eta\zeta)$ with respect to the immobile system (xyz). Let x, y, and z also be the coordinates of the point O. We now use the kinematic Euler formulas

$$(\dot{\theta}, \dot{\psi}, \dot{\varphi})^T = B(p, q, r)^T \qquad (2.2)$$

and the formulas for the passage from a mobile trihedron to the immobile one

$$(\dot{x}, \dot{y}, \dot{z})^T = D(v_1, v_2, v_3)^T. \qquad (2.3)$$

The expressions for the elements of matrices B and D (D is the orthogonal matrix) in terms of the Euler angles are well known (see, for example, [11]). Equations (2.1)–(2.3) represent the total set of equations of motion for the system under consideration.

We assume that the system begins to move from the quiescent state. In this case, the integrals of momentum and of the angular momentum take the form

$$\frac{\partial T}{\partial v} = \frac{\partial T}{\partial \omega} = 0.$$

By virtue of the positive definiteness of the form T', these equations can be solved with respect to v and ω. Substituting the obtained expressions into kinematic relationships (2.2) and (2.3), we arrive at

$$(\dot{x}, \dot{y}, \dot{z}, \dot{\theta}, \dot{\varphi}, \dot{\psi})^T = U\dot{\xi} + V\dot{\eta} + W\dot{\zeta}. \qquad (2.4)$$

The components of the six-dimensional vectors U, V, and W depend parametrically on the functions $\xi(t)$, $\eta(t)$, $\zeta(t)$, and the Euler angles, as well as on the coefficients of the form T'. Equations (2.4) represent a closed set of first-order differential equations on the $e(3)$ group of motions in three-dimensional space. The functions ξ, η, and ζ serve as controls. The position of a body is determined by six parameters $(x, y, z, \theta, \varphi, \psi) = z$, $z \in e(3)$.

Remark. The indicated reduction is an example of a more general construction for mechanical systems with a configuration space in the form of the Lie group and the left-invariant kinetic energy. If the motion proceeds without the action of external forces, the role of integrals for the momentum and for the angular momentum is played by the total set of Noether integrals [12].

The system under consideration is called completely controllable if, for an arbitrary $\varepsilon > 0$ and two arbitrary positions z_1 and z_2 of the body, it is possible to find the piecewise smooth functions $\xi(t)$, $\eta(t)$, and $\zeta(t)$ with $t_1 \le t \le t_2$ such that

$$|\xi(t)| \le \varepsilon, \quad |\eta(t)| \le \varepsilon, \quad |\zeta(t)| \le \varepsilon,$$
$$z(t_1) = z_1, \quad z(t_2) = z_2.$$

The time $t_2 - t_1$ of the motion substantially depends on the parameter ε.

Theorem. *The system is quite controllable if and only if not all the associated masses a_1, a_2, and a_3 are equal to each other.*

Indeed, x, y, and z are limited as functions of time if $a_1 = a_2 = a_3$. In turn, this fact follows from the immobility of the center of mass for the system of the body–fluid–point of the integral in equations (2.4):

$$(a + m)(x, y, z)^T + mD(\xi, \eta, \zeta)^T = \text{const}.$$

For proving the sufficiency, we introduce the widened nine-dimensional space M with the coordinates x, y, z, θ, φ, ψ, ξ, η, and ζ.

Equations (2.4) determine the distribution of three-dimensional tangential planes. We also introduce three independent admissible vector fields V_1, V_2, and V_3 with the components $(U, 1, 0, 0)$, $(V, 0, 1, 0)$, and $(W, 0, 0, 1)$, respectively. Following the Rashevskiĭ–Chow approach [13], we consider nine vector fields

$$V_1, V_2, V_3, [V_1, V_2], [V_1, V_3], [V_2, V_3],$$
$$[V_1, [V_1, V_2]], [V_3, [V_1, V_3]], [V_2, [V_2, V_3]], \qquad (2.5)$$

where $[\,,\,]$ is the Jacobi bracket. If $a_2 \ne a_3$, for small values of ξ, η, and ζ, these vectors turn out to be linearly independent at each point of $e(3)$.

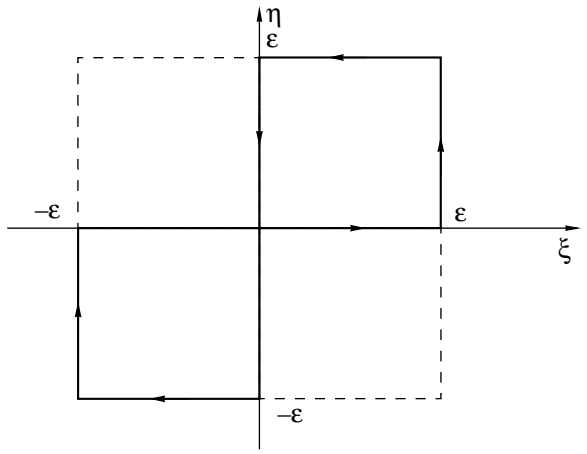

Figure.

Indeed, for $\xi = \eta = \zeta = 0$, the determinant of the matrix 9×9 composed of the components of vectors (2.5) is equal to

$$\frac{(-2a_3^2m - 3a_3^2a_2 + a_2^2m + 3a_3a_2^2 + a_3a_2m)P(a_1, a_2, a_3)}{Q(a_1, a_2, a_3)c_1^2c_2^2c_3^2\sin\theta}.$$

Here, $P(a_1, a_2, a_3)$ and $Q(a_1, a_2, a_3)$ are polynomials with positive coefficients. Since $a_k > 0$, this expression vanishes only for $a_2 = a_3$.

If commutators (2.5) are chosen in a somewhat different way, the independence condition $a_2 \neq a_3$ transforms into the condition $a_1 \neq a_2$, or $a_1 \neq a_3$.

It remains to utilize the Rashevskiĭ–Chow theorem, according to which two arbitrary points of the connected domain in M given by the inequalities $|\xi| \leq \varepsilon$, $|\eta| \leq \varepsilon$, and $|\zeta| \leq \varepsilon$ (ε is small) can be connected by the piecewise smooth curve composed of segments from the integral curvilinear fields V_1, V_2, and V_3.

3. THE GUARANTEED CONTROL

We indicate an explicit method of controlling the mass geometry of a body inside a rigid shell, which makes it possible to transfer the body with unequal associated masses from one position to another arbitrary position. For this purpose, we initially consider an auxiliary problem on a gradual plane-parallel body's motion, when one of the symmetry planes (for example, $\zeta = 0$) always remains invariable with time. The material point m also moves in this plane.

The group $e(2)$ serves as a configuration space; the generalized coordinates are x, y, i.e., the coordinates of the body's point O and the rotation angle φ. To simplify the calculation, we consider the limiting case as $a_1 \longrightarrow 0$, $a_2 \longrightarrow \infty$, and c_3 tends to a finite limit. The possibility of such a passage to the limit was substantiated in [14]. In this case, equations (2.4) take the following form:

$$\begin{aligned} &\dot{x} = v\cos\varphi, \quad \dot{y} = v\sin\varphi, \quad \dot{\varphi} = \omega, \\ &v = -\left(\dot{\xi} + \frac{\kappa\xi\eta\dot{\eta}}{1 + \kappa\xi^2}\right), \quad \omega = -\frac{\kappa\xi\dot{\eta}}{1 + \kappa\xi^2}, \end{aligned} \tag{3.1}$$

where $\kappa = \dfrac{m}{c_3}$.

Let the point m move with a constant (in its modulus) velocity along a closed curve shown in the figure. Using (3.1), we can calculate the increment of the coordinates for a period:

$$\begin{aligned} &\Delta x = 0, \quad \Delta y = -2\varepsilon\left(1 + \sin\mu - \frac{\sin\mu}{\mu}\right), \\ &\Delta\varphi = 0. \end{aligned} \tag{3.2}$$

Here, $\mu = \dfrac{\kappa\varepsilon^2}{1 + \kappa\varepsilon^2}$. For small $\varepsilon \neq 0$, it is evident that $\Delta y \neq 0$. Thus, on the average, the body is displaced forward by its wide side. By virtue of analyticity, this conclusion is also retained for almost all values of the parameters.

Remark. For the first two equations of set (3.1), we can see that motion of the body is subjected to a nonintegrable constraint $\dot{x}\sin\varphi - \dot{y}\cos\varphi = 0$. However, this motion proceeds not in accordance with laws of nonholonomic mechanics but according to the principles of vaconomic mechanics developed in [14].

Let the body occupy a given position at the time moment of t_1, and its center of mass coincide with the geometric center (the point O); in particular, let the material point m for $t = t_1$ be at the point $O_1 = O$. Using rotations of symmetric flywheels (gyrodines), the body can be turned around the point O_1 and guided to an arbitrary preassigned position. This problem is well studied from various standpoints. If $a_1 \neq a_2$, we turn the body in order for the plane of symmetry $\zeta = 0$ to involve a preassigned point O_2 at which the body's center must be at the time moment t_2.

We now use formulas (3.2) valid for the plane-parallel motion. It is clear that $\Delta y \longrightarrow 0$ (as ε^3) when $\varepsilon \longrightarrow 0$. Hence, selecting a small ε, it is possible to attain the situation when the spacing between the points O_1 and O_2 equals $n\Delta y$, where n is a certain integer. Thus, if the point m starting from the point O makes exactly n rotations along the eight-shaped curve shown in the figure, then the body's center occupies the position O_2. In this case, the point m turns out anew at the point O.

After this, it is necessary once more (for example, using symmetric flywheels) to turn the body around the point O_2 and to orient the body in a preassigned way.

ACKNOWLEDGMENTS

This work was supported by the Leading Science-School Program (project no. 00-15-96196) and by the Integration Program (project A-00-97).

REFERENCES

1. G. I. Taylor, Proc. R. Soc. London, Ser. A **214**, 158 (1952).
2. J. M. Lighthill, J. Fluid Mech. **9**, 305 (1960).
3. T. Y. Wu, J. Fluid Mech. **10**, 321 (1961).
4. M. A. Lavrent'ev and M. M. Lavrent'ev, Prikl. Mekh. Tekh. Fiz., No. 4, 3 (1962).
5. T. B. Benjamin and A. T. Ellis, Philos. Trans. R. Soc. London, Ser. A **260**, 221 (1966).
6. P. G. Saffman, J. Fluid Mech. **28**, 385 (1967).
7. O. V. Voinov and A. G. Petrov, Dokl. Akad. Nauk SSSR **212**, 1086 (1973) [Sov. Phys. Dokl. **18**, 634 (1973)].
8. V. M. Kuznetsov, B. A. Lugovtsov, and Y. N. Sher, Arch. Ration. Mech. Anal. **25**, 367 (1967).
9. A. Galper and T. Miloh, Proc. R. Soc. London A **442**, 273 (1993).
10. L. Landweber and T. Miloh, J. Fluid Mech. **96**, 33 (1980).
11. E. Whitteker, *A Treatise on the Analytical Dynamics of Particles and Rigid Bodies* (Cambridge Univ. Press, 1927; Otd. Nauchn. Tekh. Inform., Moscow, 1937).
12. V. V. Kozlov, *General Theory of Vortices* (Izdat. Dom Udmurt. Universitet, Izhevsk, 1998).
13. P. K. Rashevskiĭ, Uch. Zap. Mosk. Ped. Inst. im. K. Libknekhta, Ser. Fiz.-Mat. Nauk, No. 2, 83 (1938).
14. V. V. Kozlov, Vestnik Mosk. Gos. Univ. Ser. 1. Mat., Mekh., No. 3, 102 (1983).

Translated by V. Bukhanov

Doklady Physics, Vol. 47, No. 2, 2002, pp. 136–140. Translated from Doklady Akademii Nauk, Vol. 382, No. 4, 2002, pp. 482–487.

MECHANICS

On the Construction of Effective Constitutive Relations for Porous Elastic Materials Subjected to Finite Deformations Including the Case of Their Superposition

V. A. Levin* and K. M. Zingerman**

Presented by Academician V.P. Myasnikov June 22, 2001

Received July 5, 2001

This study deals with a new approach to the construction of effective constitutive relations for porous nonlinearly elastic materials subjected to finite deformations. The approach allows for superimposing the deformations when pores are formed after a preliminary loading. The effective constitutive relations based on this approach are shown to remain unchanged in the case of a superimposed rigid motion.

The construction of the effective constitutive relations is performed on the basis of well-known general principles [1, 2]. We isolate in a material a certain representative volume (for the two-dimensional case, this is a certain area) and, studying its mechanical behavior under loading, we can determine properties of the material as a whole. For this volume (area), the static problem of nonlinear elasticity is solved for a given stress at the boundary. Furthermore, deformations and stresses are averaged over the representative volume (area), and the effective constitutive relations are constructed as a dependence between averaged deformations and averaged stresses.

When solving problems on effective properties of inhomogeneous materials, a question arises: how to define an effective material in order that this definition would have both a clear physical meaning (for use in experiments) and a sufficiently simple mathematical representation. In addition, in the process of seeking average deformations of porous media, a problem arises associated with the fact that the deformations are not defined in the interior of pores (this is the difference between porous materials and those with elastic inclusions). In the case of small deformations, these issues are solved in a rather simple manner [1, 3, 4]. For example, the deformation tensor of an effective material is described by the relation

$$\mathbf{E}^{e} = \frac{1}{V}\int_{V}\mathbf{E}\,dV = \frac{1}{2V}\int_{V}(\nabla\mathbf{u} + \mathbf{u}\nabla)\,dV.$$

After using the Gauss–Ostrogradskiĭ formula, this relation is reduced to the form

$$\mathbf{E}^{e} = \frac{1}{2V}\int_{\Gamma}(\mathbf{nu} + \mathbf{un})\,d\Gamma,$$

where V is the representative volume and Γ is its boundary. Then, for porous materials, it is possible to formally find the average deformations inside pores [3] under the assumption that the pores are filled with a certain elastic material whose deformations are such that displacements of boundary points of this special material coincide with those for corresponding points of the matrix material at pore boundaries. At the same time, stresses are equal to zero (provided that the pressure inside the pores is absent). Such an approach makes it possible, without determining deformations inside the pores, to find their average value according to displacements of the pore boundary, which are calculated while solving the elastic problem.

For finite deformations, and especially in the case of their superposition, this approach cannot be directly applied, since any deformation tensor (e.g., the Green tensor or the Almansi tensor) exhibits a nonlinear behavior with respect to the displacement-vector gradient in the basis of the initial or final states [5]. Thus, when averaging, it is impossible to replace the integral over a volume by the surface integral using the Gauss–Ostrogradskiĭ formula. Therefore, for porous materials a certain difficulty arises; namely, the result of averaging for any deformation tensor over a representative volume depends on how this tensor is defined inside the pores, but this definition can be done even if we require the displacements at pore boundaries to be continuous.

Therefore, for finite deformations, the approach used in [3, 4] in the case of small deformations should be modified. For example, this can be done by the following way. We average the deformation gradient over

* *Moscow State University, Vorob'evy gory, Moscow, 119899 Russia*

** *Faculty of Applied Mathematics and Informatics, Tver State University, Sadovyĭ per. 35, Tver, 170000 Russia*

1028-3358/02/4702-0136$22.00

an undeformed representative volume (area) rather than the deformation tensor. Next, the deformation tensor of an effective material is determined with the help of the averaged gradient.

We consider the shape of pores to be given in an undeformed configuration in which V_0 is the representative volume. Let Γ_0 be its boundary and $\overset{0}{\mathbf{n}}$ be the normal to Γ_0 (we assume that hollows do not intersect or touch on Γ_0). We now use the following notation in the deformed configuration: V is the representative volume, Γ is its boundary, and $\mathbf{n}$ is the normal to Γ. We denote gradient operators in the initial and deformed configurations as $\overset{0}{\nabla}$ and ∇, respectively, $\boldsymbol{\Psi} = \mathbf{I} + \overset{0}{\nabla}\mathbf{u}$ is the deformation gradient, and $\mathbf{u}$ is the displacement vector.

In what follows, we used the elements of the averaging scheme considered in [1]. Let the following condition be set at the boundary of the deformed volume V:

$$\mathbf{n} \cdot \sigma|_\Gamma = \mathbf{n} \cdot \tilde{\sigma}|_\Gamma. \tag{1}$$

Here, σ is the true-stress tensor and $\tilde{\sigma}$ is the arbitrary constant (i.e., independent of coordinates) symmetric tensor.

Taking into account the linearity of the equilibrium equations $\nabla \cdot \sigma = 0$ and boundary conditions (1) with respect to the tensor σ, and following [1], we can show that, in the absence of mass forces and in the case when condition (1) is fulfilled, the true stresses averaged over the deformed volume are equal to $\tilde{\sigma}$.

In the undeformed configuration, the boundary condition corresponding to relation (1) can be written in the form

$$\overset{0}{\mathbf{n}} \cdot \overset{0}{\boldsymbol{\Sigma}}\Big|_{\Gamma_0} = (\det\boldsymbol{\Psi})\overset{0}{\mathbf{n}} \cdot \boldsymbol{\Psi}^{*-1} \cdot \tilde{\sigma} \cdot \boldsymbol{\Psi}^{-1}\Big|_{\Gamma_0}. \tag{2}$$

Here, $\overset{0}{\boldsymbol{\Sigma}} = (\det\boldsymbol{\Psi})\boldsymbol{\Psi}^{*-1} \cdot \sigma \cdot \boldsymbol{\Psi}^{-1}$ is the second Piola–Kirchhoff stress tensor [5].

We now give a definition of an effective material. Let the outer boundary of the representative material with a volume V_0, which is taken in the undeformed configuration of the original porous material, be subjected to a load in accordance with condition (2). By an effective (averaged) material, we imply a homogeneous material satisfying the following condition: before the deformation, we fill the volume V_0 (including pores) with this material and set the uniform stress state in it so that true stresses are equal to true stresses in the original material averaged over the deformed volume (which, taking into account the aforesaid, are equal to $\tilde{\sigma}$). In this case, the deformation gradient of the effective material becomes equal to the deformation gradient (averaged over the undeformed volume V_0) of the original material.

Furthermore, we use the superscript e to denote quantities corresponding to the effective material. According to the above definition, we can write:

$$\sigma^e = \tilde{\sigma} = \frac{1}{V}\int_V \sigma dV, \quad \boldsymbol{\Psi}^e = \frac{1}{V_0}\int_{V_0} \boldsymbol{\Psi} dV_0. \tag{3}$$

With the help of the Gauss–Ostrogradskiĭ formula, this equality can be transformed to the form

$$\boldsymbol{\Psi}^e = \frac{1}{V_0}\int_{V_0} (\mathbf{I} + \overset{0}{\nabla}\mathbf{u}) dV_0 = \mathbf{I} + \frac{1}{V_0}\int_{\Gamma_0} \overset{0}{\mathbf{n}}\mathbf{u} d\Gamma_0. \tag{4}$$

In previous studies [6–8], we gave another definition of the effective material. In a solid, we isolated a representative volume (area) in the form of a parallelepiped (in the two-dimensional case, a parallelogram). Then, the effective material was defined as a homogeneous material satisfying the following condition. If we fill the representative volume (area), including pores, with this material and apply to it the same load as to the original porous body, then the average displacements along faces of this volume (or sides of the representative area) should be the same. The definition given in this study is more general compared to those given in [6–8], since it imposes no constraints on the shape of the representative volume. In addition, when this volume (area) represents a parallelepiped (a parallelogram), the formulas for seeking $\boldsymbol{\Psi}^e$ turn out to be the same.

Using this definition, we now pass to the construction of constitutive relations for a porous elastic material. In a porous body (for the undeformed configuration), we take a representative volume V_0 and solve the boundary value problem of nonlinear elasticity for this volume under given condition (2) set at the boundary Γ_0. The solution to this problem makes it possible to find the displacement vector $\mathbf{u}$. Next, using formula (4), we determine the deformation gradient $\boldsymbol{\Psi}^e$ for the effective material. Hence, we find the Green deformation tensor $\overset{0}{\mathbf{E}}{}^e$ for the effective material

$$\overset{0}{\mathbf{E}}{}^e = \frac{1}{2}(\boldsymbol{\Psi}^e \cdot \boldsymbol{\Psi}^{e*} - \mathbf{I}) \tag{5}$$

and one of the stress tensors, e.g., the second Piola–Kirchhoff stress tensor for the effective material

$$\begin{aligned}\overset{0}{\boldsymbol{\Sigma}}{}^e &= (\det\boldsymbol{\Psi}^e)(\boldsymbol{\Psi}^e)^{*-1} \cdot \sigma^e \cdot (\boldsymbol{\Psi}^e)^{-1} \\ &= (\det\boldsymbol{\Psi}^e)(\boldsymbol{\Psi}^e)^{*-1} \cdot \tilde{\sigma} \cdot (\boldsymbol{\Psi}^e)^{-1}.\end{aligned} \tag{6}$$

Then, the effective constitutive relations are constructed in the form of a dependence between $\overset{0}{\boldsymbol{\Sigma}}{}^e$ and $\overset{0}{\mathbf{E}}{}^e$, for example, in the form $\overset{0}{\boldsymbol{\Sigma}}{}^e = \mathcal{F}(\overset{0}{\mathbf{E}}{}^e)$.

Using the formulas for the tensor transformation in the case of rigid motion [5], it is possible to show that

the tensors $\overset{0}{\mathbf{E}}{}^{e}$ and $\overset{0}{\mathbf{\Sigma}}{}^{e}$ evaluated with the help of the approach under consideration remain unchanged when the porous body together with the representative volume isolated inside it participates in a rigid motion after deformation (although these tensors are nonindifferent). Therefore, the dependences between them, i.e., the effective constitutive relations, also remain unchanged.

The approach under consideration to the construction of effective constitutive relations can be formally applied to arbitrarily large deformations. However, it is unclear whether this approach adequately describes the deformation of materials if the components of the tensor $\overset{0}{\nabla}\mathbf{u}$ considerably exceed unity in absolute value. For small deformations, this approach coincides with the generally accepted approach described, e.g., in [3, 4].

If the pore shape is set in the final state, it is appropriate to use another definition of the effective material; when the averaging is performed over a deformed representative volume, not for the deformation gradient but rather for its reciprocal tensor,

$$\mathbf{\Phi} = \mathbf{\Psi}^{-1} = \mathbf{I} - \nabla\mathbf{u}.$$

Let, in accordance with condition (1), a load be applied to the outer boundary of the representative volume V isolated in the deformed configuration of the original porous material. We imply as an effective material a homogeneous material satisfying the following condition. If after a deformation we fill the volume V, including pores, with this material and set in it a uniform stress state so that the true stresses are equal to those in the original material averaged over this volume (i.e., equal to $\tilde{\sigma}$) then the tensor reciprocal to the deformation gradient of the effective material would be equal to the tensor $\mathbf{\Phi}$ of the original material averaged over the deformed volume V.

According to this definition, we can write:

$$\mathbf{\Psi}^{e-1} = \frac{1}{V}\int_V \mathbf{\Phi}\,dV$$

$$= \frac{1}{V}\int_V (\mathbf{I} - \nabla\mathbf{u})\,dV = \mathbf{I} - \frac{1}{V}\int_\Gamma \mathbf{n}\mathbf{u}\,d\Gamma.$$

We now pass to the construction of effective constitutive relations for porous materials in which the pore formation occurs after preliminary loading. We use the terminology and notation usual for the theory of repeated superposition of large deformations [9]. We consider two schemes of constructing effective constitutive relations for preloaded porous materials.

1. A defect-free solid body is subjected to preloading. In the body, there appear initial (not small) deformations, and it passes to an intermediate state. In this state, the pores are formed (opened) in the body according to the model proposed in [9]. Because of the formation of the pores, additional finite deformations appear in the body that are superimposed onto initial ones. In addition, it is assumed that the average stresses in the body remain unchanged. No additional external loads are applied to the body either. Then, the effective constitutive relations are constructed as a dependence between the averaged total deformations and the averaged stresses caused by preloading.

2. A solid body is subjected to a preloading. As a result, initial deformations arise in it and then the opening of pores occurs. Next, additional external loads are applied to the body. Due to the formation of pores and the additional loading, there appear additional deformations in the body that are superimposed onto initial ones. The effective constitutive relations are constructed as a dependence either between the average additional deformations and average additional stresses or average total deformations and average total stresses. These relations parametrically depend on the initial stresses (or on the initial deformations).

Furthermore, we use the same approach to constructing the effective constitutive relations for both schemes. The initial deformation is considered to be affine. Let $\mathbf{\Psi}^e$ be the deformation gradient for the effective material; $\mathbf{\Psi}_{0,1}$ and $\mathbf{\Psi}_{1,2}$ are the initial and additional deformation gradients of the original material, respectively; $\mathbf{u}_2$ is the additional displacement vector for the original material; and $\sigma_{0,1}$ and $\sigma_{0,2}$ are, respectively, the initial and the total (for the final state) true-stress tensors. We isolate a representative volume V_0 in the initial state. We denote as V_1 and V_2, respectively, the volumes through which the volume V_0 passes after initial and total deformations. The boundaries of the representative volume in the initial, intermediate, and final states are denoted by Γ_0, Γ_1, and Γ_2, respectively; the normal to Γ_i is $\overset{i}{\mathbf{n}}$ ($i = 0, 1, 2$).

Let the following boundary condition be set in terms of the coordinates of the final state at the boundary Γ_2

$$\overset{2}{\mathbf{n}} \cdot \sigma_{0,2}\big|_{\Gamma_2} = \overset{2}{\mathbf{n}} \cdot \tilde{\sigma}|_{\Gamma_2}, \qquad (7)$$

where $\tilde{\sigma}$ is the constant symmetric tensor.

As in the case when superposition is absent, it is possible to show that, if condition (7) is fulfilled, the total true stress averaged over the volume V_2 is equal to $\tilde{\sigma}$.

In the coordinates of the intermediate state, the boundary condition corresponding to condition (7) can be written in the form

$$\overset{1}{\mathbf{n}} \cdot \overset{1}{\mathbf{\Sigma}}_{0,2}\big|_{\Gamma_1} = (\det\mathbf{\Psi}_{1,2})\overset{1}{\mathbf{n}} \cdot \mathbf{\Psi}^{*-1}_{1,2} \cdot \tilde{\sigma} \cdot \mathbf{\Psi}^{-1}_{1,2}\big|_{\Gamma_1}. \qquad (8)$$

We now give the definition of an effective material. We suppose that a representative volume V_0 taken in the original material before the deformation passes into the volume V_1 after the initial deformation. We also suppose that, in the material being contained in this vol-

ume, pores are formed according to the model developed in [9] and the loads are applied to its outer boundary in accordance with boundary condition (8). Then this volume passes into the volume V_2. In this case, we imply as an effective material a homogeneous material satisfying the following condition. Let us fill the volume V_0 with this material before deformation and set in it a uniform stress state so that the true stresses in this volume are equal to the true total stresses averaged over the volume V_2 in the original material (which, with allowance for the aforesaid, are equal to $\tilde{\sigma}$). Then, the deformation gradient of the effective material should be equal to the product of the initial-deformation gradient by the additional-deformation gradient of the original material, which is averaged over the volume V_1.

Thus, for preloaded materials, the deformation of an effective material is formally considered as a sequence of two deformation stages, the first stage of the deformation being assumed to coincide with the initial deformation of the original material.

According to the given definition, we can write:

$$\sigma^e = \tilde{\sigma} = \frac{1}{V_2}\int_{V_2} \sigma_{0,2}\,dV_2, \quad \boldsymbol{\Psi}^e = \boldsymbol{\Psi}_{0,1}\cdot\boldsymbol{\Psi}^e_{1,2},$$
$$\boldsymbol{\Psi}^e_{1,2} = \frac{1}{V_1}\int_{V_1} \boldsymbol{\Psi}_{1,2}\,dV_1. \tag{9}$$

We take into account in this equality that $\boldsymbol{\Psi}_{1,2} = \mathbf{I} + \overset{1}{\nabla}\mathbf{u}_2$ and apply the Gauss–Ostrogradskiĭ formula. Then we arrive at

$$\boldsymbol{\Psi}^e_{1,2} = \mathbf{I} + \frac{1}{V_1}\int_{\Gamma_1} \overset{1}{\mathbf{n}}\mathbf{u}_2\,d\Gamma_1. \tag{10}$$

An approach to constructing effective constitutive relations on the basis of the given definition mainly coincides with the aforesaid in the case when the superposition of the deformations is absent. Let the shape of pores be given at the moment of their formation. For the first turn, using the given initial stress $\sigma_{0,1}$, we determine the initial deformation gradient $\boldsymbol{\Psi}_{0,1}$. Next, we isolate a representative volume V_1 in the body and solve the boundary value problem of nonlinear elasticity for this volume under condition (8) set at its outer boundary Γ_1 and under conditions set at the pore boundaries. The solution to this problem, in particular, makes it possible to find the vector $\mathbf{u}_2$ of additional displacements. Furthermore, using formulas (9) and (10), we determine the deformation gradient $\boldsymbol{\Psi}^e$ of the effective material. Next, using formulas (5) and (6), we find the tensors $\overset{0}{\mathbf{E}}{}^e$ and $\overset{0}{\boldsymbol{\Sigma}}{}^e$. As a result, the effective constitutive relations are constructed in the form of a dependence between $\overset{0}{\boldsymbol{\Sigma}}{}^e$ and $\overset{0}{\mathbf{E}}{}^e$.

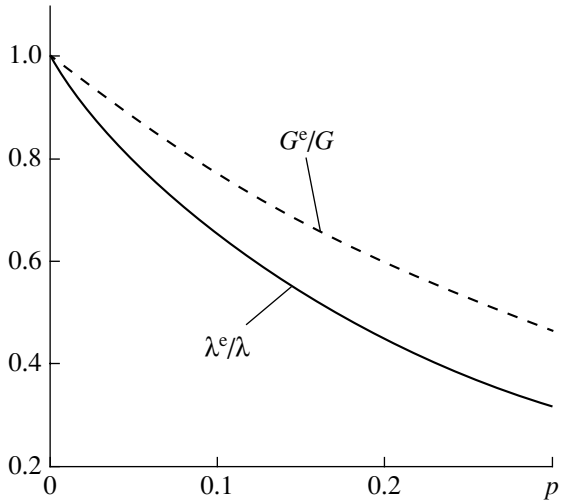

Fig. 1. Effective moduli λ^e and G^e as functions of porosity.

The calculations of effective moduli were performed for the two-dimensional case (plane deformation) when the mechanical properties of the matrix material are described by the Murnaghan potential [5]:

$$\overset{0}{\boldsymbol{\Sigma}} = \lambda(\overset{0}{\mathbf{E}} : \mathbf{I})\mathbf{I} + 2G\overset{0}{\mathbf{E}} + 3C_3(\overset{0}{\mathbf{E}} : \mathbf{I})^2\mathbf{I}$$
$$+ C_4(\overset{0}{\mathbf{E}}{}^2 : \mathbf{I})\mathbf{I} + 2C_4(\overset{0}{\mathbf{E}} : \mathbf{I})\overset{0}{\mathbf{E}} + 3C_5\overset{0}{\mathbf{E}}{}^2.$$

The problem of nonlinear elasticity was solved by the (Signorini) method of successive approximations [5, 6] within the accuracy to second-order effects. An approximate approach was applied to constructing effective constitutive relations on the basis of the method of successive approximations described in [6–8]. The application of the technique of averaging over an ensemble (which was considered in [8, 9]) made it possible to obtain the effective constitutive relations in the form:

$$\overset{0}{\boldsymbol{\Sigma}}{}^e = \lambda^e(\overset{0}{\mathbf{E}}{}^e : \mathbf{I})\mathbf{I} + 2G^e\overset{0}{\mathbf{E}}{}^e + 3C_3^e(\overset{0}{\mathbf{E}}{}^e : \mathbf{I})^2\mathbf{I}$$
$$+ C_4^e[(\overset{0}{\mathbf{E}}{}^e)^2 : \mathbf{I}]\mathbf{I} + 2C_6^e(\overset{0}{\mathbf{E}}{}^e : \mathbf{I})\overset{0}{\mathbf{E}}{}^e + 3C_5^e(\overset{0}{\mathbf{E}}{}^e)^2, \tag{11}$$

where λ^e and G^e are the effective first-order elasticity moduli and C_i^e ($i = 3, 4, 5, 6$) are the effective second-order moduli.

According to [6], in the case of plane deformation, one of the effective moduli C_i^e can be chosen arbitrarily. In calculations, we assumed that $C_4^e = C_4(1-p)^2$.

Since in this case the solution to the problem of nonlinear elasticity, which was obtained by the method of successive approximations (the solution is correct up to the terms of the second order of smallness), linearly depends on the material constants C_3, C_4, and C_5. The effective moduli evaluated with the help of the scheme

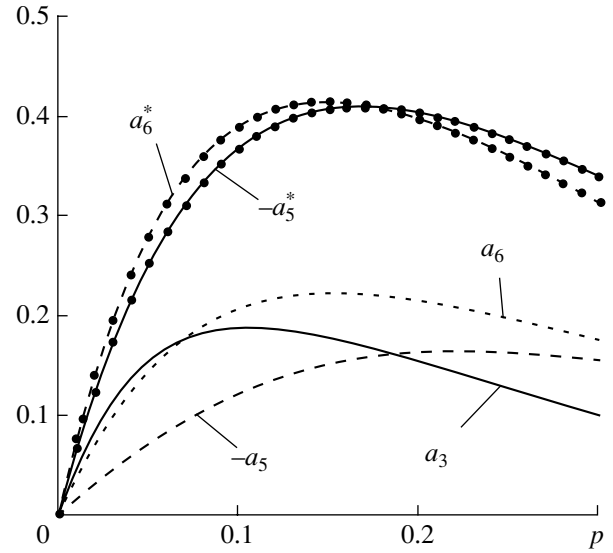

Fig. 2. Dependence of the coefficients a_i on porosity. For the case of pore formation in the loaded body, the coefficients are marked by asterisks.

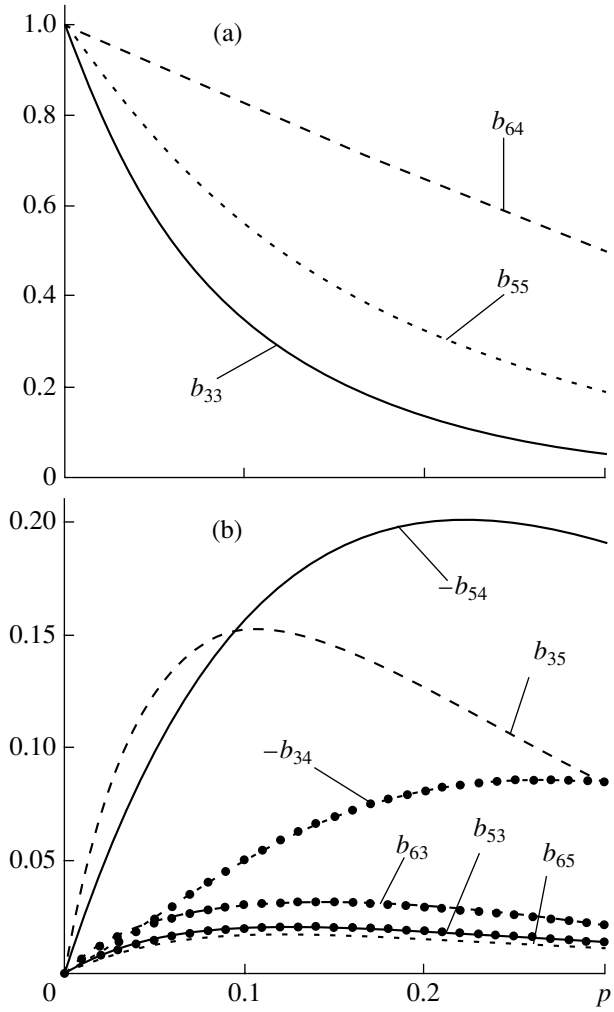

Fig. 3. Coefficients b_{ij} as functions of porosity.

described above also linearly depend on these constants; i.e.,

$$C_i^e = a_i + \sum_{j=3}^{5} b_{ij} C_j, \quad i = 3, 5, 6. \tag{12}$$

The calculations were performed for both the case when the pores are available in the unloaded body and the case when the formation of pores occurs after preloading (for scheme 1, i.e., when after the formation of pores, additional loads are not applied to the body). The calculations have demonstrated that the values of λ^e, G^e, and a_3 and of all coefficients b_{ij} for the case of the formation of pores in the loaded body are the same as in the absence of a superposition of deformations (when pores are available in the unloaded body) but the coefficients a_5 and a_6 are different for these two cases. Figures 1–3 show the dependences of the effective moduli λ^e and G^e and coefficients a_i and b_{ij} entering into formula (12) on the porosity factor p for the case $\frac{\lambda}{G} = 2$. For the case of the pore formation in the loaded body, the coefficients a_i are marked by asterisks.

ACKNOWLEDGMENTS

This work was supported by the Russian Foundation for Basic Research (project no. 98-01-00458), by the Ministry of Education of Russia, grant of the Competitive Center for Basic Natural Science for 1998–2000, and by the Program “Universities of Russia” (project no. 990858).

REFERENCES

1. B. E. Pobedrya, *Mechanics of Composite Materials* (Mosk. Gos. Univ., Moscow, 1984).
2. T. D. Shermergor, *Theory of Elasticity for Microinhomogeneous Media* (Nauka, Moscow, 1977).
3. A. S. Vavakin and R. L. Salganik, Izv. Akad. Nauk SSSR, Mekh. Tverd. Tela, No. 3, 65 (1975).
4. M. Kachanov, I. Tsukrov, and B. Shafiro, Appl. Mech. Revs. **47** (1), Pt. 2, 151 (1994).
5. A. I. Lur’e, *Nonlinear Elasticity Theory* (Nauka, Moscow, 1980).
6. V. A. Levin, V. V. Lokhin, and K. M. Zingerman, Izv. Ross. Akad. Nauk, Mekh. Tverd. Tela, No. 4, 45 (1997).
7. V. A. Levin, V. V. Lokhin, and K. M. Zingerman, Izv. Vyssh. Uchebn. Zaved. Severo-Kavkazskiĭ Region, Estestv. Nauki. 2000. Special issue: *Nonlinear Problems in Mechanics of Continuum*, 107 (2000).
8. V. A. Levin, V. V. Lokhin, and K. M. Zingerman, Trans. ASME, J. Appl. Mech. **67**, 667 (2000).
9. V. A. Levin, *Repeated Superposition of Large Strains in Elastic and Viscoelastic Bodies* (Nauka, Moscow, 1999).

Translated by Yu. Vishnyakov

Doklady Physics, Vol. 47, No. 2, 2002, pp. 141–144. Translated from Doklady Akademii Nauk, Vol. 382, No. 5, 2002, pp. 625–628.

MECHANICS

Solution to the Problem on Vibration of an Elastic Solid with Inner Cavities

Academician V. A. Babeshko*, R. Williams, A. V. Pavlova*, and S. V. Ratner***

Received October 23, 2001

We consider the vibration of an elastic solid containing plane parallel inhomogeneities. The inhomogeneities considered are cracks. Such objects were named vibration-strength viruses in [1–4]. Numerous problems in seismology, flaw detection, and the theories of acoustic emission and fracture involve consideration of the localization of a wave process by inner cracks–cavities. These problems are currently of great importance but are poorly studied in a rigorous mathematical sense.

In this study, we reveal the effect of spacing between cracks on the wave-process localization and further develop the approach described in [2, 3].

1. We consider an elastic medium containing L plane parallel horizontal inhomogeneities in the Cartesian coordinate system (x_1, x_2, x_3) at heights $h_1, h_2, \ldots$, and h_L; the lth crack occupies the domain Ω_l with interfaces S_l, $l = 1, 2, \ldots$, and L. For the sake of simplicity, we assume that all h_1 are different.

For a steady process with a frequency of ω, stresses with the amplitudes $\boldsymbol{\tau}_l = (\tau_{l1}, \tau_{l2}, \tau_{l3})$ act on the interfaces $x_3 = h_l$ of the cavities. Let $\mathbf{u}_l^{\pm} = (u_{l1}^{\pm}, u_{l2}^{\pm}, u_{l3}^{\pm})$ be the displacements in the sections $x_3 \longrightarrow \pm h_l$. Then, according to [1, 2], the boundary value problem for a layer is equivalent to the set of the integral equations

$$i\sum_{k=1}^{3}\sum_{m=1}^{3}\iint_{S_l}[\lambda\sigma^2 l_m + 2\mu\alpha_k n_k^l \alpha_m]u_{lm}(\xi_1, \xi_2, \xi_3)e^{i\langle\sigma\xi\rangle}ds \tag{1}$$

$$= \sum_{m=1}^{3}\left[\alpha_m\iint_{S_l}\tau_{lm}(\xi_1, \xi_2, \xi_3)e^{i\langle\sigma\xi\rangle}ds\right],$$

$$\alpha_3 = \pm\sqrt{\gamma_1^2 - \alpha^2}, \quad \alpha_3 = \pm\sqrt{\gamma_2^2 - \alpha^2},$$

$$\alpha^2 = \alpha_1^2 + \alpha_2^2;$$

$$i\mu\sum_{s=1}^{3}\sum_{m=1}^{3}\iint_{S_l}\{(\alpha_3 l_k - \alpha_k l_3)\alpha_m$$

$$+ \alpha_s n_s^l(\alpha_3\delta_{km} - \alpha_k\delta_{3m})\}u_{lm}(\xi_1, \xi_2, \xi_3)e^{i\langle\sigma\xi\rangle}ds \tag{2}$$

$$= \iint_{S_l}[\alpha_3\tau_{lk}(\xi_1, \xi_2, \xi_3) - \alpha_k\tau_{l3}(\xi_1, \xi_2, \xi_3)]e^{i\langle\alpha\xi\rangle}ds,$$

$$\alpha_3 = \pm\sqrt{\gamma_2^2 - \alpha^2}, \quad \sigma\xi = \alpha_1\xi_1 + \alpha_2\xi_2 + \alpha_3\xi_3,$$

$$k = 1, 2, \ldots$$

In both relationships, $l = 0, 1, 2, \ldots, L+1$; $-\infty \le \alpha_1, \alpha_2 \le \infty$, $n^l = (n_1^l, n_2^l, n_3^l)$ is the outer normal to the interface S_l; and λ and μ are the Lame parameters of the elastic medium, ρ is its density, $\gamma_1 = \dfrac{\omega}{v_1}$, $\gamma_2 = \dfrac{\omega}{v_2}$, $v_1 = \sqrt{\dfrac{\lambda + 2\mu}{\rho}}$, and $v_2 = \sqrt{\dfrac{\mu}{\rho}}$.

The relationships obtained represent the integral equations relating the stresses and displacements near a crack. For a layer with plane-parallel interfaces and plane cracks ($n_1^l = n_2^l = 0$, $n_3^l = \pm 1$), we obtain the following matrix representation of Eqs. (1), (2):

$$\mathbf{L}_l^{\pm}\mathbf{U}_l^{\pm} - \mathbf{L}_{l+1}^{\pm}\mathbf{U}_{l+1}^{\pm} = \mathbf{D}_l^{\pm}\mathbf{T}_l^{\pm} - \mathbf{D}_{l+1}^{\pm}\mathbf{T}_{l+1}^{\pm}. \tag{3}$$

Here,

$$U_{l,m}^{\pm}(\alpha_1, \alpha_2) = \int_{-\infty}^{\infty}\int_{-\infty}^{\infty}u_m^{\pm}(\xi_1, \xi_2, h_l)e^{i(\alpha_1\xi_1 + \alpha_2\xi_2)}d\xi_1 d\xi_2;$$

$$T_{l,m}(\alpha_1, \alpha_2) = \int_{-\infty}^{\infty}\int_{-\infty}^{\infty}\tau_m(\xi_1, \xi_2, h_l)e^{i(\alpha_1\xi_1 + \alpha_2\xi_2)}d\xi_1 d\xi_2,$$

$$m = 1, 2, 3;$$

$$\mathbf{U}_l^{\pm} = \{U_{l,m}^{\pm}\}, \quad \mathbf{T}_l^{+} = \mathbf{T}_l^{-}, \quad \mathbf{T}_l = \{T_{l,m}\};$$

* *Kuban State University, ul. Stavropol'skaya 149, Krasnodar, 350040 Russia*

** *University of Tennessee, Knoxville, Tennessee 37996-1410, USA*

1028-3358/02/4702-0141$22.00

$$\mathbf{L}_l^{\pm} = \begin{pmatrix} \pm\alpha_1\alpha_{31}e^{i\alpha_{31}h_l} & \pm\alpha_2\alpha_{31}e^{i\alpha_{31}h_l} & se^{i\alpha_{31}h_l} \\ \pm\alpha_2\alpha_{32}e^{i\alpha_{32}h_l} & \mp\alpha_1\alpha_{32}e^{i\alpha_{32}h_l} & 0 \\ (2s+\alpha_2^2)e^{i\alpha_{32}h_l} & -\alpha_1\alpha_2e^{i\alpha_{32}h_l} & \mp 2\alpha_1\alpha_{32}e^{i\alpha_{32}h_l} \end{pmatrix};$$

$$\mathbf{D}_l^{\pm} = \frac{i}{\mu}\begin{pmatrix} \frac{\alpha_1}{2}e^{\pm i\alpha_{31}h_l} & \frac{\alpha_2}{2}e^{\pm i\alpha_{31}h_l} & \frac{\pm\alpha_{31}}{2}e^{\pm i\alpha_{31}h_l} \\ \alpha_2e^{i\alpha_{32}h_l} & -\alpha_1e^{\pm i\alpha_{32}h_l} & 0 \\ \pm\alpha_{32}e^{\pm i\alpha_{32}h_l} & 0 & -\alpha_1e^{\pm i\alpha_{32}h_l} \end{pmatrix};$$

$$s = 0.5\gamma_2^2 - \alpha_1^2 - \alpha_2^2,$$

where the matrices $\mathbf{L}_l^+$, $\mathbf{D}_l^+$ and $\mathbf{L}_l^-$, $\mathbf{D}_l^-$ describe the reflection of waves propagating upwards and downwards in the layer, respectively.

The above relationships make it possible to construct the set of integral equations relating the edge displacements $\mathbf{u}_l^{\pm}$ and the stresses $\boldsymbol{\tau}_l$ in the section of the cracks for the space $-\infty \le z \le \infty$ ($-h_0$, $h_{N+1} \longrightarrow \infty$) with the plane cracks.

When a medium includes only one plane crack at a height of h_1, Eq. (3) takes the form

$$\mathbf{L}_1^+\mathbf{U}_1^+ = \mathbf{D}_1^+\mathbf{T}_1,$$
$$\mathbf{L}_1^-\mathbf{U}_1^- = \mathbf{D}_1^-\mathbf{T}_1^-.$$

where $\mathbf{U}_l^{\pm}$ and $\mathbf{T}_l$ are the Fourier transforms of the stresses $\boldsymbol{\tau}_l$ and displacements $\mathbf{u}_l^{\pm}$ at the upper and lower edges of the crack, respectively.

In this case, the jump $\mathbf{U}_1 = \mathbf{U}_1^+ - \mathbf{U}_1^-$ of the displacements is written as

$$\mathbf{U}_1 = \mathbf{M}\mathbf{T}_1,$$

where $(\mathbf{L}_1^+)^{-1}\mathbf{D}_1^+ - (\mathbf{L}_1^-)^{-1}\mathbf{D}_1^- = \mathbf{M}$,

$$\mathbf{M} = \frac{i}{\mu\alpha_{32}(\nu^2\alpha_{31}\alpha_{32} + s^2)}$$
$$\times\begin{pmatrix} \alpha_1^2\alpha_{32}^2 + 2\alpha_2^2\alpha_{31}\alpha_{32} + s(\alpha_{32}^2 - \alpha_2^2) & \alpha_1\alpha_2(\alpha_{32}^2 + s - 2\alpha_{31}\alpha_{32}) & 0 \\ \alpha_1\alpha_2(\alpha_{32}^2 + s - 2\alpha_{31}\alpha_{32}) & \alpha_2^2\alpha_{32}^2 + 2\alpha_1^2\alpha_{31}\alpha_{32} + s(\alpha_{32}^2 - \alpha_1^2) & 0 \\ 0 & 0 & 0.5\gamma_2\alpha_{31}\alpha_{32} \end{pmatrix}.$$

In turn, the stresses $\mathbf{T}_1$ can be expressed in terms of the jump of the displacements

$$\mathbf{T}_1 = \mathbf{M}^{-1}\mathbf{U}_1. \tag{4}$$

Thus, Eq. (4) expresses the dependence between the known integral characteristic of a stress on crack edges and the unknown integral characteristic of the jump of the displacements.

It is evident that the above relationships can be generalized to the case of an arbitrary number of cracks. For L cracks in the medium, we have

$$\begin{aligned} &\mathbf{U}_1 + \mathbf{A}_{12}^+\mathbf{U}_2 + \mathbf{A}_{13}^+\mathbf{U}_3 + \ldots + \mathbf{A}_{1L}^+\mathbf{U}_L = \mathbf{M}\mathbf{T}_1, \\ &\mathbf{A}_{12}^-\mathbf{U}_1 + \mathbf{U}_2 + \mathbf{A}_{23}^+\mathbf{U}_3 + \ldots + \mathbf{A}_{2L}^+\mathbf{U}_L = \mathbf{M}\mathbf{T}_2, \\ &\ldots \\ &\mathbf{A}_{1k}^-\mathbf{U}_1 + \ldots + \mathbf{U}_k + \ldots + \mathbf{A}_{kL}^+\mathbf{U}_L = \mathbf{M}\mathbf{T}_k, \\ &\ldots \\ &\mathbf{A}_{1L}^-\mathbf{U}_1 + \ldots + \mathbf{A}_{kL}^-\mathbf{U}_k + \ldots + \mathbf{U}_L = \mathbf{M}\mathbf{T}_L. \end{aligned} \tag{5}$$

Here,

$$\mathbf{T}_l = \mathbf{T}_l^+ = \mathbf{T}_l^-.$$

$$\mathbf{A}_{mk}^+ = (\mathbf{L}_m^+)^{-1}\mathbf{L}_k^+, \quad \mathbf{A}_{mk}^- = (\mathbf{L}_k^-)^{-1}\mathbf{L}_m^-, \quad m < k.$$

Equations (5) can be written in the matrix form

$$\begin{pmatrix} \mathbf{M}^{-1} & \mathbf{M}^{-1}\mathbf{A}_{12}^+ & \ldots & \mathbf{M}^{-1}\mathbf{A}_{1L}^+ \\ \mathbf{M}^{-1}\mathbf{A}_{12}^- & \mathbf{M}^{-1} & \ldots & \mathbf{M}^{-1}\mathbf{A}_{2L}^+ \\ \ldots & \ldots & \ldots & \ldots \\ \mathbf{M}^{-1}\mathbf{A}_{1k}^- & \ldots & \mathbf{M}^{-1}\mathbf{A}_{L-1L}^- & \mathbf{M}^{-1} \end{pmatrix}\begin{pmatrix} \mathbf{U}_1 \\ \mathbf{U}_2 \\ \vdots \\ \mathbf{U}_L \end{pmatrix} = \begin{pmatrix} \mathbf{T}_1 \\ \mathbf{T}_2 \\ \vdots \\ \mathbf{T}_L \end{pmatrix}. \tag{6}$$

Thus, the method used provides the set of integral equations in unknown jumps of displacements on the crack edges in the matrix form for an arbitrary number

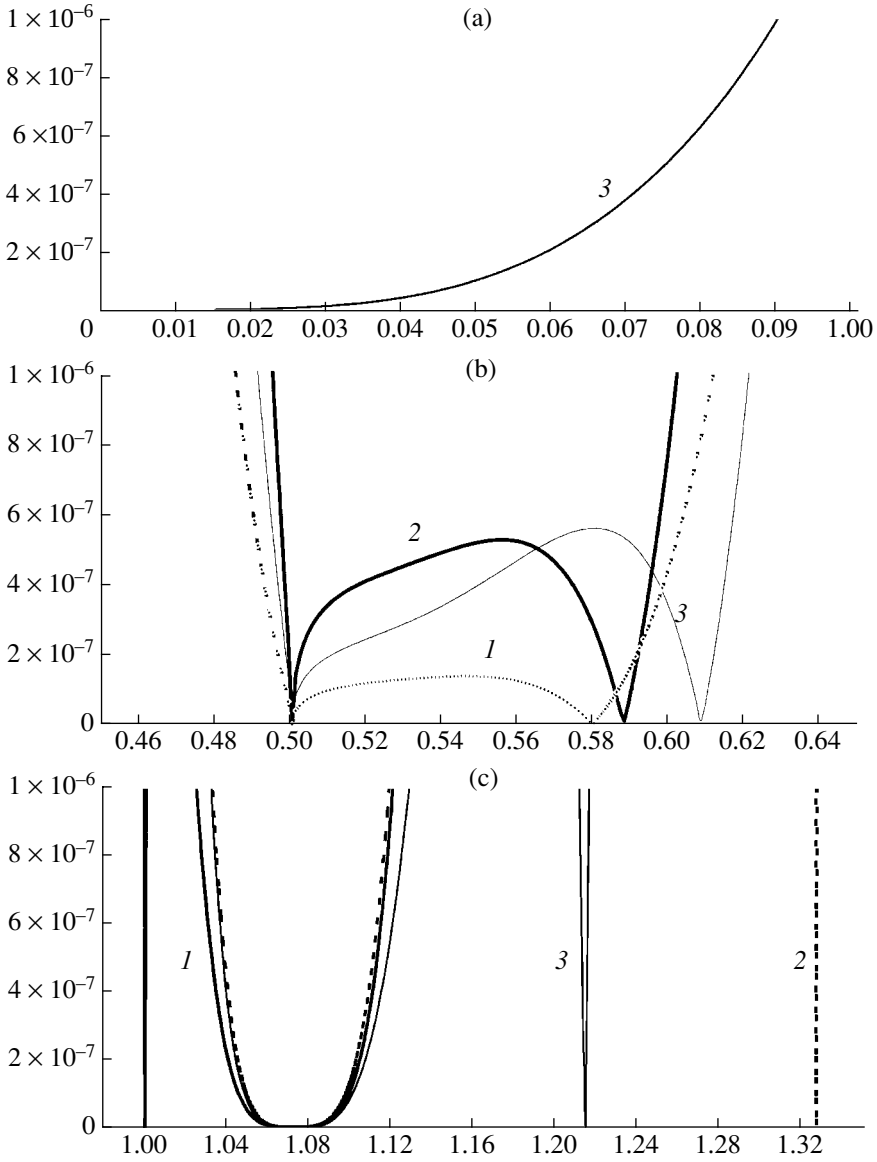

Fig. 1. Function of the determinant modulus for $L = 2$, $\varepsilon = 0.5$, $\gamma_2 h_{12} = (1) \frac{\pi}{3}$, $(2) \frac{2\pi}{3}$, $(3)\ \pi$, and $\beta \in$ (a) [0, 0.2], (b) [0.45, 0.65], (c) [0.96, 1.35].

of plane-parallel cavities called the vibration-strength virus $V(2/h_1; S_1/\ldots/h_L; S_L)$ [3, 4].

2. To solve the above set by the method discussed in [3, 4] and to determine the condition of the localization of the wave process by an aggregate of inhomogeneities, it is necessary to know the real singularities of the elements of the matrix appearing in Eq. (6). This matrix is a function of the kernel symbol for the conventional set of integral equations of the mixed problem. The properties of this set make it possible to use known algorithms for calculating the determinants of block matrices [5, 6]. The numerical investigation of the determinant shows that the number of its real zeros increases with the vertical spacing between cracks. When the spacing between cracks increases by half the length of the transverse wave in the medium, an additional real zero appears. Upon substituting dimensionless coordinates $\beta_{31} = \sqrt{\varepsilon^2 - \beta^2}$, $\beta_{32} = \sqrt{1 - \beta^2}$, $\beta = \frac{\alpha}{\gamma_2}$, and $\varepsilon = \frac{\gamma_1}{\gamma_2}$, these regularities are easily traced in the graphs of the determinant modulus in β as a function of the spacing between the cracks for the case of two cracks ($L = 2$) in the medium. Figure 1 shows the determinant modulus of the matrix of set (6) (the points of tangency with the real axis correspond to real zeros) when the cracks are spaced by $(1) \frac{\pi}{3}$, $(2) \frac{2\pi}{3}$, and $(3)\ \pi$. In this case, we take $\varepsilon = 0.5$.

Furthermore, the determinant of the matrix of the set has a repeated real zero $\beta^2\beta_{31}\beta_{32} + (0.5 - \beta^2)^2 = 0$ and the real branch points $\beta = \varepsilon, 1$.

For the antiplane two-crack problem, Eq. (6) takes the form

$$\begin{pmatrix} T_1 \\ T_2 \end{pmatrix} = \frac{-i\mu\alpha_{32}}{2}\begin{pmatrix} 1 & e^{i\alpha_{32}h} \\ e^{i\alpha_{32}h} & 1 \end{pmatrix}\begin{pmatrix} U_1 \\ U_2 \end{pmatrix},$$

$$\Delta(\alpha) = \frac{\mu^2\alpha_{32}^2}{4}(1 - e^{2i\alpha_{32}h}),$$

where $h = h_2 - h_1$ is the spacing between cracks. It is easy to understand that, after substitution of the dimensionless parameters

$$\Delta(\beta) = \frac{\mu^2\gamma_2^2}{4}(1 - \beta^2)\left(1 - e^{2i\sqrt{1-\beta^2}h_1}\right),$$

we have $h_1 = \gamma_2 h$ and the condition of appearing real zeros can be obtained analytically.

ACKNOWLEDGMENTS

This work was supported by the Russian Foundation for Basic Research (project no. 99-01-00787), r2000South (project nos. 00-01-96024, 00-01096019), the US Civilian Research and Development Foundation for the Independent States of the Former Soviet Union (project no. REC-004), and Integration (project no. A 0017).

REFERENCES

1. V. A. Babeshko, *Dynamics of Inhomogeneous Linear-Elastic Media* (Nauka, Moscow, 1989).
2. V. A. Babeshko, Izv. Vyssh. Uchebn. Zaved. Sev.-Kavk. Reg., Estest. Nauki, No. 3, 5 (2000).
3. V. A. Babeshko, Dokl. Akad. Nauk **373**, 191 (2000) [Dokl. Phys. **45**, 342 (2000)].
4. V. A. Babeshko, Izv. Akad. Nauk, Mekh. Tverd. Tela, No. 3, 5 (2000).
5. V. V. Voevodin, *The Computational Methods in Linear Algebra* (Nauka, Moscow, 1977).
6. F. R. Gantmacher, *Theory of Matrices* (Nauka, Moscow, 1988, 4th ed.; Chelsea, New York, 1959).

Translated by V. Bukhanov

Doklady Physics, Vol. 47, No. 2, 2002, pp. 145–147. Translated from Doklady Akademii Nauk, Vol. 382, No. 5, 2002, pp. 629–631.

MECHANICS

The Shear Correction Factor in the Geometrically Nonlinear Theory of Timoshenko Shells

Corresponding Member of the RAS É. I. Grigolyuk* and G. M. Kulikov**

Received October 15, 2001

The necessity of considering transverse shears in the problems of beam bending was first recognized by Timoshenko [1]. On the basis of the virtual work principle, the Timoshenko's theory was extended in [2] to the case of isotropic plates. In order to take into account a nonuniformity in the distribution of transverse shears over cross sections of a shell, the shear correction factor k is introduced in this theory. To date, this factor is usually taken to be equal to $k = \frac{5}{6}$ or $\frac{\pi^2}{12}$ [3]. In [4], it was shown that a value of $k = 1$ is more preferable when the procedure of recovering the transverse components of the stress tensor by integrating the equations of the three-dimensional elasticity theory is used in the linear theory of Timoshenko shells in the approach proposed in [2]. It was this choice that made it possible to construct the mathematically consistent and geometrically noncontradictory linear theory of Timoshenko shells. In this study, the results obtained in [4] are extended to anisotropic shells with finite deflection.

1. Let us consider a thin anisotropic shell of a constant thickness h. We assume that an elastic-symmetry surface parallel to the face surfaces S^- and S^+ exists at each point of the shell. As an initial surface S, we take a shell surface spaced from the face surfaces by δ^- and δ^+; i.e., $h = \delta^+ - \delta^-$. Let the initial surface be associated with the orthogonal curvilinear coordinates α_1 and α_2 measured along the lines of principal curvatures. The coordinate α_3 is measured in the direction of increasing the outer normal to the surface S (see figure).

The equilibrium equations of the elasticity theory for a thin shell, which has a finite deflection and whose face-surface metrics can be identified with the metric of the initial surface, have the form [5]

$$\begin{aligned}
&\frac{1}{A_i}\frac{\partial \sigma_{ii}}{\partial \alpha_i} + \frac{1}{A_j}\frac{\partial \sigma_{ij}}{\partial \alpha_j} + \frac{\partial \sigma_{i3}}{\partial \alpha_3} + B_i(\sigma_{ii} - \sigma_{jj}) \\
&\quad + 2B_j\sigma_{ij} + k_j\Sigma_{i3} = 0 \quad (i \neq j), \\
&\frac{1}{A_1}\frac{\partial \Sigma_{13}}{\partial \alpha_1} + \frac{1}{A_2}\frac{\partial \Sigma_{23}}{\partial \alpha_2} + \frac{\partial \sigma_{33}}{\partial \sigma_3} + B_1\Sigma_{13} \\
&\quad + B_2\Sigma_{23} - k_1\sigma_{11} - k_2\sigma_{22} = 0, \\
&\Sigma_{i3} = \sigma_{i3} + \Theta_1\sigma_{1i} + \Theta_2\sigma_{i2}, \\
&\Theta_i = \frac{1}{A_i}\frac{\partial u_3}{\partial \alpha_i} - k_i u_i, \quad B_i = \frac{1}{A_1 A_2}\frac{\partial A_j}{\partial \alpha_j},
\end{aligned} \tag{1}$$

where u_α are the displacements of the shell points, $\sigma_{\alpha\beta}$ are the stresses, A_i are the Lamé constants, and k_i are the curvatures of the coordinate lines. Hereafter, $i, j = 1, 2$ and $\alpha, \beta = 1, 2, 3$.

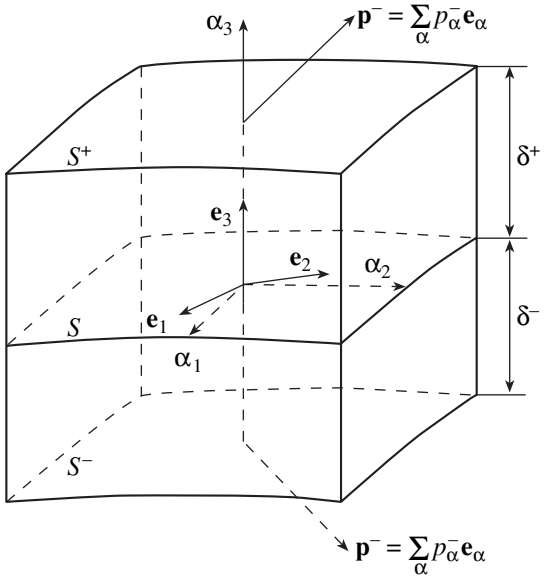

Shell element.

* *Moscow State Technical University (MAMI), Moscow, Russia*

** *Tambov State Technical University, Tambov, Russia*

1028-3358/02/4702-0145$22.00 © 2002 MAIK "Nauka/Interperiodica"

The relationships of the generalized Hooke's law can be written in the form [4]

$$\sigma_{ij} = \sum_{l \le m} b_{ijlm}\varepsilon_{lm}, \quad \sigma_{i3} = \sum_{l} b_{i3l3}\varepsilon_{l3}, \qquad i, j, l, m = 1, 2. \tag{2}$$

When constructing our theory, we used the modified Timoshenko hypothesis [4, 6] on the linear distribution of tangential displacements over the shell thickness:

$$u_i = N^-(\alpha_3)v_i^- + N^+(\alpha_3)v_i^+, \quad u_3 = v_3,$$
$$N^-(\alpha_3) = \frac{\delta^+ - \alpha_3}{h}, \quad N^+(\alpha_3) = \frac{\alpha_3 - \delta^-}{h}, \tag{3}$$

where $v_i^\pm(\alpha_1, \alpha_2)$ are the tangential displacements of the face surfaces $S^\pm$ and $v_3(\alpha_1, \alpha_2)$ is the transverse displacement of the surface S.

Introducing displacements (3) into the stress–strain relationship of the nonlinear theory of elasticity [5] for a thin finite-deflection shell and assuming that the transverse shear strains and tangential strains are distributed, respectively, uniformly and linearly over the shell thickness [7], we obtain

$$\varepsilon_{ij} = N^-(\alpha_3)E_{ij}^- + N^+(\alpha_3)E_{ij}^+, \quad \varepsilon_{i3} = E_{i3}, \quad \varepsilon_{33} = 0,$$
$$E_{ii}^\pm = \frac{1}{A_i}\frac{\partial v_j^\pm}{\partial\alpha_i} + B_j v_j^\pm + k_i v_3 + \frac{1}{2}(\theta_i^\pm)^2 \quad (i \ne j),$$
$$E_{12}^\pm = \frac{1}{A_1}\frac{\partial v_2^\pm}{\partial\alpha_1} + \frac{1}{A_2}\frac{\partial v_1^\pm}{\partial\alpha_2} - B_2 v_1^\pm - B_1 v_2^\pm + \theta_1^\pm\theta_2^\pm, \tag{4}$$
$$E_{i3} = \beta_i - \theta_i,$$
$$\beta_i = \frac{1}{h}(v_i^+ - v_i^-), \quad \theta_i^\pm = k_i v_1^\pm - \frac{1}{A_i}\frac{\partial v_3}{\partial\alpha_i},$$
$$\theta_i = \frac{1}{2}(\theta_i^- + \theta_i^+).$$

Multiplying the first two of the equilibrium Eqs. (1) by the functions of the shape $N^\pm(\alpha_3)$ and integrating the resulting equations along with the third equation with respect to the transverse coordinate from δ^- to δ^+ with allowance for the boundary conditions at the face surfaces $S^\pm$,

$$\sigma_{\alpha 3}(\delta^\pm) = p_\alpha^\pm, \tag{5}$$

we obtain the expressions consistent with the virtual work principle. Here, $p_\alpha^\pm$ are the components of the surface-load vectors $\mathbf{p}^\pm$ at the face surfaces $S^\pm$ (see figure). As a result, taking into account Eqs. (3) and (4), we arrive at the following nonlinear equilibrium equations for the shell with respect to the stress and moment resultants:

$$\frac{1}{A_i}\frac{\partial H_{ii}^\pm}{\partial\alpha_i} + \frac{1}{A_j}\frac{\partial H_{ij}^\pm}{\partial\alpha_j} + B_i(H_{ii}^\pm - H_{jj}^\pm) + 2B_j H_{ij}^\pm + k_i S_{i3}^\pm \mp \frac{1}{h}T_{i3} = \mp p_i^\pm \quad (i \ne j),$$
$$\frac{1}{A_1}\frac{\partial N_{13}}{\partial\alpha_1} + \frac{1}{A_2}\frac{\partial N_{23}}{\partial\alpha_2} + B_1 N_{13} + B_2 N_{23} - k_1 T_{11} - k_2 T_{22} = p_3^- - p_3^+, \tag{6}$$

where $T_{i\alpha}$, $H_{ij}^\pm$, H_{ij}^{pq}, N_{i3}, and $S_{i3}^\pm$ are the stress and generalized moment resultants determined by the formulas

$$N_{i3} = T_{i3} - \theta_1^- H_{1i}^- - \theta_1^+ H_{1i}^+ - \theta_2^- H_{i2}^- - \theta_2^+ H_{i2}^+,$$
$$S_{i3}^- = \frac{1}{2}T_{i3} - \theta_1^- H_{1i}^{00} - \theta_1^+ H_{1i}^{01} - \theta_2^- H_{i2}^{00} - \theta_2^+ H_{i2}^{01},$$
$$S_{i3}^+ = \frac{1}{2}T_{i3} - \theta_1^- H_{1i}^{01} - \theta_1^+ H_{1i}^{11} - \theta_2^- H_{i2}^{01} - \theta_2^+ H_{i2}^{11},$$
$$T_{i\alpha} = \int_{\delta^-}^{\delta^+}\sigma_{i\alpha}d\alpha_3, \quad H_{ij}^\pm = \int_{\delta^-}^{\delta^+}\sigma_{ij}N^\pm(\alpha_3)d\alpha_3, \tag{7}$$
$$H_{ij}^{pq} = \int_{\delta^-}^{\delta^+}\sigma_{ij}[N^-(\alpha_3)]^{2-p-q}[N^+(\alpha_3)]^{p+q}d\alpha_3, \qquad p, q = 0, 1.$$

The elasticity relationships for the stress and generalized moment resultants (7) with allowance for Eqs. (2) and (4) can be represented in the form

$$H_{ij}^{00} = \frac{1}{12}h\sum_{l \le m} b_{ijlm}(3E_{lm}^- + E_{lm}^+),$$
$$H_{ij}^{01} = \frac{1}{12}h\sum_{l \le m} b_{ijlm}(E_{lm}^- + E_{lm}^+),$$
$$H_{ij}^{11} = \frac{1}{12}h\sum_{l \le m} b_{ijlm}(E_{lm}^- + 3E_{lm}^+), \tag{8}$$
$$H_{ij}^- = H_{ij}^{00} + H_{ij}^{01}, \quad H_{ij}^+ = H_{ij}^{01} + H_{ij}^{11},$$
$$T_{ij} = H_{ij}^- + H_{ij}^+, \quad T_{i3} = h\sum_{l} k_{il}b_{i3l3}e_{l3},$$

where we take $k_{il} = 1$ for the shear correlation factors. Formula (8) for the transverse forces T_{i3} has simple meaning: the elasticity relationships for transverse shear stresses (2) in the theory of Timoshenko shells are

satisfied not pointwise but integrally over the shell thickness [6–8].

Integrating elasticity-theory Eqs. (1) with respect to the transverse coordinate from δ^- to α_3 with allowance for boundary conditions (5) at the face surface S^-, we arrive at the following formulas for the transverse components of the stress tensor:

$$\begin{aligned}\sigma_{i3} &= p_i^- - \frac{1}{A_i}\frac{\partial Q_{ii}}{\partial \alpha_i} - \frac{1}{A_j}\frac{\partial Q_{ij}}{\partial \alpha_j} - B_i(Q_{ii} - Q_{jj}) \\ &\quad - 2B_jQ_{ij} - k_iR_{i3} \quad (i \neq j), \\ \sigma_{33} &= p_3^- - \frac{1}{A_1}\frac{\partial R_{13}}{\partial \alpha_1} - \frac{1}{A_2}\frac{\partial R_{23}}{\partial \alpha_2} - B_1R_{13} \\ &\quad - B_2R_{23} + k_1Q_{11} + k_2Q_{22},\end{aligned} \tag{9}$$

where

$$\begin{aligned}R_{i3} &= Q_{i3} - \theta_1^-M_{1i}^- - \theta_1^+M_{1i}^+ - \theta_2^-M_{i2}^- - \theta_2^+M_{i2}^+, \\ Q_{i\alpha} &= \int_{\delta^-}^{\alpha_3}\sigma_{i\alpha}d\alpha_3, \quad M_{ij}^{\pm} = \int_{\delta^-}^{\alpha_3}\sigma_{ij}N^{\pm}(\alpha_3)d\alpha_3.\end{aligned} \tag{10}$$

In view of the equalities $Q_{i\alpha}(\delta^+) = T_{i\alpha}$, $M_{ij}^{\pm}(\delta^+) = H_{ij}^{\pm}$ and shell equilibrium equations (6), the boundary conditions (5) at the face surface S^+ result immediately from Eqs. (9).

2. Now, we discuss the question (that is of importance for the theory of Timoshenko shells) of whether or not the stress field, which is specified by Eqs. (2) and (9) and was found by solving the problem, satisfies equilibrium shell equations (6). The shell equilibrium equations (6) can be no longer exactly satisfied with the transverse forces T_{i3}^s evaluated on the basis of the refined transverse shear stress σ_{i3} determined by Eq. (9). The reason is that the transverse forces T_{i3} evaluated on the basis of Hooke's law (2), i.e., by Eq. (8), can generally differ from T_{i3}^s.

To solve this problem, we use the following formulas obtained from Eqs. (2), (4), (8), and (10):

$$\begin{aligned}&\int_{\delta^-}^{\delta^+}Q_{ij}d\alpha_3 = hH_{ij}^-, \quad \int_{\delta^-}^{\delta^+}Q_{i3}d\alpha_3 = \frac{1}{2}hT_{i3}, \\ &\int_{\delta^-}^{\delta^+}M_{ij}^-d\alpha_3 = hH_{ij}^{00}, \quad \int_{\delta^-}^{\delta^+}M_{ij}^+d\alpha_3 = hH_{ij}^{01}.\end{aligned}$$

With allowance for these formulas and Eqs. (9), we obtain

$$\begin{aligned}T_{i3}^s &= \int_{\delta^-}^{\delta^+}\sigma_{i3}d\alpha_3 = h\Big[p_i^- - \frac{1}{A_i}\frac{\partial H_{ii}^-}{\partial \alpha_j} - \frac{1}{A_j}\frac{\partial H_{ij}^-}{\partial \alpha_j} \\ &\quad - B_i(H_{ii}^- - H_{jj}^-) - 2B_jH_{ij}^- - k_iS_{i3}^-\Big] \quad (i \neq j).\end{aligned} \tag{11}$$

Taking the shell equilibrium equations (6) into account, we derive from Eq. (11) that $T_{i3}^s = T_{i3}$, as we wished prove.

Thus, on the basis of the physically clear supposition that the equations of Hooke's law (2) for transverse shear stresses are integrally satisfied, we succeeded in constructing the self-consistent geometrically nonlinear theory of Timoshenko shells. In this theory, the nonlinear shell equilibrium equations (6) and Eqs. (9) are satisfied together. For this reason, $k_{il} = 1$ was taken in Eq. (8) for the transverse forces. In conclusion, it must be emphasized that, from the standpoint of the approach developed in this study, efforts on constructing a geometrically nonlinear theory of Timoshenko shells on the basis of various ways of evaluating the shear correlation factors k_{il} will lead to a mathematically inconsistent and contradictory theory.

REFERENCES

1. S. P. Timoshenko, *The Course of Elasticity Theory*, Vol. 2: *Bars and Plates* (St. Petersburg, Kollins Printing House, 1916).
2. R. D. Mindlin, J. Appl. Mech. **18**, 31 (1951).
3. É. I. Grigolyuk and I. T. Selezov, in *Nonclassical Theories of Vibrations of Bars, Plates, and Shells: Mechanics of Deformable Solids* (VINITI, Moscow, 1973), Vol. 5.
4. É. I. Grigolyuk and G. M. Kulikov, Dokl. Akad. Nauk **381**, 47 (2001) [Dokl. Phys. **46**, 797 (2001)].
5. V. V. Novozhilov, *The Theory of Elasticity* (Sudpromgiz, Leningrad, 1958).
6. G. M. Kulikov, J. Eng. Mech. **127**, 119 (2001).
7. G. M. Kulikov and S. V. Plotnikova, Mekh. Kompoz. Mater. **35**, 347 (1999) [Mech. Compos. Mater. **35**, 241 (1999)].
8. É. I. Grigolyuk and G. M. Kulikov, *Multilayer Reinforced Shells: Analysis of Pneumatic Tires* (Mashinostroenie, Moscow, 1988).

Translated by Yu. Vishnyakov

Doklady Physics, Vol. 47, No. 2, 2002, pp. 148–152. Translated from Doklady Akademii Nauk, Vol. 382, No. 5, 2002, pp. 632–636.

MECHANICS

Effect of High-Frequency Vibration on the Onset of Convection in a Horizontal Fluid Layer

S. M. Zen'kovskaya and A. L. Shleykel'

Presented by Academician I.I. Vorovich August 1, 2001

Received August 15, 2001

INTRODUCTION

As is well known, the averaging method is efficient in investigating dynamical systems under the action of high-frequency vibration. This method allows motion to be separated into slow and rapid components, where the latter can be expressed in terms of the former. The slow component satisfies averaged equations that, being autonomous, contain vibration-caused forces arising as a result of the interaction of vibration fields. For parent systems dependent on a certain additional parameter λ [in problems of convection, it is presented by the Rayleigh (Ra) or Marangoni (Ma) numbers], it is of interest to study the effects of both the vibration character and the vibration amplitude on the critical value λ_*. If this value grows modulo, vibration is said to be of a stabilizing nature, otherwise, to be destabilizing.

It is quite noteworthy that vibration can stabilize and destabilize a given steady-state regime. In certain cases, even absolute stabilization (i.e., stability at an arbitrary value of λ) can be attained. These are diverse possibilities that lead to the necessity of investigating the vibrational stability and allow prediction of nontrivial effects that can be observed experimentally. The classical model of a pendulum with a vibrating suspension point, which was considered by Bogolyubov and Kapitza, can serve as a good guiding line in such investigations. Maintaining stability of the lower position, vertical vibrations can stabilize the unstable upper position. At the same time, the horizontal vibrations can destabilize even the lower pendulum position.

In the problem on thermal convection in a layer with rigid boundaries or with free undistorted boundaries, vibration affects it in a similar way. In particular, vertical vibrations turn out to be stabilizing [1, 2], horizontal vibrations are destabilizing, and oblique vibrations can either stabilize or destabilize relative equilibrium [3–5]. Some of these effects were verified experimentally in [6].

Rostov State University,
ul. Zorge 5, Rostov-on-Don, 344090 Russia

For convection occurring in a region with rigid boundaries, the averaging method is substantiated in [7, 8]. For mechanical systems with constraints imposed, this method is developed in [9], where a unified standpoint was presented for numerous vibration effects.

In the present paper, we investigate the effect of high-frequency translational vibration of the form $\frac{a}{\tilde{\omega}}\cos\tilde{\omega}t$, which occurs along the vector $\mathbf{s} = (\cos\varphi, 0, \sin\varphi)$, on the onset of two types of convection. We imply the Marangoni convection in a thin uniform fluid layer with a deformable free boundary and the Rayleigh–Benard convection in a nonuniform fluid layer bounded by rigid walls. The averaging method is applied to equations of convection, which is written in the Oberbeck–Boussinesq approximation. Conditions for the applicability of these equations are considered in [10]. It is characteristic that in a layer with a free boundary the vibration generates both mass forces and surface stresses. It is shown that the effect of vibration on the thermocapillary convection is determined by the single parameter $\mu_s = \frac{(\mathrm{Re}\sin\varphi)^2}{2}$, where the vibrational Reynolds number $\mathrm{Re} = \frac{ah}{\nu}$ and φ is the vibration angle. With increasing μ_s, the Marangoni numbers Ma grow and approach their values corresponding to an undistorted free boundary. Thermal gravitational convection in a layer bounded by rigid walls depends on two vibrational parameters: the dimensionless vibration velocity $r = \frac{a\sqrt{\chi\nu}}{\sqrt{2}gh^2}$ and the angle φ.

The critical Rayleigh number $\mathrm{Ra}_*(r, \varphi)$ is plotted in Figs. 1 and 2. It turns out that in the case of heating from below ($\mathrm{Ra} > 0$) the strong vibration ($r \gg 1$) destabilizes the equilibrium for any arbitrary angle φ except 90°. There exists a critical angle $\varphi_* \approx 52°$ such that at $0° \le \varphi \le \varphi_*$ the destabilization occurs at an arbitrary r. However, for small values of r when $\varphi_* < \varphi < 90°$, the

1028-3358/02/4702-0148$22.00

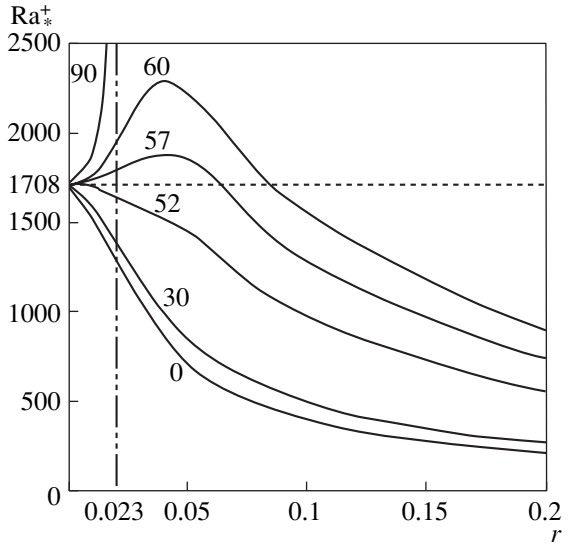

Fig. 1.

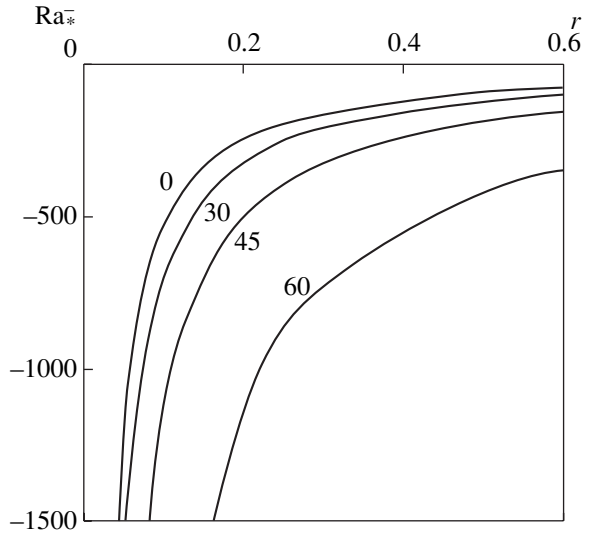

Fig. 2.

vibration stabilizes the equilibrium. In this case, there is a single optimal value $r_*(\varphi)$ such that the stabilizing effect of the vibration decreases and gradually becomes destabilizing at $r > r_*$. In the case of heating from above (Ra < 0, Fig. 2), the vibration destabilizes the relative equilibrium at an arbitrary angle $\varphi \neq 90°$. With increasing r, this destabilizing effect is intensified; i.e., $\mathrm{Ra} \longrightarrow 0$ as $r \longrightarrow \infty$.

FORMULATION OF THE PROBLEM

We consider an infinite horizontal layer of a viscous incompressible heat-conducting fluid with the density $\rho = \rho_0 (1 - \beta(T - T_0))$. From below ($x_3' = h$), the layer is bounded by a rigid wall, while its upper boundary can be either rigid or free. In the latter case, the boundary is considered as a deformable surface ($x_3' = \zeta'(x_1', x_2', t)$) with acting forces of surface tension, which are characterized by the coefficient $\sigma = \sigma_0 - \sigma_T(T - T_0)$, where $\sigma_T = \left|\frac{\partial\sigma}{\partial T}\right|$. Heat-exchange boundary conditions of the generalized form are specified at each boundary. It is assumed that the layer, as a whole, executes plane translational harmonic vibrations along the vector $\mathbf{s} = (\cos\varphi, 0, \sin\varphi)$ according to the law $\frac{a}{\tilde{\omega}}\cos\tilde{\omega}t$. The coordinate system is chosen in such a manner that the x_3-axis coincides with the direction of gravity force, the origin being situated on the unperturbed upper boundary.

Equations of convection written out in the Oberbeck–Boussinesq approximation in the coordinate system moving together with the vibrating layer are of the form

$$\frac{d\mathbf{v}'}{dt} = -\nabla p' + \Delta\mathbf{v}' + (1 - \varepsilon T')(\mathrm{Ga}\boldsymbol{\gamma} + \omega\mathrm{Re}\cos\omega t\mathbf{s}),$$
$$\mathrm{div}\mathbf{v}' = 0, \quad \frac{dT'}{dt} = \mathrm{Pr}^{-1}\Delta T', \quad \frac{d}{dt} = \frac{\partial}{\partial t} + \mathbf{v}'\nabla. \tag{1}$$

Boundary conditions specified at the free deformable boundary $x_3' = \zeta'(x_1', x_2', t)$ have the form

$$(\mathbf{v}', \mathbf{l}') = \frac{\partial\zeta'}{\partial t}, \quad \mathbf{l}' = \left(-\frac{\partial\zeta'}{\partial x_1}, -\frac{\partial\zeta'}{\partial x_2}, 1\right), \quad \mathbf{n} = \frac{\mathbf{l}'}{|\mathbf{l}'|},$$
$$\tau_{ik}'n_k' - p'n_i = -2\left(C - \frac{\mathrm{Ma}}{\mathrm{Pr}}T'\right)Kn_i + \frac{\mathrm{Ma}}{\mathrm{Pr}}\frac{\partial T'}{\partial x_i}, \tag{2}$$
$$i = 1, 2;$$

$$\tau_{3k}'n_k' - p' = -2\left(C - \frac{\mathrm{Ma}}{\mathrm{Pr}}T'\right)K, \quad \tau_{ik}' = \frac{\partial v_i'}{\partial x_k} + \frac{\partial v_k'}{\partial x_i}, \tag{3}$$

$$2K = \nabla_2\left(\frac{\nabla_2\zeta'}{\sqrt{1 + |\nabla_2\zeta'|^2}}\right), \quad \nabla_2 = \left(\frac{\partial}{\partial x_1}, \frac{\partial}{\partial x_2}\right);$$
$$\frac{\partial T'}{\partial n} - \mathrm{Bi}T' = \delta_1. \tag{4}$$

At the rigid wall, $x_3' = 1$, the boundary conditions are specified as

$$\mathbf{v}' = 0, \quad \frac{\partial T'}{\partial x_3} + B_0T' = \delta_2. \tag{5}$$

Problem (1)–(5) contains the following dimensionless parameters, namely, the vibration frequency $\omega =$

$\frac{\tilde{\omega}h^2}{\nu}$, the vibrational Reynolds number $\mathrm{Re} = \frac{ah}{\nu}$, the Boussinesq parameter $\varepsilon = Ah\beta$ (A is the characteristic temperature gradient), the Galilei number $\mathrm{Ga} = \frac{gh^3}{\nu^2}$, the Prandtl number $\mathrm{Pr} = \frac{\nu}{\chi}$, the Marangoni number $\mathrm{Ma} = \frac{A\sigma_T h^2}{\rho_0 \chi \nu}$, the surface-tension coefficient $C = \frac{\sigma_0 h}{\rho_0 \nu^2}$, and the heat-transfer parameters $\mathrm{Bi} = \frac{b_1 h}{k_1}$ and $B_0 = \frac{b_2 h}{k_2}$.

AVERAGING

Furthermore, we assume that the frequency ω is high and the vibrational Reynolds number is finite; i.e., $\omega \longrightarrow \infty$ and $\mathrm{Re} = O(1)$. Similar to [1, 3], we apply the Van der Pol–Krylov–Bogolyubov averaging method to problem (1)–(5). Along with the slow time t, we introduce the rapid time $\tau = \omega t$ and present the unknowns as sums of smooth components and fast components that have zero average (over τ) values:

$$\begin{aligned} \mathbf{v}' &= \mathbf{v}(x, t) + \tilde{\mathbf{v}}(x, t, \tau), \\ p' &= p(x, t) + \omega\tilde{p}(x, t, \tau), \\ T' &= T(x, t) + \frac{1}{\omega}\tilde{T}(x, t, \tau), \\ \zeta' &= \zeta(x_1, x_2, t) + \frac{1}{\omega}\tilde{\zeta}(x_1, x_2, t, \tau). \end{aligned} \tag{6}$$

After selecting principal vibrational terms, substituting relations (6) into the system of equations (1) as $\omega \longrightarrow \infty$ yields the system

$$\begin{aligned} \frac{\partial\tilde{\mathbf{v}}}{\partial\tau} &= -\nabla\tilde{p} + (1 - \varepsilon T)\mathrm{Re}\cos\tau \cdot \mathbf{s}, \\ \mathrm{div}\tilde{\mathbf{v}} &= 0, \quad \frac{\partial\tilde{T}}{\partial\tau} + (\tilde{\mathbf{v}}, \nabla T) = 0. \end{aligned} \tag{7}$$

Conserving the principal terms with respect to ω in relations (2) and (3), we arrive at the following conditions at the free boundary:

$$\begin{aligned} x_3 &= \zeta(x_1, x_2, t): \ \frac{\partial\tilde{\zeta}}{\partial\tau} = (\mathbf{l}, \tilde{\mathbf{v}}), \\ \mathbf{l} &= \left(-\frac{\partial\zeta}{\partial x_1}, -\frac{\partial\zeta}{\partial x_2}, 1\right), \quad \tilde{p} = 0. \end{aligned} \tag{8}$$

At the rigid wall $x_3 = 1$, there remains only one boundary condition $\tilde{v}_n = 0$.

Problem (7), (8) has the solution

$$\begin{aligned} \tilde{\mathbf{v}} &= \mathrm{Re}\mathbf{w}(x, t)\sin\tau, \quad \tilde{p} = \mathrm{Re}\Phi(x, t)\cos\tau, \\ \tilde{T} &= \mathrm{Re}(\mathbf{w}, \nabla T)\cos\tau, \quad \tilde{\zeta} = -\mathrm{Re}(\mathbf{w}, \mathbf{l})\cos\tau, \end{aligned} \tag{9}$$

which is 2π-periodic in τ, where $\mathbf{w}(x, t)$ and $\Phi(x, t)$ are the amplitudes of pulsatory velocity and of pulsatory pressure, respectively. These amplitudes satisfy the equations

$$\begin{aligned} \mathbf{w} &= -\nabla\Phi + (1 - \varepsilon T)\mathbf{s}, \quad \mathrm{div}\mathbf{w} = 0, \\ \Phi|_{x_3 = \zeta(x_1, x_2, t)} &= 0, \quad w_n|_{x_3 = 1} = 0. \end{aligned} \tag{10}$$

Substituting relations (9) into formulas (6) and, then, the latter into system (1)–(5), averaging the result over τ, and retaining the terms on the order of $O(1)$ as $\omega \longrightarrow \infty$ in the equations derived, we obtain the following autonomous system for average values of the unknowns:

$$\begin{aligned} \frac{d\mathbf{v}}{dt} &= -\nabla q + \Delta\mathbf{v} - \mathrm{Ga}\varepsilon T\gamma + \frac{\mathrm{Re}^2}{2}(\mathbf{w}, \nabla)\nabla\Phi, \\ \mathrm{div}\mathbf{v} &= 0; \\ \frac{dT}{dt} &= \mathrm{Pr}^{-1}\Delta T, \quad \mathbf{w} = -\nabla\Phi + (1 - \varepsilon T)\mathbf{s}, \\ \mathrm{div}\mathbf{w} &= 0. \end{aligned} \tag{11}$$

At the averaged free boundary, $x_3 = \zeta(x_1, x_2, t)$, the boundary conditions take the form

$$\begin{aligned} (\mathbf{v}, \mathbf{l}) &= \frac{\partial\zeta}{\partial t}, \quad \mathbf{l} = \left(-\frac{\partial\zeta}{\partial x_1}, -\frac{\partial\zeta}{\partial x_2}, 1\right), \\ \tau_{ik}n_k - &\left(q + \mathrm{Ga}\zeta - \frac{\mathrm{Re}^2}{2}\frac{\partial\Phi}{\partial x_3}(\mathbf{w}, \mathbf{l})\right)n_i \\ &= -2\left(C - \frac{\mathrm{Ma}}{\mathrm{Pr}}T\right)Kn_i + \frac{\mathrm{Ma}}{\mathrm{Pr}}\frac{\partial T}{\partial x_i}, \quad i = 1, 2; \\ \tau_{3k}n_k - &\left(q + \mathrm{Ga}\zeta - \frac{\mathrm{Re}^2}{2}\frac{\partial\Phi}{\partial x_3}(\mathbf{w}, \mathbf{l})\right) = -2\left(C - \frac{\mathrm{Ma}}{\mathrm{Pr}}T\right)K, \\ 2K &= \nabla_2\left(\frac{\nabla_2\zeta}{\sqrt{1 + |\nabla_2\zeta|^2}}\right), \quad \frac{\partial T}{\partial n} - \mathrm{Bi}T = \delta_1, \quad \Phi = 0. \end{aligned} \tag{12}$$

At the rigid wall, $x_3 = 1$, boundary conditions are

$$\mathbf{v} = 0, \quad \frac{\partial T}{\partial x_3} + B_0 T = \delta_2, \quad w_3 = 0. \tag{13}$$

Thus, as a result of the nonlinear interaction of the vibration fields, there appears a vibration-caused force in the averaged equations of motion and vibration-caused stresses in the dynamic boundary condition, where both quantities vary as the square of the vibrational Reynolds number.

Furthermore, Eqs. (11)–(13) are used to consider thermocapillary convection in a thin layer of a uniform

fluid and thermal vibrational convection in a layer bounded by rigid walls.

THERMOCAPILLARY MARANGONI CONVECTION

Under the assumption that $\varepsilon = 0$ in (11), the vibration-caused force

$$F_v = \frac{\mathrm{Re}^2}{2}(\mathbf{w}, \nabla)\nabla\Phi = \left(-\frac{\mathrm{Re}^2}{4}\right)\nabla w^2$$

is potential and can be included into the pressure term. Thus, vibration effects occur only provided that the free surface is, on the average, deformable.

We assume that $\delta_1 B_0 + \delta_2 \mathrm{Bi} = B_0(1 + \mathrm{Bi}) + \mathrm{Bi} \neq 0$ if $\mathrm{Bi}^2 + B_0^2 \neq 0$ and $\delta_1 = \delta_2 = 1$ at $\mathrm{Bi} = B_0 = 0$. Then, problem (11)–(13) has the equilibrium solution $\mathbf{v}_0 = 0$, $T_0 = z$, $q_0 = \frac{\mathrm{Re}^2}{4}\cos^2\varphi$, $\mathbf{w}_0 = (\cos\varphi, 0, 0)$, $\Phi_0 = x_3 \sin\varphi$, and $\zeta_0 = 0$. While analyzing the stability of the solution, we derive the following system for the amplitudes $v(z)$ and $\theta(z)$ of δ-components for normal perturbations proportional to $\exp(\lambda t + i\alpha_1 x_1 + i\alpha_2 x_2)$:

$$\lambda L v = L^2 v, \quad \lambda \mathrm{Pr}\theta = L\theta - v; \tag{14}$$

$$x_3 = 0: \; v = \lambda \mathrm{Pr}\delta, \quad D^2 v + \alpha^2 v = \mathrm{Ma}\alpha^2(\theta + \delta), \tag{15}$$

$$D\theta - \mathrm{Bi}(\theta + \delta) = 0;$$

$$(3\alpha^2 + \lambda)Dv - D^3 v = \mathrm{Pr}\alpha^2(C\alpha^2 + \mathrm{Ga} + \mu_s \alpha \tanh\alpha)\delta; \tag{16}$$

$$x_3 = 1: \; v = Dv = 0, \quad D\theta + B_0\theta = 0. \tag{17}$$

Here, $D = \frac{d}{dz}$, $\alpha^2 = \alpha_1^2 + \alpha_2^2$, $L = D^2 - \alpha^2$, and $\mu_s = \frac{(\mathrm{Re}\sin\varphi)^2}{2}$ is the vibrational Galilei number. The presented expression for the parameter μ_s shows that horizontal ($\varphi = 0$) high-frequency vibrations do not affect (in the limit $\omega \longrightarrow \infty$) the onset of the thermocapillary convection in a thin layer of a uniform fluid. Moreover, the vibration increases the effective surface tension

$$C_s = C + \frac{\mathrm{Ga}}{\alpha^2} + \frac{\mu_s \alpha \tanh\alpha}{\alpha^2}.$$

For example, $C = 7 \times 10^4$, $\mathrm{Ga} = 0.98 \times 10^4$, and $\mu_s = 0.5 \times 10^4 \sin^2\varphi$ for a water layer with $h = 1$ mm, $\nu = 0.01$ cm^2/s if $\tilde{\omega} = 100$ Hz and $a/\tilde{\omega} = 1$ mm. Additional terms (gravitational and vibrational) also depend on the wave number α. They can be noticeable already at $\alpha \sim 1$ and even principal at small α.

We can assume that at $\alpha \neq 0$ critical values of the Marangoni number grow modulo with increasing μ_s and tend to the values corresponding to the undistorted free boundary. Then, the strongest stabilizing effect is attained for vertical vibrations. Calculation results and asymptotic formulas corresponding to $\alpha \longrightarrow 0$ [11] confirm this assumption. Monotone ($\lambda = 0$) and oscillatory ($\lambda = ic$) instabilities existing at $\alpha \gg 1$ [$\mathrm{Ma}(\alpha) > 0$] and $\alpha \ll 1$ [$\mathrm{Ma}(\alpha) < 0$] have been studied numerically.

THERMAL VIBRATIONAL CONVECTION IN A HORIZONTAL LAYER BOUNDED BY RIGID WALLS

We assume that the fluid is nonuniform ($\varepsilon \neq 0$) and the layer boundaries ($z = 0$ and h) represent rigid isothermal walls with given temperatures T_1 and T_2, respectively. Then, heating from below corresponds to the condition $A = \frac{T_2 - T_1}{h} > 0$. The averaged equations can be written as

$$\frac{d\mathbf{u}}{dt} = -\nabla q + \Delta\mathbf{u} - \mathrm{Gr}T\boldsymbol{\gamma} + \mathrm{Gv}(\mathbf{w}, \nabla)\nabla\tilde{\Phi},$$

$$\mathrm{div}\mathbf{u} = 0,$$

$$\frac{dT}{dt} = \mathrm{Pr}^{-1}\Delta T, \quad \mathbf{w} = -\nabla\tilde{\Phi} - T\mathbf{s}, \quad \mathrm{div}\mathbf{w} = 0, \tag{18}$$

$$z = 0; 1: \; \mathbf{u} = 0, \quad T = z, \quad w_3 = 0.$$

Here, $\mathrm{Gr} = \mathrm{Ga} \times \varepsilon$ is the gravitational Grashof number and $\mathrm{Gv} = \frac{(\mathrm{Re}\varepsilon)^2}{2}$ is the vibrational Grashof number [1]. This system has the following equilibrium solution:

$$\mathbf{v}_0 = 0, \quad T_0 = z, \quad q_0 = -\frac{\mathrm{Gr}z^2}{2} + \mathrm{const},$$

$$w_0 = (-z\cos\varphi, 0, 0), \quad \tilde{\Phi}_0 = -\frac{z^2}{2}\sin\varphi + \mathrm{const}.$$

The corresponding spectral problem for amplitudes of normal perturbations (in the form described in the preceding section) can be reduced to the system

$$\lambda L u = L^2 u + \mathrm{Ra}\alpha^2\theta$$

$$+ \mu(\alpha^2\cos^2\varphi\theta + \alpha^2\sin\varphi w + i\alpha\cos\varphi Dw),$$

$$\lambda\mathrm{Pr}\theta = L^2\theta - u, \quad D = \frac{d}{dz}, \quad L \equiv D^2 - \alpha^2, \tag{19}$$

$$Lw = \alpha^2\sin\varphi\theta + i\alpha\cos\varphi D\theta,$$

$$z = 0; 1: \; u = Du = \theta = w = 0.$$

Here, $\mathrm{Ra} = \mathrm{GrPr}$ and $\mu = \mathrm{GvPr}$ represent the gravitational and vibrational Rayleigh numbers, respectively.

They are related by the equality $\mu = \mathrm{Ra}^2 r^2$, where the parameter $r^2 = \dfrac{a^2 \chi \nu}{2g^2 h^4}$ characterizes the ratio between vibration-caused and gravitation-caused forces.

Numerical investigation of the spectral problem (19) yields only the monotone instability ($\lambda = 0$). The behavior of neutral curves $\mathrm{Ra}_*(r, \varphi) = \min\limits_{\alpha} \mathrm{Ra}(r, \varphi, \alpha)$ is illustrated in Figs. 1 and 2. We can see (Fig. 1) that the direction $\varphi = 90°$ is exclusive, because the absolute stabilization is possible only in this case: namely, at $r > 0.023$, the layer is stable at any value of the Rayleigh number. However, if $52° < \varphi < 90°$, there are values of the parameter $r_*(\varphi)$ at which the layer is the most stable, and $\mathrm{Ra}_*^+(r_*, \varphi) > \mathrm{Ra}_*(0)$. For the angles $0° < \varphi < 52°$, the vibration destabilizes the layer: $\mathrm{Ra}_*^+(r, \varphi) < \mathrm{Ra}_*(0)$.

One of the most interesting vibration effects is the existence of negative Rayleigh numbers at $r \neq 0$ and $0° \leq \varphi < 90°$ (see Fig. 2). This fact implies that the thermal vibrational convection can arise not only if a layer is heated from below but also if it is heated from above.

At sufficiently large values of the parameter r, the critical numbers Ra_* tend to zero so that $\mathrm{Ra}_*^2 r^2 = \mu_*(\varphi)$, where $\mu_*(\varphi)$ determines convection under the condition of zero gravity. According to calculations, the asymptotic behavior corresponding to $r \longrightarrow \infty$ is attained already at $r \approx 10$. For $\mathrm{Ra} = 0$, problem (18) was first considered in [12], where the functions $\mu_*(\varphi)$ were calculated.

Following to Yudovich [13], we apply the Krein–Gantmakher theory of oscillation operators to problem (19) for $\mathrm{Ra} = 0$, $\lambda = 0$ and attain a rather complete description of the spectrum at $\varphi = 0°$ and 90°. In both cases, the eigenvalues $\mu_k(\alpha)$ are simple, while the eigenfunctions form the Markovian chain. All values of $\mu_k(\alpha)$ are positive at $\varphi = 0°$ and negative at $\varphi = 90°$. This fact implies that, in the conditions of zero gravity, monotone instability is absent in the case of vertical vibrations and is present when the vibrations are horizontal.

ACKNOWLEDGMENTS

This work was supported by the Russian Foundation for Basic Research (project nos. 00–15–96188 and 01–01–22002) and INTAS (project no. 99–01505).

REFERENCES

1. S. M. Zen'kovskaya and I. B. Simonenko, Izv. Akad. Nauk SSSR, Mekh. Zhidk. Gaza, No. 5, 51 (1966).
2. S. M. Zen'kovskaya, Izv. Akad. Nauk SSSR, Mekh. Zhidk. Gaza, No. 1, 55 (1968).
3. S. M. Zen'kovskaya (Available from VINITI, Moscow, No. 2437-78, VINITI, 1978; Ref. Zh. Mekh., No. 11, 30 (1978)).
4. S. M. Zen'kovskaya, in *Proceedings of VII All-Union Seminar on Numerical Methods for Viscous Liquids, Novosibirsk, Russia, 1979* (Inst. Teor. Prikl. Mekh. Sib. Otd. Akad. Nauk SSSR, Novosibirsk, 1979), p. 116.
5. S. M. Zen'kovskaya, Izv. Sev.-Kavkaz. Nauchn. Tsentra, Estestv. Nauki, No. 4, 43 (1981).
6. M. P. Zavarykin, S. V. Zorin, and G. F. Putin, Dokl. Akad. Nauk SSSR **299**, 309 (1988) [Sov. Phys. Dokl. **33**, 174 (1988).
7. I. B. Simonenko, Mat. Sborn. **87**, 236 (1972).
8. V. B. Levenshtam, Sib. Mat. Zh., No. 2, 105 (1993).
9. V. I. Yudovich, Dokl. Akad. Nauk **354**, 622 (1997) [Phys. Dokl. **42**, 322 (1997)].
10. D. V. Lyubimov, Eur. J. Mech. B, Fluids **14**, 439 (1995).
11. S. M. Zen'kovskaya and A. L. Shleykel', in *Proceedings of VII Ross. Symposium on Zero-Gravity Mechanics, Russia, 2001* (Moscow, 2001), p. 248.
12. G. Z. Gershuni and E. M. Zhukhovitsky, Dokl. Akad. Nauk SSSR **249**, 580 (1979) [Sov. Phys. Dokl. **24**, 894 (1979)].
13. V. I. Yudovich, Prikl. Mat. Mekh. **30**, 1000 (1966).

Translated by Yu. Verevochkin

Doklady Physics, Vol. 47, No. 2, 2002, pp. 153–155. Translated from Doklady Akademii Nauk, Vol. 382, No. 5, 2002, pp. 637–640.

MECHANICS

Pressure-Wave Damping in a Liquid with Bubbles Produced by Two Kinds of Gases

Academician V. E. Nakoryakov and V. E. Dontsov

Received November 1, 2001

Evolution of pressure waves in a liquid with gas bubbles is investigated sufficiently well from both the experimental and theoretical standpoints (see, e.g., [1, 2]). In particular, it is shown that an initial perturbation in a gas–liquid medium can decay into solitary waves, i.e., solitons, whose properties are studied in detail. It is revealed that the principal mechanism of wave dissipation in bubble media is the heat exchange between bubbles and the surrounding liquid. In [3, 4], the structure and damping of solitary pressure waves of moderate intensity in a gas–liquid mixture was experimentally investigated. In [5, 6], it was shown that allowance for polydispersivity in a gas–liquid medium leads to additional pressure-perturbation damping without qualitatively changing the wave structure. The effect of the inhomogeneity of a gas–liquid mixture and of the compressibility of a liquid on the pressure-wave structure are investigated in [7, 8]. In [9, 10], the appearance of two kinds of oscillatory solitary waves in a liquid with gas bubbles was discovered. These waves, called multisolitons, are caused by the existence of two degrees of freedom in a medium. The structure and damping of oscillatory solitary waves in liquids with gas bubbles in the case of various relations between bubble radii was experimentally studied in [11, 12].

In the present paper, we experimentally investigated the structure and damping of moderate-amplitude pressure waves in a liquid containing a bubble mixture of two gases (freon and helium) for the cases of one and two different bubble sizes.

The experiments were carried out with a setup of the shock-tube type. The basic section of the setup was a vertical thick-walled steel tube with an internal diameter of 0.053 m and a length of 1.5 m. This section filled with a liquid was then saturated with gas bubbles through two independent bubble sources situated in the lower part of the section. The bubble-size spread was within ±5%. A solution of glycerin (50 wt %) in distilled water was used as a working liquid. Freon-12 (CCl_2F_2) and helium, whose thermal diffusivities differ by a factor of more than 50, were used as a gas phase. The mean (over the basic section length) volume gas contents $\varphi_{f,h}$ for bubbles of each gas were determined by the increase in the level of the liquid in the basic section after the bubbles (with a diameter $d_{f,h}$) of the (f, h)-kind gas had been introduced. (The subscripts f and h correspond to freon and helium, respectively.) The experiments were performed under a static atmospheric pressure P_0. Bell-shaped pressure waves were generated by means of an electromagnetic vibrator located in the bottom of the basis section. The signals were formed by the repulsion of a thin copper plate from an electromagnetic coil when an electric-current pulse flowed through it. Pressure-wave profiles were registered by six piezoelectric sensors located along the basic-section length. The sensor signals were transmitted to amplitude-to-digital converters and then processed by a computer.

As a result of these experimental studies, it was established that the relationship between the relative concentrations of poorly heat-conducting freon bubbles and highly heat-conducting helium bubbles in the gas–liquid mixture qualitatively defines the wave structure and significantly affects the wave damping. While propagating waves in the liquid containing the low heat-conducting gas (freon), a solitary wave (soliton) or a group of solitary waves are formed from the initial signal, which damp due to dissipative processes. The principal mechanism for the dissipation of the solitary waves in a liquid with gas bubbles is the heat exchange between the bubble gas and the surrounding liquid [1–3]. The main parameters defining the damping of solitary waves are the gas heat diffusivity in bubbles, their size, the volume gas content in a liquid, and the wave amplitude.

Figure 1 displays the evolution of a pressure wave in a liquid with freon bubbles and a small volume concentration of helium bubbles of the same size. The time scales in Figs. 1a and 1b are 10^{-3} s. Above each wave profile, the wave amplitude (or the amplitude of the first oscillation for a group of solitary waves and oscillating shock waves) is indicated. As is seen, for the wave amplitudes with $\Delta P_0/P_0 \sim 1$ (Fig. 1a), a small addition of helium bubbles to the medium does not qualitatively change the wave structure. From an initial signal, a sol-

Kutateladze Institute of Thermal Physics, Siberian Division, Russian Academy of Sciences, pr. Lavrent'eva 1, Novosibirsk, 630090 Russia

E-mail: dontsov@itp.nsc.ru

1028-3358/02/4702-0153$22.00

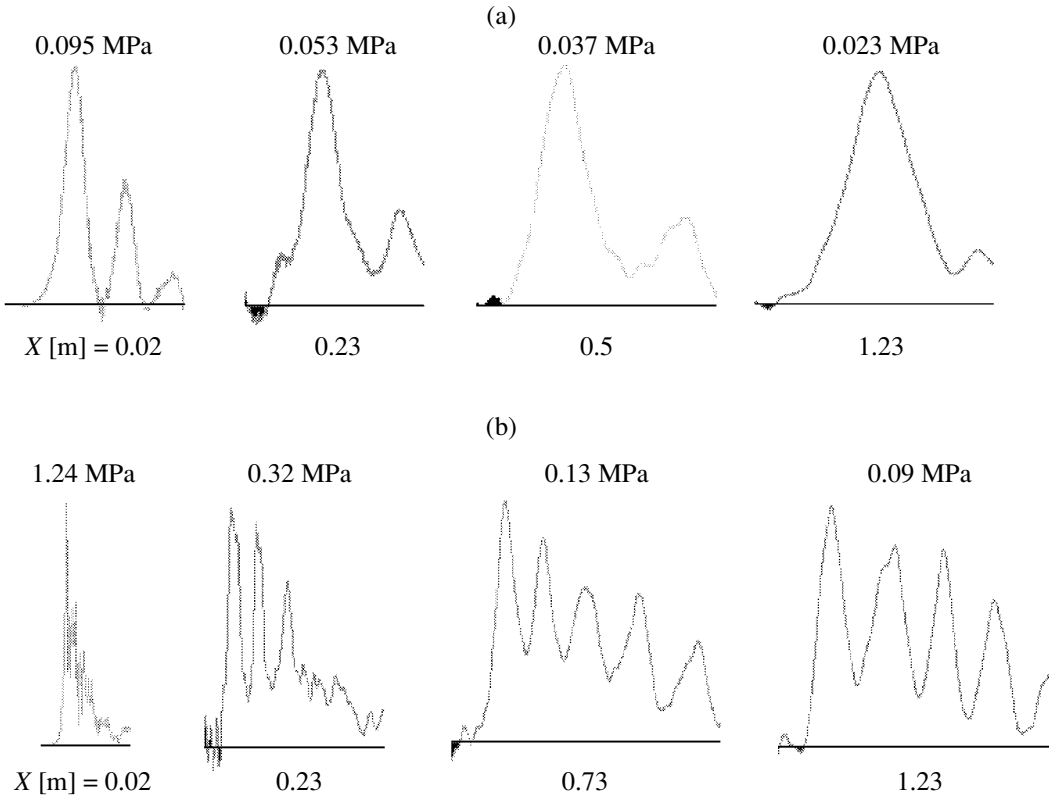

Fig. 1. Evolution of a pressure wave in a liquid containing a mixture of freon bubbles and helium bubbles at the distance X [m] from the inlet to the medium: (a) $\Delta P_0 = 0.095$ and (b) 1.24 MPa ($d_f = d_h = 2.3$ mm; $\varphi_f = 1.0\%$, $\varphi_h = 0.2\%$). The time scale is 1 ms.

itary wave is formed. However, the damping of the solitary wave is considerably stronger than in the liquid containing freon bubbles. This is explained by the fact that the wave structure is, basically, previously formed by freon bubbles, whereas helium bubbles mainly contribute to damping.

The dissipative energy loss increases with the amplitude of the wave incoming onto the medium, which is accompanied by the formation of an oscillating shock wave from the initial signal (Fig. 1b). The qualitative change in the wave structure leads, in turn, to a decrease in its damping, due to additional energy feeding the forward front of the oscillating shock wave. As a result, the effect of the increase in wave damping due to introducing helium bubbles into the medium is less pronounced for large-amplitude waves.

One of the possible ways to enhance damping for large wave amplitudes is an increase in the size of gas bubbles in the liquid. This makes it possible to form from the initial signal a series of solitary waves whose damping is considerably stronger than that for oscillating shock waves.

An increase in the volume concentration of helium bubbles in a gas–liquid mixture results in enhancing the pressure-wave damping. In the case of a high concentration of helium bubbles ($\varphi_h = 1\%$, $\varphi_f = 0.2\%$), shock waves, whose oscillations rapidly damp, are immediately formed from an initial signal. In this case, dissipative processes predominate over nonlinear and dispersive processes even for large wave amplitudes. This fact leads to both rapidly smoothing pulsations and the formation of a monotonous shock wave.

Figure 2 displays the pressure-wave damping in the liquid with bubbles of freon and helium of various volume concentrations as a function of the wave amplitude at a distance $X = 1.23$ m from the inlet of the wave into the medium. Here, ΔP is the (first-oscillation) wave amplitude at a given distance X from the inlet to the medium. As is seen, the helium-bubble concentration in the gas–liquid density strongly affects the wave damping. An effect of small relative concentrations of helium bubbles on damping waves with an amplitude $\Delta P_0/P_0 \sim 1$ (points *1* and *2*) is the most pronounced. The wave damping increases with the relative concentration of helium bubbles in the medium (under the condition of preserving the total volume gas content). At the same time, the effect of helium-bubble concentration on the wave damping noticeably decreases. For example, points *5* and *6*, which, respectively, correspond to relatively high concentrations of helium bubbles and pure helium bubbles (without freon bubbles) virtually coincide. With increasing the relative amplitude $\Delta P_0/P_0$ of a wave entering into the medium, the effect of the helium-bubble concentration on the wave damping

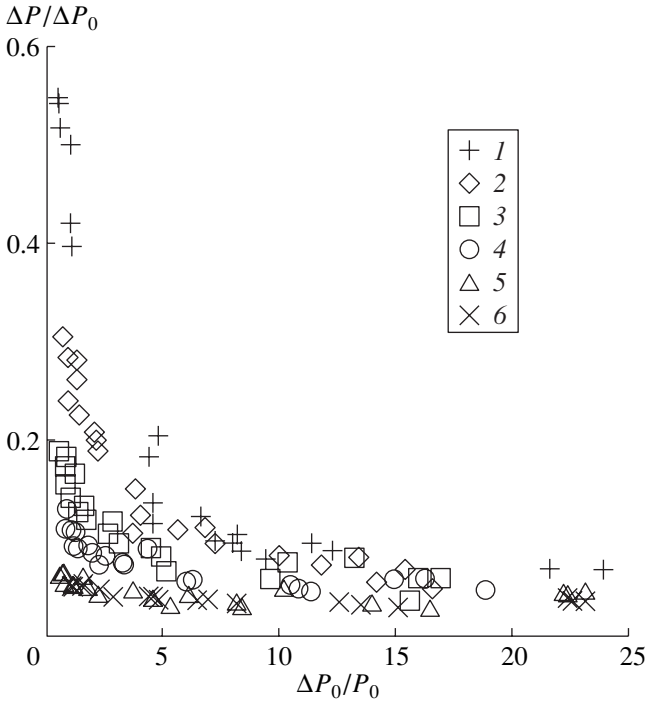

Fig. 2. Damping of a pressure wave in a liquid containing a mixture of freon bubbles and helium bubbles as a function of the wave amplitude ($d_f = d_h = 2.3$ mm): (*1*) $\varphi_f = 1.2\%$, $\varphi_h = 0$; (*2*) $\varphi_f = 1.0\%$, $\varphi_h = 0.2\%$; (*3*) $\varphi_f = 0.8\%$, $\varphi_h = 0.4\%$; (*4*) $\varphi_f = 0.4\%$, $\varphi_h = 0.8\%$; (*5*) $\varphi_f = 0.2\%$, $\varphi_h = 1.0\%$; (*6*) $\varphi_f = 0$, $\varphi_h = 1.2\%$.

decreases. As was shown above, this fact is explained by coupling solitary waves and the formation of an oscillating shock wave.

The damping of a pressure wave increases with the distance X. The strongest effect of this distance on the wave damping is observed for small wave amplitudes $\Delta P_0/P_0 \sim 1$ when solitary waves are not even coupled into an oscillating shock wave. With an increase in X and the relative concentration of helium bubbles in the gas–liquid medium, the damping depends less on the shock-wave amplitude; this is caused by the structural reconstruction of the wave profile.

As it was shown in [4, 11], the solitary-wave damping in a liquid that contains gas bubbles of two different sizes is stronger than in a liquid with gas bubbles of a single size under similar other parameters for the wave and the medium. This fact is explained by the resonant behavior of the bubbles of two kinds, which form an oscillating solitary wave called multisoliton. In this study, experimental data are obtained related to the structure and damping of moderate-amplitude pressure waves in a liquid with freon bubbles and a relatively low concentration of smaller-size helium bubbles. It was shown that the variation of the helium-bubble size by a factor of more than two virtually affects neither the wave structure nor the wave damping. Apparently, the dissipative energy loss in the case of compressing small-sized helium bubbles is so high that the bubbles fail to execute resonant-frequency oscillations and to form (together with freon bubbles) an oscillating solitary wave. The helium bubbles follow only the pressure in the wave being formed by freon bubbles and insignificantly affect the structure and damping of the wave.

While investigating wave damping in a liquid with larger size bubbles, when the general dissipation is lower, the effect of an increase in the wave damping is apparently possible in the case of introducing bubbles into the gas–liquid mixture that correspond to a highly heat-conducting gas.

Thus, we have demonstrated the possibility of a considerable increase in the damping of moderate-amplitude pressure waves in a liquid containing gas bubbles by introducing small relative volume concentrations of bubbles with a highly heat-conducting gas into the medium.

ACKNOWLEDGMENTS

This work was supported by the Russian Foundation for Basic Research, project nos. 00-01-00831 and 00-15-96177.

REFERENCES

1. V. E. Nakoryakov, B. G. Pokusaev, and I. R. Shreiber, *Wave Dynamics of Gas–Liquid and Vapor–Liquid Media* (Énergoatomizdat, Moscow, 1990).
2. R. I. Nigmatulin, *Dynamics of Multiphase Media* (Nauka, Moscow, 1987).
3. V. E. Dontsov, V. E. Kuznetsov, P. G. Markov, and V. E. Nakoryakov, Akust. Zh. **33**, 1041 (1987) [Sov. Phys. Acoust. **33**, 605 (1987)].
4. V. E. Nakoryakov, V. E. Kuznetsov, V. E. Dontsov, and P. G. Markov, Int. J. Multiphase Flow **16**, 741 (1990).
5. V. K. Kedrinskiĭ, Zh. Prikl. Mekh. Tekh. Fiz., No. 4, 29 (1968).
6. V. Sh. Shagapov, Izv. Akad. Nauk SSSR, Mekh. Zhidk. Gaza, No. 6, 145 (1976).
7. A. E. Beylich and A. Gulhan, Phys. Fluids A **2**, 1412 (1990).
8. M. Kameda, N. Shimaura, F. Higashino, and Y. Matsumoto, Phys. Fluids **10**, 2661 (1998).
9. V. G. Gasenko, V. E. Dontsov, V. V. Kuznetsov, and V. E. Nakoryakov, Izv. Sibirsk. Otd. Akad. Nauk SSSR, Tekh. Nauki **6**, 43 (1987).
10. V. G. Gasenko and V. P. Izergin, in *Proceedings of XI Intern. Symp. on Nonlinear Acoustics* (Novosibirsk, 1987), Chap. 2, p. 23.
11. V. E. Dontsov, V. E. Kuznetsov, P. G. Markov, and V. E. Nakoryakov, Akust. Zh. **35**, 157 (1989) [Sov. Phys. Acoust. **35**, 95 (1989)].
12. V. E. Nakoryakov and V. E. Dontsov, Dokl. Akad. Nauk **378**, 483 (2001) [Dokl. Phys. **46**, 422 (2001)].

Translated by G. Merzon

Doklady Physics, Vol. 47, No. 2, 2002, pp. 156–158. Translated from Doklady Akademii Nauk, Vol. 382, No. 6, 2002, pp. 765–767.

MECHANICS

Localization of a Vibrational Process in an Elastic Solid by an Array of Rigid Planar Inclusions

Academician V. A. Babeshko*, V. V. Buzhan*, and R. Williams**

Received October 23, 2001

We consider a problem concerning the localization of a vibrational process in an elastic space by an array of rigid parallel planar inclusions. These inclusions, described in the framework of the Griffith theory [1], were called in [2, 3] vibration-strength "viruses". Although this class of problems is rather topical, its rigorous mathematical study commenced only recently. This type of defects (inhomogeneities) most often arises in nonuniformly strengthened structural elements, as well as in heterogeneous-layer geological structures. In the latter case, such defects are inherent in tectonic plates of break zones and can trigger a brittle fracture. Methods suggested in the present paper are also applicable to the mathematical analysis of phenomena arising in three-dimensional integral circuits used as elements of electronic devices.

In previous papers [2, 3], methods applicable to the analysis of general integral-equation sets were used to find out the conditions for the localization of wave processes. In the present paper, studying this problem in an infinite medium, we confirm the concepts of [2, 3] and demonstrate the ways for practically solving the problem.

1. We consider an elastic space with L horizontal inhomogeneities (inclusions) in the orthogonal (x_1, x_2, x_3) reference system. The lth inhomogeneity ($l = 1, 2, \ldots, L$) is located in the $x_3 = h_l$ plane and occupies a domain Ω_l. The $x_3 = h_l$ boundaries of the inclusions are subjected to the actions of displacements with amplitudes $\mathbf{u}_l$ and a frequency ω. We denote the stresses at the boundaries of inclusions as $\boldsymbol{\tau}_l^{\pm}$. According to the definition of [2], this set of inhomogeneities is the L-level virus of the class 1 and of the type Ω, which is denoted as $V(1/h_1; \Omega_1/\ldots/h_L; \Omega_L)$. To construct a system of integral equations relating the displacements and stresses at the inclusion boundaries, we apply the method of the Fourier transform with respect to the variables x_1 and x_2 introducing the following notation for the displacement vectors $\mathbf{u}$ and stresses $\boldsymbol{\tau}_l^{\pm}$:

$$V\mathbf{u} \equiv \mathbf{U}(\alpha_1, \alpha_2, x_3) = \int_{-\infty}^{\infty}\int \mathbf{u}(x_1, x_2, x_3) e^{i(\alpha_1 x_1 + \alpha_2 x_2)} dx_1 dx_2,$$

$$V\boldsymbol{\tau} \equiv \mathbf{T}(\alpha_1, \alpha_2, x_3) = \int_{-\infty}^{\infty}\int \boldsymbol{\tau}(x_1, x_2, x_3) e^{i(\alpha_1 x_1 + \alpha_2 x_2)} dx_1 dx_2.$$

The integral relationships (similar to those we are searching for) were derived in [3] but for a level $-\infty \le x_1, x_2 \le +\infty$, $h_{l-1} \le x_3 \le h_l$. We now represent them in the vector form

$$\begin{aligned} D_{l-1}^{+}\mathbf{T}_{l-1}^{+} - D_l^{+}\mathbf{T}_l^{-} &= L_{l-1}^{+}\mathbf{U}_{l-1}^{+} - L_l^{+}\mathbf{U}_l^{-}, \\ D_{l-1}^{-}\mathbf{T}_{l-1}^{+} - D_l^{-}\mathbf{T}_l^{-} &= L_{l-1}^{-}\mathbf{U}_{l-1}^{+} - L_l^{-}\mathbf{U}_l^{-}, \end{aligned} \tag{1}$$

$$L_l^{\pm} = \begin{bmatrix} \pm\alpha_1\alpha_{31}e^{\pm i\alpha_{31}h_l} & \pm\alpha_2\alpha_{31}e^{\pm i\alpha_{31}h_l} & se^{\pm i\alpha_{31}h_l} \\ \pm\alpha_2\alpha_{31}e^{\pm i\alpha_{32}h_l} & \mp\alpha_1\alpha_{32}e^{\pm i\alpha_{32}h_l} & 0 \\ (2s+\alpha_2^2)e^{\pm i\alpha_{32}h_l} & -\alpha_1\alpha_2 e^{\pm i\alpha_{32}h_l} & \mp 2\alpha_1\alpha_{32}e^{\pm i\alpha_{32}h_l} \end{bmatrix},$$

$$D_l^{\pm} = \frac{i}{\mu}\begin{bmatrix} \frac{\alpha_1}{2}e^{\pm i\alpha_{31}h_l} & \frac{\alpha_2}{2}e^{\pm i\alpha_{31}h_l} & \pm\frac{\alpha_{31}}{2}e^{\pm i\alpha_{31}h_l} \\ \alpha_2 e^{\pm i\alpha_{32}h_l} & -\alpha_1 e^{\pm i\alpha_{32}h_l} & 0 \\ \pm\alpha_{32}e^{\pm i\alpha_{32}h_l} & 0 & -\alpha_1 e^{\pm i\alpha_{32}h_l} \end{bmatrix},$$

where $\alpha_{3j} = \sqrt{\gamma_j^2 - \alpha^2}$, $s = 0.5\gamma_j^2 - \alpha^2$, $\gamma_1 = \dfrac{\omega}{c_l}$, $\gamma_2 = \dfrac{\omega}{c_t}$; $c_l = \sqrt{\dfrac{\lambda + 2\mu}{\rho}}$ and $c_t = \sqrt{\dfrac{\mu}{\rho}}$ are velocities of longitudinal and transverse waves in the medium; ω is the circular frequency; λ and μ are the Lamé coefficients; and $\alpha^2 =$

* *Kuban State University, Stavropol'skaya ul. 149, Krasnodar, 350040 Russia*

** *University of Tennessee, Knoxville, Tennessee, 37996-1410 USA*

1028-3358/02/4702-0156$22.00 © 2002 MAIK "Nauka/Interperiodica"

$\alpha_1^2 + \alpha_2^2$. The branch α_{3j} of the square root is chosen from the condition

$$\alpha_{3j} = \begin{cases} \left|\gamma_j^2 - \alpha^2\right|^{1/2}, & \gamma_j^2 > \alpha^2 \\ i\left|\gamma_j^2 - \alpha^2\right|^{1/2}, & \gamma_j^2 < \alpha^2. \end{cases}$$

It is evident that the matrices $L_l^{\pm}$ and $D_l^{\pm}$ are associated with effects related to interactions of waves propagating inside the layer with its inhomogeneities.

To derive integral equations, we should eliminate from relationships (1) (for $l = 1$) the first equation and all terms with $e^{-i\alpha_{3j}h_0}$ from the second equation. At the same time, for $l = L + 1$, we should omit the second equation and all terms with $e^{i\alpha_{3j}h_{L+1}}$. In the case of inclusions, we take into account that $\mathbf{U}_l^+ = \mathbf{U}_l^- = \mathbf{U}_l$. As a result, we arrive at the following set of integral relationships

$$\begin{gathered} D_1^-\mathbf{T}_1^- = L_1^-\mathbf{U}_1, \\ D_1^+\mathbf{T}_l^+ - D_2^+\mathbf{T}_2^- = L_1^+\mathbf{U}_1 - L_2^+\mathbf{U}_2, \\ D_1^-\mathbf{T}_1^+ - D_2^-\mathbf{T}_2^- = L_1^-\mathbf{U}_1 - L_2^-\mathbf{U}_2, \\ \cdots\cdots\cdots\cdots\cdots\cdots\cdots\cdots \\ D_{L-1}^+\mathbf{T}_{L-1}^+ - D_L^+\mathbf{T}_L^- = L_{L-1}^+\mathbf{U}_{L-1} - L_L^+\mathbf{U}_L, \\ D_{L-1}^-\mathbf{T}_{L-1}^+ - D_L^-\mathbf{T}_L^- = L_{L-1}^-\mathbf{U}_{L-1} - L_L^-\mathbf{U}_L, \\ D_L^+\mathbf{T}_L^+ = L_L^+\mathbf{U}_L. \end{gathered} \tag{2}$$

Solving Eqs. (2) with respect to vectors $\mathbf{U}_1, \mathbf{U}_2, \ldots, \mathbf{U}_L$, we derive a set of integral equations

$$S_L\mathbf{T} = \mathbf{U}, \tag{3}$$

$$\mathbf{T} = \{\mathbf{T}_1, \mathbf{T}_2, \ldots, \mathbf{T}_L\}, \quad \mathbf{U} = \{\mathbf{U}_1, \mathbf{U}_2, \ldots, \mathbf{U}_L\},$$

$$S_L = \Theta_L J_L, \tag{4}$$

$$\Theta_L = \operatorname{diag}\{S_1^{-1}, S_1^{-1}, \ldots, S_1^{-1}\},$$

$$J_L = \begin{bmatrix} I & J_{12}^+ & J_{13}^+ & \ldots & J_{1,N-1}^+ & J_{1N}^+ \\ J_{12}^- & I & J_{23}^+ & \ldots & J_{2,N-1}^+ & J_{2N}^+ \\ J_{13}^- & J_{23}^- & I & \ldots & J_{2,N-1}^+ & J_{3N}^+ \\ \ldots & \ldots & \ldots & \ldots & \ldots & \ldots \\ J_{1,N-1}^- & J_{2,N-1}^- & J_{3,N-1}^- & \ldots & I & J_{N-1,N}^+ \\ J_{1N}^- & J_{2N}^- & J_{3N}^- & \ldots & J_{N-1,N}^- & I \end{bmatrix}.$$

Here, $\mathbf{T}_l = \mathbf{T}_l^+ - \mathbf{T}_l^-$ is the jump of stresses at the boundary of the lth inclusion

$$S_1 = D_+^{-1}L_+ - D_-^{-1}L_-, \quad J_{kl}^{\pm} = D_{\pm}^{-1}P_{kl}D_{\pm},$$

$$P_{kl} = \operatorname{diag}\{e^{i\alpha_{31}H_{kl}}, e^{i\alpha_{32}H_{kl}}, e^{i\alpha_{32}H_{kl}}\},$$

$$H_{kl} = h_l - h_k.$$

The matrix $D_{\pm}$ can be found from the matrix $D_l^{\pm}$ by eliminating exponentials from the matrix elements. Note that in the case of $L = 2$, representation (3) coincides with the similar representation for the case of antiplanar strain $\mathbf{u} = (u_1, 0, 0)$, $u_1 = u_1(x_2, x_3)$, $\tau = (\tau_{13}, 0, 0)$, $\tau_{13} = \tau_{13}(x_2, x_3)$, for which it is possible to obtain the equations in the analytical form

$$\begin{aligned} U_1 &= \frac{i}{2\mu\gamma_2\beta_{32}}[T_1 + e^{i\beta_{32}H_{12}}T_2], \\ U_2 &= \frac{i}{2\mu\gamma_2\beta_{32}}[e^{i\beta_{32}H_{12}}T_1 + T_2]. \end{aligned} \tag{5}$$

Here, the functions U_1, U_2, T_1, and T_2 are the first components of the corresponding vector functions $\mathbf{U}_1$, $\mathbf{U}_2$, $\mathbf{T}_1$, and $\mathbf{T}_2$.

2. For set (3), the method of solution was thoroughly described in [2, 3], so we do not repeat it here. Note only that in order to use this method we need information concerning the real-valued singularities of the matrix-function elements describing the set of equations in the symbolic form and also zeroes of the determinant for this set.

According to expansion (4), the problem of determining these singularities reduces to analyzing the functions Θ_L and J_L. The block-matrix theory yields the following relationships expressed in dimensionless coordinates:

$$\det\Theta = (\det S_1^{-1})^L,$$

$$\det S_1^{-1} = \frac{\delta^2(u)}{8i(\mu\gamma_2)^3\beta_{31}\beta_{32}^2},$$

$$\beta_{31} = \sqrt{\varepsilon^2 - u^2}, \quad \beta_{32} = \sqrt{1 - u^2},$$

$$u = \frac{\alpha}{\gamma_2}, \quad \delta(u) = u^2 + \beta_{31}\beta_{32}, \quad \varepsilon = \frac{c_t}{c_l}.$$

In the case of two inclusions, by virtue of the structure of the J_L matrix, it is easily reduced to the third-order determinant that can be calculated on the basis of the Sarrus rule. For the larger number of inclusions, the use of this approach is not reasonable, because it calls for the inversion of high-order matrices. Therefore, the other methods are used. For example, according to the compact Gauss scheme [5], the initial matrix J_L is rep-

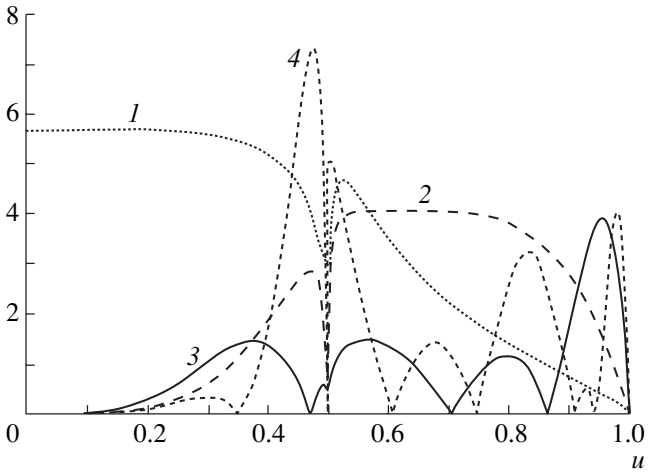

Absolute values of the determinant for $L = 2$, $\varepsilon = 0.5$, and different values of $\gamma_2 H_{12}$: (*1*) $\gamma_2 H_{12} = \frac{\pi}{2}$; (*2*) π; (*3*) 2π; and (*4*) 3π.

resented as a product of triangular matrices. Then, it is easy to calculate the determinant in itself.

The presence of the exponentials $\exp\{i\beta_{3k}\gamma_2 H_{pq}\}$ in the elements of the J_L matrix can cause pronounced oscillations of its determinant at large values of the normalized frequency $\gamma_2 H_{pq} = \frac{2\pi H_{pq}}{\lambda_t}$ (λ_t is the wavelength of the transverse wave), when $0 \le u \le 1$. This feature can give rise to regular real-valued zeros in the segment [0, 1] that was confirmed by results of numerous calculations. In particular, the condition of the existence for the root subsets $\gamma_2 H_{pq} \ge \pi$ was determined, namely, the fact that the distance between the neighboring inclusions should exceed the half-wavelength of the transverse wave in the medium. This condition can be obtained in the analytical form for antiplanar case (5) having the root subset

$$\left\{\sqrt{1-\left(\frac{\pi k}{\gamma_2 H_{12}}\right)^2}\right\}.$$

As an illustration confirming the above conclusions, we display in the figure the behavior of the determinant absolute value as a function of the parameter u at $L = 2$ for different values of the normalized frequency, which are multiple to π.

Thus, the matrix of the set S_L has real singularities, such as branch points $u = \varepsilon$, 1, and the main factor determining the existence of the root subsets [0, 1] of its determinant is the relative distance between neighboring inhomogeneities, which is equal to the half-wavelength.

ACKNOWLEDGMENTS

This work was supported by the Russian Foundation for Basic Research (project nos. 99-01-00787, r2000South 00101-96024, and 00-01-96019), by the Civilian Research and Development Foundation (CRDF) (project no. REC-004), and by the "Integratsiya" State Program (project no. A0017).

REFERENCES

1. V. M. Aleksandrov, B. I. Smetanin, and B. V. Sobol', *Thin Stress Concentrations in Elastic Bodies* (Nauka, Moscow, 1993).
2. V. A. Babeshko, Izv. Akad. Nauk, Mekh. Tverd. Tela, No. 3, 5 (2000).
3. V. A. Babeshko, Izv. Vyssh. Uchebn. Zaved., Sev.-Kav. Region. Estestv. Nauki, No. 3, 1 (2000).
4. R. A. Horn and C. R. Johnson, *Matrix Analysis* (Cambridge Univ. Press, Cambridge, 1985; Mir, Moscow, 1989).
5. V. V. Voevodin, *Computational Foundations of Linear Algebra* (Nauka, Moscow, 1977).

Translated by K. Kugel'

Doklady Physics, Vol. 47, No. 2, 2002, pp. 159–162. Translated from Doklady Akademii Nauk, Vol. 382, No. 6, 2002, pp. 768–771.

MECHANICS

Method of Differential Constraints in the Problem of a Stratified Shear-Free Turbulent Mixing Layer

V. N. Grebenev* and B. B. Ilyushin**

Presented by Academician A.K. Rebrov August 10, 2001

Received August 30, 2001

INTRODUCTION

In [1, 2], a self-similar solution to the problem of a shear-free turbulent unstratified mixing layer is presented. The characteristic property of this solution lies in the existence of differential constraints [3] isolating the given class of solutions. It is established that the differential constraint derived coincides with the algebraic relation (closing relation) for triple correlations found in [4]. Therefore, we can say that the tensor-invariant model [4] is substantiated within the framework of the method of differential constraints.

In this paper, we study the dynamics of a shear-free stratified mixing layer. Our principal result is presented by the theorem for the existence of an invariant manifold for the model. This makes it possible to solve the problem for the cases of both stable and unstable flow stratification. It turns out that the algebraic parameterization for the third moments, which corresponds to the Zeman–Lumley model [5], defines an equation for the invariant manifold of the model under consideration, while the Brunt–Väisälä frequency represents a bifurcation parameter in analyzing solutions to the equation for the turbulence time scale.

1. INVARIANT MANIFOLDS OF THE MODEL

The model [1] used here to describe a shear-free mixing layer has the third order of closure and is based on the hypothesis [6] that cumulants of the fifth and fourth orders are zero and nonzero, respectively. Thus, this model is represented by the equations

$$\frac{\partial\langle w^2\rangle}{\partial t} = -\frac{\partial\langle w^3\rangle}{\partial z} - \alpha(1 + a\hat{\tau}^2N^2)\frac{\langle w^2\rangle}{\hat{\tau}}, \qquad (1.1)$$

$$\frac{\partial\langle w^3\rangle}{\partial t} = \frac{\partial}{\partial z}\left[\kappa\hat{\tau}\langle w^2\rangle\frac{\partial\langle w^3\rangle}{\partial z}\right] - 3\langle w^2\rangle\frac{\partial\langle w^2\rangle}{\partial z} - \gamma(1 + a\hat{\tau}^2N^2)\frac{\langle w^3\rangle}{\hat{\tau}}, \qquad (1.2)$$

$$\frac{\partial\epsilon}{\partial t} = \frac{\partial}{\partial z}\left[\delta\hat{\tau}\langle w^2\rangle\frac{\partial\epsilon}{\partial z}\right] - \rho(1 + a\hat{\tau}^2N^2)\frac{\epsilon}{\hat{\tau}}, \qquad (1.3)$$

where $\alpha = \frac{2}{3}$, $\kappa = \frac{6c_1}{c_3(c_1+2)}$, $\gamma = \frac{2c_2(c_1+1)}{3c_1}$, $\delta = \frac{3c_1c_d}{2(c_1+2)}$, $\rho = \frac{2c_{\epsilon_2}(c_1+2)}{3c_1}$, $\hat{\tau} = \frac{\langle w^2\rangle}{\epsilon}$, and $a = \frac{c_1^2\pi}{8(c_1+2)^2}$. In addition, w is the vertical pulsatory velocity component; $\langle w^2\rangle$ is the single-point second-order pulsation correlation for the vertical velocity component; $\langle w^3\rangle$ is the third-order correlation; ϵ is the spectral flux of the turbulence kinetic energy; $N^2 = \beta g\frac{\partial\Theta}{\partial z}$, where N is the Brunt–Väisälä frequency; $\beta = \frac{1}{\Theta}$ is the coefficient of volume expansion; Θ is the average potential temperature; g is acceleration of gravity; c_{**} are the model coefficients; and the sign $\langle\cdot\rangle$ denotes averaging.

Since the system of evolution equations has an invariant manifold, its structure can be simplified [7]. Namely, the existence of differential constraints defining the invariant manifold makes it possible to reduce the number of equations and replace the differentiation operation by a certain algebraic procedure.

One of the invariant manifolds of system (1.1)–(1.3) has the form

$$D = \{\langle w^2\rangle, \langle w^3\rangle, \hat{\tau}: \mathcal{H}^1(\langle w^2\rangle, \langle w^3\rangle, \hat{\tau}) \equiv \langle w^3\rangle + \delta\hat{\tau}\langle w^2\rangle\langle w^2\rangle_z = 0\}. \qquad (1.4)$$

To prove invariance of the set D with respect to the flux generated by system (1.1)–(1.3), we make certain that

* *Institute of Computer Technologies, Siberian Division, Russian Academy of Sciences, pr. Akademika Lavrent'eva 6, Novosibirsk, 630090 Russia*

** *Kutateladze Institute of Thermal Physics, Siberian Division, Russian Academy of Sciences, pr. Akademika Lavrent'eva 1, Novosibirsk, 630090 Russia*

1028-3358/02/4702-0159$22.00 © 2002 MAIK "Nauka/Interperiodica"

on the set of smooth solutions to system (1.1)–(1.3) the operator $\mathcal{H}^1(\langle w^2\rangle, \langle w^3\rangle, \hat{\tau})$ does not change sign [8].

Theorem 1.1. *Let $\langle w^2\rangle$, $\langle w^3\rangle$, and ϵ be sufficiently smooth solutions to system* (1.1)–(1.3) *and, in addition,*

$$\frac{\partial\hat{\tau}}{\partial z} = 0, \quad \frac{\partial\hat{\tau}}{\partial t} = (2\alpha-\gamma)(1+a\hat{\tau}^2N^2) + \frac{3}{\delta}, \qquad (1.5)$$
$$\kappa = \delta.$$

Then, the operator $\mathcal{H}^1$ has the property of conserving the sign [8].

Corollary 1.1. *The set D represents the invariant manifold of system* (1.1)–(1.3).

Corollary 1.2. *The differential constraint $\mathcal{H}^1(\langle w^2\rangle, \langle w^3\rangle, \hat{\tau}) = 0$, which defines the invariant manifold of system* (1.1)–(1.3), *coincides with the algebraic model of triple correlations* [5].

The theorem formulated below forms a basis for finding different classes of the solutions.

Theorem 1.2. *Let constants of model* (1.1)–(1.3) *satisfy the equalities*

$$a(2\alpha-\gamma) = \alpha(\rho-a),$$
$$\frac{3}{\delta} + 2\alpha - \gamma = \rho - \alpha, \quad \kappa = \delta.$$

Then, on the invariant manifold D, system (1.1)–(1.3) *can be reduced to the form*

$$\langle w^2\rangle = \hat{\tau}\epsilon, \quad \langle w^3\rangle = -\delta\hat{\tau}\langle w^2\rangle\frac{\partial\langle w^2\rangle}{\partial z}, \qquad (1.6)$$

$$\frac{\partial\epsilon}{\partial t} = \frac{\partial}{\partial z}\left[\delta\hat{\tau}\langle w^2\rangle\frac{\partial\epsilon}{\partial z}\right] - \rho(1+a\hat{\tau}^2N^2)\frac{\epsilon}{\hat{\tau}}, \qquad (1.7)$$

where $\hat{\tau} = \hat{\tau}(t)$ is the solution to the equation

$$\frac{\partial\hat{\tau}}{\partial t} = (2\alpha-\gamma)(1+a\hat{\tau}^2N^2) + \frac{3}{\delta}. \qquad (1.8)$$

2. SOLUTIONS ON THE INVARIANT SET

We consider equation (1.8) written out as

$$\frac{\partial\hat{\tau}}{\partial t} = BN^2\hat{\tau}^2(t) + D, \qquad (2.1)$$

where $B = a(2\alpha-\gamma)$ and $D = \frac{3}{\delta} + 2\alpha - \gamma$. The form of a solution to Eq. (2.1) depends on signs of the quantities B, D, and N^2. According to calculations, $B < 0$ and $D > 0$. Positive (negative) definiteness of N^2 corresponds to the cases of stable (unstable) stratification.

2.1. Stable stratification. Integration of equation (2.1) allows its solution to be expressed as

$$\hat{\tau}^s(t) = A\tanh\left(4\sqrt{\left(\frac{D}{-B}\right)}BNt + C_0\right),$$

where $A = \sqrt{\frac{D}{-BN^2}}$ and C_0 is an integration constant determined by the specified initial value $\hat{\tau}_s(0)$; $\hat{\tau}_s(t) \longrightarrow A$ as $t \longrightarrow \infty$.

Initial conditions for equation (1.7) are determined by the formulation of the problem. They are

$$\epsilon_0(z) \equiv \epsilon(z, 0) = \begin{cases}\epsilon_-, & \text{if } z < 0\\ \epsilon_+, & \text{if } z \geq 0,\end{cases}$$

where ϵ_- and ϵ_+ are positive numbers such that $\epsilon_- < \epsilon_+$. We introduce the notation

$$\theta \equiv \theta(t) = \int_0^t \hat{\tau}_s^2(p)dp, \quad \varsigma(\theta) = \hat{\tau}_s^2(\theta^{-1}(t)),$$

$$\psi(\theta) = \frac{1+a\varsigma^2(\theta)N^2}{\varsigma^3(\theta)},$$

$$\hat{\epsilon}(z, \theta) = u_s(z, \theta)\exp\left(-\int_0^\theta \psi(p)dp\right),$$

where $\hat{\epsilon}(z, \theta) = \epsilon(z, t)$. Then the function u_s satisfies the equation

$$\frac{\partial u_s}{\partial\hat{\theta}} = \frac{\partial}{\partial z}\left[\partial u_s\frac{\partial u_s}{\partial z}\right], \quad \hat{\theta} = \int_0^\theta \exp\left(-\int_0^\xi \psi(p)dp\right)d\xi, \qquad (2.2)$$

$$u_s(z, 0) = \epsilon_-, \text{ if } z < 0,$$
$$u_s(z, 0) = \epsilon_+, \text{ if } z \geq 0. \qquad (2.3)$$

It is easy to verify that $\hat{\theta}: [0, +\infty) \longrightarrow [0, \hat{\theta}_0)$, where $\hat{\theta}_0 < \frac{A}{aN^2}$, and

$$\exp\left(-\int_0^\theta \psi(p)dp\right) \longrightarrow 0 \text{ at } \theta \longrightarrow +\infty.$$

The solution to problem (2.2), (2.3) is unique and invariant with respect to the parametric transformation group presented in [9]. Thus, u_s is a self-similar solution of the form

$$u_s(z, \hat{\theta}) = u_s(\hat{\xi}), \quad \hat{\xi} = \frac{z - z_c}{\sqrt{2\hat{\theta}}}, \quad z_c(\hat{\theta}) = \lambda_0\sqrt{2\hat{\theta}},$$

where λ_0 is a certain constant and problem (2.2), (2.3) turns into the equation

$$2\delta\frac{d^2u_s}{d\hat{\xi}^2} + 2\delta\left(\frac{du_s}{d\hat{\xi}}\right)^2 + (\hat{\xi}+\lambda_0)\frac{du_s}{d\hat{\xi}} = 0, \qquad (2.4)$$

$$u_s(-\infty) = \epsilon_-, \quad u_s(+\infty) = \epsilon_+. \tag{2.5}$$

Setting $u_s(\hat{\xi}) = \dfrac{d\hat{\xi}}{d\zeta}$, where ζ is the new variable, we obtain the following boundary value problem for the Blasius equation:

$$2\delta\frac{d^3\hat{\xi}}{d\zeta^3} + (\hat{\xi} + \lambda_0)\frac{d^2\hat{\xi}}{d\zeta^2} = 0, \tag{2.6}$$

$$\left.\frac{d\hat{\xi}}{d\zeta}\right|_{-\infty} = \epsilon_-, \quad \left.\frac{d\hat{\xi}}{d\zeta}\right|_{+\infty} = \epsilon_+. \tag{2.7}$$

Lemma 2.1. *For arbitrary positive numbers* ϵ_- *and* ϵ_+ ($\epsilon_- \le \epsilon_+$), *there exists a unique positive solution* u_s *to problem* (2.4), (2.5) [*correspondingly,* (2.2), (2.3)] *such that convex* ($\hat{\xi} < 0$) *or concave* ($\hat{\xi} > 0$) *function* u_s *is monotonically increasing in the interval* $(-\infty, +\infty)$.

Having determined u_s, we easily find $\langle w^2\rangle$ and $\langle w^3\rangle$ by the formulas

$$\langle \hat{w}^2(z, \theta)\rangle = \hat{\tau}_s\hat{\epsilon}(z, \theta) = \hat{\tau}_s u_s(z, \theta)\exp\left(-\int_0^\theta \psi(p)dp\right),$$

$$\langle \hat{w}^3(z, \theta)\rangle = -\delta\hat{\tau}_s\langle \hat{w}^2(z, \theta)\rangle\frac{\partial\langle \hat{w}^2(z, \theta)\rangle}{\partial z},$$

$$\langle w^3(z, t)\rangle = \langle \hat{w}^3(z, \theta)\rangle.$$

2.2. Unstable stratification. For $N^2 < 0$, the solution to equation (2.1) has the form

$$\hat{\tau}_{ns} = A\tanh(\sqrt{(DBN^2)}t + C_1),$$

where C_1 is determined by the value $\hat{\tau}_{ns}(0)$. We introduce the notation

$$\theta = \theta(t) \equiv \int_0^t \hat{\tau}_{ns}^2(p)dp.$$

Then, the function u_{ns}, defined as

$$u_{ns}(z, \theta) = \hat{\epsilon}(z, \theta)\exp\left(\int_0^\theta \psi(p)dp\right),$$

$$\psi(\theta) = \frac{1 + a\varsigma^2(\theta)N^2}{\varsigma^3(\theta)},$$

$$\varsigma(\theta) = \hat{\tau}_{ns}^2(\theta^{-1}(t)),$$

satisfies the equation

$$\frac{\partial u_{ns}}{\partial\hat{\theta}} = \frac{\partial}{\partial z}\left[\partial u_{ns}\frac{\partial u_{ns}}{\partial z}\right].$$

Here,

$$\hat{\theta} = \int_0^\theta \exp\left(-\int_0^\xi \psi(p)dp\right)d\xi.$$

It is evident that $\hat{\theta} \longrightarrow +\infty$ as $\sqrt{(DBN^2)}\,t + C_1 \longrightarrow \dfrac{\pi}{2}$. Further analysis is similar to the case of the stable stratification.

Lemma 2.1 allows formulation of the following theorem:

Theorem 2.1. *Let* $\kappa = \delta$ *and*

$$a(2\alpha - \gamma) = \alpha(\rho - a), \quad \frac{3}{\delta} + 2\alpha - \gamma = \rho - \alpha.$$

Then, there is a solution to system (1.1)–(1.3) *of the form*

(a) *for* $N^2 > 0$,

$$\hat{\epsilon}(z, \theta) = u_s(z, \theta)\exp\left(-\int_0^\theta \psi(s)ds\right),$$

$$\theta = \theta(t) \equiv \int_0^t \hat{\tau}_s^2(p)dp,$$

$$\langle w^2(z, t)\rangle = \hat{\tau}_s\epsilon(z, t),$$

$$\langle w^3(z, t)\rangle = -\delta\hat{\tau}_s\langle w^3(z, t)\rangle\frac{\partial\langle w^2(z, t)\rangle}{\partial z};$$

(b) *for* $N^2 < 0$,

$$\hat{\epsilon}(z, \theta) = u_{ns}(z, \theta)\exp\left(-\int_0^\theta \psi(s)ds\right),$$

$$\theta = \theta(t) \equiv \int_0^t \hat{\tau}_{ns}^2(p)dp,$$

$$\langle w^2(z, t)\rangle = \hat{\tau}_s\epsilon(z, t),$$

$$\langle w^3(z, t)\rangle = -\delta\hat{\tau}_s\langle w^2(z, t)\rangle\frac{\partial\langle w^2(z, t)\rangle}{\partial z}.$$

Here, u_s (u_{ns}) *represents the self-similar solution to problem* (2.4), (2.5).

ACKNOWLEDGMENTS

The authors are grateful to G.G. Chernykh for his participation in discussions of the results of this study.

This work was supported by the Russian Foundation for Basic Research (project nos. 00-15-96810 and 01-01-00783), by the Integration Project of the

Siberian Division of the Russian Academy of Sciences (project no. 2000-1), and by INTAS (project no. 97-2022).

REFERENCES

1. V. N. Grebenev and V. V. Ilyushin, Dokl. Akad. Nauk **374**, 761 (2000) [Dokl. Phys. **45**, 550 (2000)].
2. V. N. Grebenev, V. V. Ilyushin, and Yu. I. Shokin, J. Nonlin. Sci. and Numer. Simulation **1**, 305 (2000).
3. A. F. Sidorov, V. P. Shapeev, and N. N. Yanenko, *The Method of Differential Constraints and Its Application to Gas Dynamics* (Nauka, Novosibirsk, 1984).
4. K. Hanjalic and B. E. Launder, J. Fluid Mech. **52**, 609 (1972).
5. O. Zeman and J. L. Lumley, J. Atmos. Sci. **33**, 1974 (1976).
6. B. B. Ilyushin, in *Closure Strategies for Turbulent and Transition Flows* (Cambridge, 1999).
7. V. K. Andreev, O. V. Kaptsov, V. V. Pukhnachev, and A. A. Rodionov, *The Application of Group Theoretical Methods in Fluid Mechanics* (Nauka, Novosibirsk, 1994).
8. V. A. Galaktionov, Nonlin. Anal. Theory Methods and Applications **23**, 1595 (1994).
9. J. Vazques, Trans. Am. Math. Soc. **285**, 717 (1984).

Translated by Yu. Verevochkin

Doklady Physics, Vol. 47, No. 2, 2002, pp. 163–167. Translated from Doklady Akademii Nauk, Vol. 382, No. 6, 2002, pp. 772–776.

MECHANICS

A New Mechanism of the Nonlinear Generation of Internal Waves

Yu. V. Kistovich and Yu. D. Chashechkin

Presented by Academician A.Yu. Ishlinskiĭ August 8, 2001

Received August 27, 2001

The exact solution to the linearized problem of generating disturbances by a two-dimensional obstacle performing a periodic motion in a viscous continuously stratified liquid describes thin boundary layers [1] as well as progressive waves and makes it possible to estimate the errors of the extensively used method of sources [2]. The three-dimensional boundary-layer flow is split into layers of two types [3]. One of them (viscous periodic flow) is analogous to the Stokes layer in a homogeneous fluid and has a thickness depending on the kinematic viscosity and frequency. The spatial scale of the second (internal boundary) layer depends on the geometric parameters of the problem [3]. Since the governing equations are nonlinear, the moving boundary layers are direct sources of waves. The parameters of waves generated by a boundary-layer flow on a horizontal disc performing torsional vibrations are in satisfactory agreement with measurements [4]. For the first time, we consider here the generation of internal waves through new mechanisms attributed to the nonlinear interaction of boundary-layer flows with each other and with progressive internal waves or residual motions into which the internal waves transform when the disturbance frequency ω exceeds the buoyancy frequency N of a media. As a source of waves, we consider an infinite immovable vertical plane whose part performs complex two-dimensional motion, which is the superposition of two vertical oscillations with frequencies ω_1 and ω_2. In this case, only the vertical component of the surface velocity is nonzero:

$$U(z, t) = U_1(z)e^{-i\omega_1 t} + U_2(z)e^{-i\omega_2 t}. \quad (1)$$

The equations of two-dimensional motion of a viscous incompressible stratified liquid without diffusion have the form

$$(\rho_0 + \rho)\left(\frac{\partial u_x}{\partial t} + u_x\frac{\partial u_x}{\partial x} + u_z\frac{\partial u_x}{\partial z} - \nu\Delta u_x\right) = -\frac{\partial P}{\partial x},$$

$$(\rho_0 + \rho)\left(\frac{\partial u_z}{\partial t} + u_x\frac{\partial u_z}{\partial x} + u_z\frac{\partial u_z}{\partial z} - \nu\Delta u_z\right) = -\frac{\partial P}{\partial z} - \rho g, \quad (2)$$

$$\frac{\partial \rho}{\partial t} + u_z\frac{d\rho_0}{dz} + u_x\frac{\partial \rho}{\partial x} + u_z\frac{\partial \rho}{\partial z} = 0, \quad \frac{\partial u_x}{\partial x} + \frac{\partial u_z}{\partial z} = 0,$$

where $\rho_0(z)$ is the undisturbed density profile, ρ is the density disturbance, u_x and u_z are the velocity components, P is the pressure minus the hydrostatic pressure, ν is the kinematic viscosity, g is the acceleration of gravity directed opposite to the vertical z-axis, and $\Delta = \frac{\partial^2}{\partial x^2} + \frac{\partial^2}{\partial z^2}$. The boundary conditions are the no-slip condition in the plane,

$$u_x(x = 0, z, t) = 0, \quad u_z(x = 0, z, t) = U(z, t), \quad (3)$$

and damping of the disturbances at infinity.

In the approximation of weak nonlinearity, the solution of the problem in the first-order perturbation theory is represented as the sum of solutions of linearized system (2) with boundary conditions (3) and the solutions of the inhomogeneous linearized system

$$\rho_0\frac{\partial \tilde{u}_x}{\partial t} = -\frac{\partial \tilde{P}}{\partial x} + \rho_0\nu\Delta\tilde{u}_x + \rho_0 f^x,$$

$$\rho_0\frac{\partial \tilde{u}_z}{\partial t} = -\frac{\partial \tilde{P}}{\partial z} + \rho_0\nu\Delta\tilde{u}_z - \tilde{\rho}g + \rho_0 f^z, \quad (4)$$

$$\frac{\partial \tilde{\rho}}{\partial t} + \tilde{u}_z\frac{d\rho_0}{dz} = m, \quad \frac{\partial \tilde{u}_x}{\partial x} + \frac{\partial \tilde{u}_z}{\partial z} = 0$$

with zero boundary conditions in the plane. The sources f^x, f^z, and m appear in Eqs. (4) upon substituting the stream function Ψ, which is the solution of the linearized system, into the quadratic terms of Eqs. (2) and have the form

$$f^x = \Psi_x\Psi_{zz} - \Psi_z\Psi_{xz},$$
$$f^z = \Psi_z\Psi_{xx} - \Psi_x\Psi_{xz}, \quad m = \Psi_x\rho_z - \Psi_z\rho_x, \quad (5)$$

Institute for Problems of Mechanics,
Russian Academy of Sciences,
pr. Vernadskogo 101, Moscow, 117526 Russia

1028-3358/02/4702-0163$22.00

where the subscripts x and z denote the partial derivatives with respect to the corresponding variables. In Eqs. (5), the terms $\rho\frac{\partial \mathbf{u}}{\partial t}$ and $\rho\nu\Delta\mathbf{u}$ are omitted under the assumption that

$$\lambda \ll \Lambda, \quad \delta_\nu^2 \ll \lambda\Lambda,$$

where λ is the typical spatial scale, $\delta_\nu = \sqrt{\frac{2\nu}{\omega}}$ is the thickness of the viscous boundary layer, and $\Lambda = -\frac{\rho_0}{\rho_0'}$ is the stratification scale. Equations (4) lead to the following equation for the correction to the stream function, $\tilde{\Psi}$ ($\tilde{u}_x = \tilde{\Psi}_z$, $\tilde{u}_z = -\tilde{\Psi}_x$):

$$\left[\frac{\partial^2}{\partial t^2}\Delta + N^2\frac{\partial^2}{\partial x^2} - \nu\frac{\partial}{\partial t}\Delta^2\right]\tilde{\Psi} = \frac{\partial}{\partial t}\left(\frac{\partial f^x}{\partial z} - \frac{\partial f^z}{\partial x}\right) + \frac{g}{\rho_0}\frac{\partial m}{\partial x} \equiv F, \tag{6}$$

where $N = \sqrt{\frac{g}{\Lambda}}$ is the buoyancy frequency.

Entering into (5), the solution of linearized system (2) with boundary conditions (3) is represented as the plane-wave expansion [2, 6]

$$\Psi = \frac{1}{2}(\Psi_1 e^{-i\omega_1 t} + \Psi_2 e^{-i\omega_2 t}) + \text{c.c.},$$

$$\rho = \frac{i\rho_0'}{2\omega_1}\Psi_{1x}e^{-i\omega_1 t} + \frac{i\rho_0'}{2\omega_2}\Psi_{2x}e^{-i\omega_2 t} + \text{c.c.},$$

$$\Psi_j = \int_{-\infty}^{+\infty} A_j(k)(e^{ik_{j\mathrm{w}}x} - e^{ik_{j\mathrm{b}}x})e^{ikz}dk, \tag{7}$$

$$A_j(k) = \frac{i}{2\pi}\frac{1}{k_{j\mathrm{w}} - k_{j\mathrm{b}}}\int_{-\infty}^{+\infty} U_j(z)e^{-ikz}dz,$$

which describes both the internal waves and the boundary layers (the terms with the subscripts w and b). Here, the wave numbers satisfy the dispersion equation

$$\omega_j^2(k_j^2 + k^2) - N^2k_j^2 + i\omega_j\nu(k_j^2 + k^2)^2 = 0. \tag{8}$$

The substitution of solutions (7) into Eqs. (5) and (6) results in the appearance of the terms with different combination frequencies 0, $2\omega_1$, $2\omega_2$, and $\omega_1 \pm \omega_2$ on the right-hand side of Eq. (6). To calculate the generation of waves with the frequency $\Omega = \omega_1 - \omega_2$, we seek a solution of Eq. (6) in the form

$$\tilde{\Psi} = \frac{1}{2}[\psi(x, z)e^{-i\Omega t} + \psi^*(x, z)e^{i\Omega t}].$$

Here, the asterisk denotes complex conjugation and ψ satisfies the equation

$$\left[\Omega^2\Delta - N^2\frac{\partial^2}{\partial x^2} - i\Omega\nu\Delta^2\right]\psi = F_\Omega(x, z), \tag{9}$$

$$\begin{aligned} F_\Omega = \frac{i\Omega}{2}\{&(1+\alpha_1)[\Psi_{2x}^*\Psi_{1xxz} - \Psi_{2z}^*\Psi_{1xxx}] \\ &+ (1-\alpha_2)[\Psi_{1x}\Psi_{2xxz}^* - \Psi_{1z}\Psi_{2xxx}^*] \\ &+ (\alpha_1+\alpha_2)[\Psi_{1xz}\Psi_{2xx}^* - \Psi_{1xx}\Psi_{2xz}^*] + \Psi_{1x}\Psi_{2zzz}^* \\ &- \Psi_{1z}\Psi_{2xzz}^* + \Psi_{2x}^*\Psi_{1zzz} - \Psi_{2z}^*\Psi_{1xzz}\}, \end{aligned} \tag{10}$$

where $\alpha_j = \frac{N^2}{\Omega\omega_j}$.

A solution of Eq. (9) is constructed in the form of the convolution of its right-hand side with the Green's function of Eq. (9):

$$\psi(x, z) = \int_{0}^{\infty}\int_{-\infty}^{+\infty} G(x, \xi; z - \zeta)F_\Omega(\xi, \zeta)d\zeta d\xi. \tag{11}$$

The conducted calculations demonstrate that the Green's function satisfying the boundary conditions $\frac{\partial G}{\partial x} = \frac{\partial G}{\partial z} = 0$ at $x = 0$ has the form

$$G = \frac{1}{4\pi\Omega\nu}\int_{-\infty}^{+\infty}\tilde{G}(\kappa; x, \xi)e^{i\kappa(z-\zeta)}d\kappa, \tag{12}$$

$$\begin{aligned} \tilde{G} = \frac{1}{\kappa_\mathrm{b}^2 - \kappa_\mathrm{w}^2}\Bigg\{&\frac{1}{\kappa_\mathrm{w}} \\ &\times\left[e^{i\kappa_\mathrm{w}|x-\xi|} - \frac{\kappa_\mathrm{b} + \kappa_\mathrm{w}}{\kappa_\mathrm{b} - \kappa_\mathrm{w}}e^{i\kappa_\mathrm{w}(x+\xi)} + \frac{2\kappa_\mathrm{w}}{\kappa_\mathrm{b} - \kappa_\mathrm{w}}e^{i\kappa_\mathrm{w}x}e^{i\kappa_\mathrm{b}\xi}\right] \\ &- \frac{1}{\kappa_\mathrm{b}}\left[e^{i\kappa_\mathrm{b}|x-\xi|} + \frac{\kappa_\mathrm{b} + \kappa_\mathrm{w}}{\kappa_\mathrm{b} - \kappa_\mathrm{w}}e^{i\kappa_\mathrm{b}(x+\xi)} - \frac{2\kappa_\mathrm{b}}{\kappa_\mathrm{b} - \kappa_\mathrm{w}}e^{i\kappa_\mathrm{b}x}e^{i\kappa_\mathrm{w}\xi}\right]\Bigg\}, \end{aligned} \tag{13}$$

where the solutions $\kappa_\mathrm{w}(\kappa)$ and $\kappa_\mathrm{b}(\kappa)$ of the dispersion equation corresponding to Eq. (9) have the form

$$\kappa_\mathrm{w} = |\kappa|\tan\theta + \frac{i\nu|\kappa|^3}{2N\cos^5\theta}, \quad \kappa_\mathrm{b} = (i-1)\cot\theta\sqrt{\frac{\Omega}{2\nu}}. \tag{14}$$

Here, $\theta = \arcsin\left(\frac{\Omega}{N}\right)$ is the angle between the beams of the internal waves and the horizontal plane.

Substituting Eqs. (7), (10), (12), and (13) into Eq. (11) and integrating with respect to ζ, we obtain

$$\psi = \frac{i}{4\nu}\int_{-\infty}^{+\infty} e^{i\kappa z}\int_{-\infty}^{+\infty}\int_{0}^{\infty} A_1(k)A_2^*(k-\kappa) \times \tilde{G}(\kappa; x, \xi)\tilde{F}(k, \kappa; \xi)d\xi dk d\kappa, \quad (15)$$

where

$$\tilde{F} = H(k_w, \tilde{k}_w) - H(k_b, \tilde{k}_w) - H(k_w, \tilde{k}_b) + H(k_b, \tilde{k}_b),$$
$$H(\sigma, \tilde{\sigma}) = e^{i(\sigma-\tilde{\sigma})\xi}[(k-\kappa)\sigma - k\tilde{\sigma}]\{(\sigma-\tilde{\sigma}) \times [(1+\alpha_1)\sigma + (1-\alpha_2)\tilde{\sigma}] + \kappa(2k-\kappa)\}. \quad (16)$$

Here,

$$k_w = k_{1w}(k), \quad \tilde{k}_w = k_{2w}^*(k-\kappa),$$
$$k_b = k_{1b}(k), \quad \tilde{k}_b = k_{2b}^*(k-\kappa).$$

The terms entering into Eq. (16) for $\tilde{F}$ describe the nonlinear interaction between the internal waves (this interaction was calculated in [7]), the interaction of the internal waves with the boundary layers, and the interaction between the boundary layers.

When integrating in Eq. (15) with respect to the coordinate ξ in the approximation of low viscosity, we retain only the terms of the minimum order in $\nu \longrightarrow 0$. Then the terms presenting the direct interaction between internal waves disappear in Eq. (15), since they have a higher order in ν. The nonlinear interaction of the boundary layers with each other and with the internal waves leads to the generation of a wave field, whose stream function is

$$\Psi = \frac{1}{2\nu\kappa_b}\int_{-\infty}^{+\infty} e^{i\kappa_w x}e^{i\kappa z}\int_{-\infty}^{+\infty} A_1(k)A_2^*(k-\kappa) \times\left\{\frac{(1+\alpha_1)(k-\kappa)k_b}{\kappa_b + k_b} + \frac{(1-\alpha_2)k\tilde{k}_b}{\kappa_b - \tilde{k}_b}\right. \quad (17)$$
$$\left. - \frac{[(k-\kappa)k_b - k\tilde{k}_b][(1+\alpha_1)k_b + (1-\alpha_2)\tilde{k}_b]}{(\kappa_b + k_b - \tilde{k}_b)(k_b - \tilde{k}_b)}\right\}dk d\kappa.$$

Solution (17) exists for arbitrary frequencies ω_1 and ω_2, in particular, exceeding the buoyancy frequency N. Since the energy density increases with the wave frequency, only the case ω_1 is of practical importance, $\omega_2 \gg N$, where the direct generation of progressive internal waves is forbidden by the properties of the dispersion equation. In this case, it follows from Eq. (8) that the roots of the dispersion equation corresponding to the boundary layer take the form

$$k_b = (1+i)\sqrt{\frac{\omega_1^2 - N^2}{2\omega_1\nu}}, \quad \tilde{k}_b = (1-i)\sqrt{\frac{\omega_2^2 - N^2}{2\omega_2\nu}}.$$

Substituting Eq. (7) for $A_j(k)$ into Eq. (17) and performing integration, we obtain

$$\psi = -\frac{i}{4\pi\nu\kappa_b(\kappa_b + k_b - \tilde{k}_b)(k_b - \tilde{k}_b)} \times \int_{-\infty}^{+\infty} e^{i\kappa_w x}e^{i\kappa z}[\beta_1 I_1(\kappa) + \beta_2 I_2(\kappa)]d\kappa,$$

$$\beta_1 = 2 + \alpha_1 - \alpha_2 + (1-\alpha_2)\frac{k_b - \tilde{k}_b}{\kappa_b - \tilde{k}_b}, \quad (18)$$

$$\beta_2 = 2 + \alpha_1 - \alpha_2 + (1+\alpha_1)\frac{k_b - \tilde{k}_b}{\kappa_b + \tilde{k}_b},$$

$$I_1(\kappa) = \int_{-\infty}^{+\infty} U_1'(z)U_2^*(z)e^{-i\kappa z}dz,$$

$$I_2(\kappa) = \int_{-\infty}^{+\infty} U_1(z)U_2'^*(z)e^{-i\kappa z}dz.$$

If the geometry of the part of the plane moving with different frequencies is characterized by a common function $S(z)$, i.e., $U_j(z) = -i\omega_j b_j S(z)$, where b_j is the amplitude of corresponding oscillations and $\max S(z) = 1$, we have

$$\psi = \frac{\omega_1\omega_2 b_1 b_2 \beta}{8\pi\nu\kappa_b}\int_{-\infty}^{+\infty}\kappa e^{i\kappa_w x}e^{i\kappa z}\int_{-\infty}^{+\infty} S^2(\zeta)e^{-i\kappa\zeta}d\zeta d\kappa, \quad (19)$$
$$\beta = \frac{\beta_1 + \beta_2}{(\kappa_b + k_b - \tilde{k}_b)(k_b - \tilde{k}_b)}.$$

Since the frequencies ω_1 and ω_2 are high ($\omega_1 \approx \omega_2 = \omega \gg \Omega$), it follows from (19) that

$$\psi = -\frac{3\omega b_1 b_2}{8\pi\kappa_b}\int_{-\infty}^{+\infty}\kappa e^{i\kappa_w x}e^{i\kappa z}\int_{-\infty}^{+\infty} S^2(\zeta)e^{-i\kappa\zeta}d\zeta d\kappa. \quad (20)$$

As an illustration, we consider the generation of waves by an a-wide strip when $S(z) = \vartheta\left(\frac{a}{2} - |z|\right)$, where

ϑ is the unit step function. Integrating with respect to ζ in Eq. (20), we obtain the stream function in the form

$$\psi = -\frac{3\omega b_1 b_2}{4\pi\kappa_b}\int_{-\infty}^{+\infty}\sin\frac{\kappa a}{2}e^{i\kappa_w x}e^{i\kappa z}d\kappa. \quad (21)$$

For simplicity, let us consider only one beam propagating in the first quadrant. Introducing its concomitant coordinate system (p, q) with the q-axis directed along the beam, and using Eq. (14) and (21), we obtain the vertical displacements h of particles in the beam

$$h(p,q) = \frac{3\omega b_1 b_2(1+i)\sin\theta}{8\pi}\sqrt{\frac{2\nu}{\Omega}} \times\int_0^\infty\kappa\sin\frac{\kappa a\cos\theta}{2}\exp\left(i\kappa p-\frac{\nu\kappa^3 q}{2N\cos\theta}\right)d\kappa, \quad (22)$$

which can be expressed in terms of the standard work functions $F(p, q)$ [6].

The amplitude of the displacements in the axis of the single-mode beam excited by the motion of a narrow strip $\left(a<\frac{\sqrt[3]{g\nu}}{N}\right)$ for large distances from a source $\left(q\gg\frac{2Na^3\cos\theta}{\nu}\right)$ takes the form

$$h_m(q) = \frac{\omega a b_1 b_2\cos^2\theta}{4\pi q}\sqrt{\frac{\sin\theta}{\nu N}}, \quad (23)$$

which is proportional to the product of the oscillation amplitudes, average frequency, and strip width.

Under the laboratory conditions, when q = 20 cm, N = 1 s^{-1}, $a = b_1 = b_2$ = 1 cm, θ = 45°, and ω = 10 s^{-1}, Eq. (23) yields the estimate $h_m(q) \approx 2$ mm that is quite possible to observe.

The above method makes it possible to evaluate the parameters of wave beams for other combination frequencies: double, sum, and zero.

The effects of nonlinear generation are also manifested in the cases of more complex motions of a generating surface. In particular, let a part of the plane perform frequency-modulated oscillations with a constant amplitude b so that the surface velocity is

$$U(z,t) = -i\varphi'(t)be^{-i\varphi(t)}S(z),$$
$$\varphi'(t)\equiv\omega(t) = \omega_0(1+\mu\sin\Omega t), \quad (24)$$

where μ is the frequency-modulation depth and the function $S(z)$ specifies, as above, the geometry of the moving part of the plane. Following the above method, we find the stream function of the generated wave field

$$\psi = -\frac{3\omega_0 b^2\mu}{16\pi\kappa_b}\int_{-\infty}^{+\infty}\kappa J(\kappa)e^{i\kappa_w x}e^{i\kappa z}d\kappa,$$
$$J(\kappa) = \int_{-\infty}^{+\infty}S^2(z)e^{-i\kappa z}dz. \quad (25)$$

When a source of waves is an a-wide strip, we have $S(z)=\vartheta\left(\frac{a}{2}-|z|\right)$ and Eq. (25) takes the form

$$\tilde{\Psi}_\Omega = \frac{3\mu\omega_0 b^2}{8\pi\kappa_b}\int_{-\infty}^{+\infty}\sin\frac{\kappa a}{2}e^{i\kappa_w x}e^{i\kappa z}d\kappa, \quad (26)$$

which determines both the beams of internal waves propagating away from the source to the right. Considering motion only in the first quadrant of the joint coordinate system (p, q), we find the vertical displacements h of particles in the beam in the form

$$h(p,q) = \frac{3\mu\omega_0 b^2(1+i)\sin^2\theta}{16\pi\Omega}\sqrt{\frac{2\nu}{\Omega}} \times\int_0^\infty\kappa\sin\frac{\kappa a\cos\theta}{2}\exp\left(i\kappa p-\frac{\nu\kappa^3 q}{2N\cos\theta}\right)d\kappa. \quad (27)$$

At large distances from the source $\left(q\gg\frac{2Na^3\cos\theta}{\nu}\right)$, when the beam is single-mode, the integral in Eq. (27) is calculated and the expression for the displacements in the beam axis takes the form

$$h_m(q) = \frac{3\mu\omega_0 a b^2(1+i)\sin\theta\cos^2\theta}{8\pi q\sqrt{2\nu\Omega}}. \quad (28)$$

The amplitude of the generated wave is proportional to the depth of the frequency modulation.

Under natural conditions, when the flows are substantially nonstationary, the mechanisms under consideration can significantly contribute to the generation and formation of the internal-wave spectrum. Similar effects can be observed in the dynamics of other types of waves (acoustic, surface, inertial, and hybrid), which also coexist with their boundary layers classified in [8].

ACKNOWLEDGMENTS

This work was supported by the Ministry of Education of Russian Federation (State Program "Inte-

gratsiya," project no. 2.1-304) and the Russian Foundation for Basic Research (project no. 99-05-64980).

REFERENCES

1. Yu. D. Chashechkin and Yu. V. Kistovich, Dokl. Akad. Nauk **355**, 54 (1997) [Phys. Dokl. **42**, 377 (1997)].
2. M. J. Lighthill, *Waves in Fluids* (Cambridge Univ. Press, Cambridge, 1978; Mir, Moscow, 1981).
3. Yu. V. Kistovich and Yu. D. Chashechkin, Prikl. Mekh. Tekh. Fiz. **42**, 52 (2001).
4. Yu. D. Chashechkin, Yu. V. Kistovich, and Yu. S. Il'inykh, Dokl. Akad. Nauk **375**, 338 (2000) [Dokl. Phys. **45**, 627 (2000)].
5. L. D. Landau and E. M. Lifshitz, *Fluid Mechanics* (Nauka, Moscow, 1986, 3rd ed.; Pergamon Press, Oxford, 1987, 2nd ed.).
6. Yu. V. Kistovich and Yu. D. Chashechkin, Prikl. Mat. Mekh. **63**, 611 (1999).
7. A. V. Kistovich and Yu. D. Chashechkin, Izv. Akad. Nauk SSSR, Fiz. Atm. Okeana **27**, 1292 (1991).
8. Yu. V. Kistovich and Yu. D. Chashechkin, Preprint No. 674, IPM RAN (Inst. for Problems of Mechanics, Russian Academy of Sciences, 2001).

Translated by Yu. Vishnyakov

Doklady Physics, Vol. 47, No. 2, 2002, pp. 168–171. Translated from Doklady Akademii Nauk, Vol. 382, No. 6, 2002, pp. 777–780.

MECHANICS

A New Class of Exact Solutions of Euler Equations

Corresponding Member of the RAS V. V. Pukhnachov

Received November 12, 2001

1. In this paper, we consider rotationally symmetric motions of an ideal fluid in the absence of external bulk forces. The Euler equations describing such motions have the form

$$\begin{gathered} u_t + uu_r + wu_z - r^{-1}v^2 + p_r = 0, \\ v_t + uv_r + wv_z + r^{-1}uv = 0, \\ w_t + uw_r + ww_z + p_z = 0, \\ u_r + r^{-1}u + w_z = 0. \end{gathered} \tag{1}$$

Here, t is the time; u, v, and w are the velocity components along the axes r, θ, and z of the cylindrical coordinate system, respectively; and p is the pressure.

Our main result consists in finding a class of those exact solutions to system (1) that depend on four arbitrary functions of the variable z and one arbitrary function of the variable t. Using nonlinear substitutions and certain quadratures, we express these solutions in terms of solutions of linear ordinary differential equations of the second order.

2. The Euler equations admit a broad transformation group [1] that yields exact solutions to them. Until recently, invariant solutions of the Euler equations were primarily studied (see, e.g., [2]). For a more broad class of partially invariant solutions [3], only individual examples including the so-called singular vortex were found [4].

This paper is devoted to the analysis of those partially invariant solutions of system (1) that can be represented as

$$\begin{gathered} w = w(z, t), \quad u = u(r, z, t), \\ v = v(r, z, t), \quad p = p(r, z, t). \end{gathered} \tag{2}$$

As was shown in [5], these solutions are based on a six-parametric group admissible by the equations for the three-dimensional unsteady motion of an ideal fluid. These equations are of the second rank and have a defect equal to three, which is the maximum number possible for system (1). This implies that they have two invariant independent variables and three noninvariant functions to be found.

3. In order to find solutions (2) of system (1), one should supplement it with the equation $w_r = 0$ and analyze the consistency of the resulting overdetermined system of equations. Such an analysis was performed in [5]. In what follows, we will briefly formulate the results of that paper.

Let us first assume that $v \neq 0$ and $w_{zz} \neq 0$. In this case, solution (2) of system (1) can be written out in the form

$$\begin{gathered} u = fr + qr^{-1}, \quad v = r^{-1}[(a + \chi)r^4 + br^2 + K - q^2]^{1/2}, \\ p = \frac{1}{2}(\chi r^2 - w^2 - Kr^{-2}) - \int_0^z w_t(\zeta, t)d\zeta + \vartheta(t). \end{gathered} \tag{3}$$

Here, χ and ϑ are arbitrary functions of t; K is an arbitrary constant; and functions $f = -\frac{w_z}{2}$, a, q, and b of variables z and t satisfy the equations

$$\begin{gathered} f_t + wf_z + f^2 - a = 0, \\ a_t + wa_z + 4(a + \chi)f + \dot{\chi} = 0, \\ q_t + wq_z - b = 0, \\ b_t + wb_z + 2fb + 4(a + \chi)q = 0, \end{gathered} \tag{4}$$

where $\dot{\chi} = \frac{d\chi}{dt}$.

The case where $v \neq 0$ and $w_{zz} = 0$ was considered in [6]. Omitting details, we only note that, under the additional assumption $u_z = 0$, the function v is found to take the form

$$v = r^{-1}[(a + s)r^4 + \dot{q}r^2 - q^2]^{1/2}.$$

Here, a and q are arbitrary functions of t, and the function $s(r, t)$ satisfies a linear partial differential equation of the first order. Therefore, the trivial z-dependence of the velocity field is compensated by the more intricate r-dependence of the circular velocity v and pressure p.

In particular, this allows us to consider the problem on motion of a fluid with the free cylindrical boundary $r = R(t)$ and a time-dependent vorticity source at the

Lavrent'ev Institute of Hydrodynamics, Siberian Division, Russian Academy of Sciences, pr. Akademika Lavrent'eva 15, Novosibirsk, 630090 Russia

1028-3358/02/4702-0168$22.00

flow axis [6]. The fluid-cylinder bases are assumed to be solid surfaces at $z = 0$ and $z = kt + l$, where k and l are constants. This solution could be treated as the Ovsyannikov's solution [7] generalized to vortex fluid flows with singularities at the symmetry axis.

In the case where $\nu = 0$, solution (2) of system (1) is obtained in quadratures by integrating the Riccati equation with respect to the unknown t (the second variable enters into the initial conditions as a parameter).

Although this case corresponds to an axial motion, the rotational component can be added to the velocity field by the following transformation conserving the form of system (1):

$$\nu' = (\nu + cr^{-2})^{1/2}, \quad p' = p - \frac{cr^{-2}}{2},$$

where c is a constant. The other variables entering into system (1) remain as before [8]. The same transformation allows the constant K to be eliminated from Eqs. (3).

4. Let us consider solution (3) in detail. We first note that Eqs. (4) for a given function w form a hyperbolic system. The system is decomposed into two subsystems to be solved sequentially. The first subsystem consists of two semilinear equations relating the functions f and a. Upon determining them, the functions q and b can be found from the system of linear hyperbolic equations. The fact that the equations are reduced to hyperbolic system (4) is very noteworthy, because the initial system of Euler equations (1) is of the mixed type (the system has both real and complex characteristics). Another remarkable feature of system (4) is that it has a unique characteristic direction. This fact allows us to reduce Eqs. (4) to a system of ordinary differential equations by introducing the Lagrangian coordinates ζ and t. For a given function w, the relation between ζ and z is determined by the solution of the Cauchy problem

$$\frac{dz}{dt} = w(z, t), \quad z = \zeta \text{ for } t = 0. \tag{5}$$

Let us introduce the new desired functions

$$F(\zeta, t) = f(z, t), \quad A(\zeta, t) = a(z, t),$$
$$Q(\zeta, t) = q(z, t), \quad B(\zeta, t) = b(z, t).$$

In this case, the first two equations in system (4) take the form

$$F_t = F^2 - A = 0, \quad A_t + 4F(A + \chi) + \dot{\chi} = 0. \tag{6}$$

It is natural to consider the following Cauchy problem for system (6):

$$F = F_0(\zeta), \quad A = A_0(\zeta) \text{ for } t = 0. \tag{7}$$

We now prove that system (6) can be linearized exactly.

According to the second of Eqs. (6), the sign of the function $A(\zeta, t) + \chi(t)$ is fixed for any fixed value of ζ. When $A + \chi \le 0$, we can introduce the new function $G = [-(A + \chi)]^{1/2}$ and rewrite Eqs. (6) in the form

$$F_t + F^2 + G^2 + \chi = 0, \quad G_t + 2FG = 0.$$

It is evident that the functions $F + G = C$ and $F - G = D$ satisfy the Riccati equations

$$C_t + C^2 + \chi = 0, \quad D_t + D^2 + \chi = 0,$$

which, by substituting $C = (\ln\rho)_t$ and $D = (\ln\sigma)_t$, are reduced to the linear equations

$$\rho_{tt} + \chi\rho = 0, \quad \sigma_{tt} + \chi\sigma = 0. \tag{8}$$

Initial conditions (7) are satisfied by setting

$$\rho = 1, \quad \rho_t = F_0(\zeta) + G_0(\zeta), \quad \sigma = 1,$$
$$\sigma_t = F_0(\zeta) - G_0(\zeta) \text{ for } t = 0. \tag{9}$$

Here, $G_0 = [-(A_0 + \chi_0)]^{1/2}$ and $\chi_0 = \chi(0)$. In the case of $A + \chi \ge 0$, the substitution $A + \chi = G^2$ reduces system (6) to the form

$$F_t + F^2 - G^2 + \chi = 0, \quad G_t + 2FG = 0,$$

which can be rewritten as the Riccati equation $H_t + H^2 + \chi = 0$ for the complex function $F + iG + H$. In turn, substituting $H = (\ln\mu)_t$, we reduce this equation to the linear equation

$$\mu_{tt} + \chi\mu = 0, \tag{10}$$

where μ is the new complex function. According to Eqs. (7), the initial conditions for Eq. (10) take the form

$$\mu = 1, \quad \mu_t = F_0(\zeta) + iG_0(\zeta) \text{ for } t = 0, \tag{11}$$

where $G_0 = (A_0 + \chi_0)^{1/2}$.

If the functions F and A are found, the functions Q and B are determined from the linear Cauchy problem

$$Q_t - B = 0, \quad B_t + 2FB + 4(A + \chi)Q = 0, \tag{12}$$

$$Q = Q_0(\zeta), \quad B = B_0(\zeta) \text{ for } t = 0. \tag{13}$$

Thus, the equations governing the partially invariant solution under consideration admit complete linearization. Functional arbitrariness in this solution is provided by the function $\chi(t)$ entering into representation (3) and those four functions F_0, A_0, Q_0, and B_0 of the variable ζ that specify initial conditions (7) and (13) for systems (6) and (12), respectively.

It remains to transform the equation to the Eulerian coordinates. To perform this transformation, we note that, according to Eq. (5), the strain z_ζ can be expressed in terms of solutions of Eqs. (8), (9) and (10), (11):

$$z_\zeta = \frac{1}{|\rho\sigma|}, \text{ for } A + \chi \le 0,$$
$$z_\zeta = \frac{1}{|\mu^2|}, \text{ for } A + \chi \ge 0. \tag{14}$$

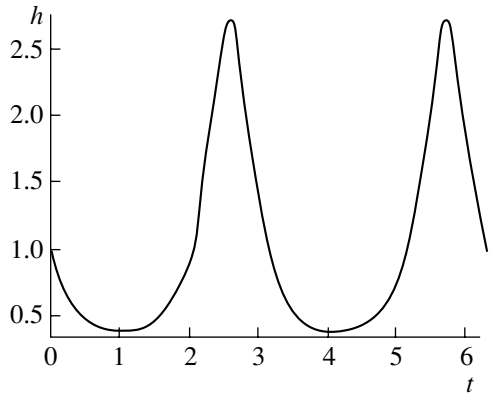

Fig. 1. Function $h(t)$.

Therefore, the function $z = Z(\zeta, t)$ is determined by a quadrature under the initial condition $z = z_0(t)$ at $t = 0$, whereas the function $w = Z_t$ of the variables z and t is found in a parametric form.

5. Although system (6) is solved independently of Eqs. (12), the functions to be found in the initial problem are coupled through the boundary conditions. It is precisely the situation that takes place for the fluid motion in the semi-infinite impenetrable cylinder ($z > 0$, $0 < r < R = \text{const}$) with sources and vortices at its axis.

In the case of $\chi = \text{const}$, system (12) has a set of the solutions $Q = -R^2F$ and $B = R^2(F^2 - A)$, where the functions F and A satisfy Eqs. (6). For these solutions, we have $u = -\frac{1}{2}(r - R^2r^{-1})w_z$ so that the impenetrability condition $u = 0$ is satisfied at the lateral surface of the semicylinder. The impenetrability condition $w = 0$ is also satisfied at the cylinder base for even functions $F_0(\zeta)$ and $A_0(\zeta)$. For such functions, $F(\zeta, t)$ and $A(\zeta, t)$ are also even functions of ζ. Moreover, with regard to Eqs. (14) and the relation $f = -\frac{w_z}{2}$, $w(z, t)$ is an odd function of z. According to Eqs. (3), (5), and (7) and the above assumption on the functions Q and B, the initial velocity field for the motion under consideration takes the form

$$\begin{aligned} u &= (r - R^2r^{-1})F_0(z), \quad w = -2\int_0^z F_0(\zeta)d\zeta, \\ v &= r^{-1}\{r^4[A_0(z) + \chi] - R^2r^2[A_0(z) - F_0^2(z)] \\ &\quad + K - R^4F_0^2(z)\}^{1/2}. \end{aligned} \tag{15}$$

For given constants R and χ and bounded functions F_0 and A_0, the positiveness of the radicand in the formula for v can be ensured by choosing a sufficiently large constant $K > 0$.

Taking into account that the solution of Eqs. (6) and (7) for $\chi = \text{const}$ can be expressed in terms of elementary functions and using Eqs. (5) and (14), we arrive at a parametric representation for the solution of the boundary value problem of the motion of an ideal fluid in a semicylinder. This solution corresponds to initial state (15) and depends on two arbitrary functions $F_0(z)$ and $A_0(z)$. We do not present this representation here and consider only a simple particular case.

Let $\chi = 1$ and both F_0 and $A_0 > -1$ be even finite functions of ζ on the segment $[-1, 1]$. Because $A_0 + \chi > 0$, we have, according to the relationships $F + iG = (\ln\mu)_t$ and $A + \chi = G^2$,

$$F = \operatorname{Re}(\ln\mu)_t, \quad A = [\operatorname{Im}(\ln\mu)_t]^2 - 1, \tag{16}$$

where μ is a solution of Cauchy problem (10) and (11). In the case under consideration, this solution takes the form

$$\mu = \cos t + \{F_0(\zeta) + i[A_0(\zeta) + 1]^{1/2}\}\sin t. \tag{17}$$

The function $z(\zeta, t)$ is determined from the second of Eqs. (14) under the condition $z(0, t) = 0$:

$$\begin{aligned} z(\zeta, t) &= \int_0^\zeta \frac{d\eta}{|\mu(t, \eta)|^2} \equiv Z(\zeta, t), \text{ for } 0 \le \zeta \le 1, \\ z(\zeta, t) &= \zeta - 1 + h(t), \text{ for } \zeta \ge 1, \end{aligned} \tag{18}$$

where $h(t) = Z(1, t)$ is a 2π-periodic function of t. When deriving the second of Eqs. (18), we take into account that $|\mu| = 1$ for $\zeta \ge 1$ as follows from Eq. (17) and the condition $F_0 = A_0 = 0$ for $\zeta \ge 1$.

Using Eqs. (16)–(18), we can describe the motion under consideration in the parametric form. In particular, $w = Z_t$ for $0 \le \zeta \le 1$ and $w = \dot{h}(t)$ for $\zeta \ge 1$. This implies that the impenetrability condition is satisfied at each plane $z = h(t) + N$, where $N = \text{const} > 0$. Moreover, $u = 0$ and $v = r^{-1}(K + r^4)^{1/2}$ for $\zeta \ge 1$.

Therefore, the fluid motion in the region bounded by the planes $z = h(t)$ and $z = h(t) + N$ is similar to the motion of a plunger. In the region $0 < r < R$ and $0 < z < h(t)$, the fluid flow is periodic in time. Such a motion is a result of interaction between the sources and vortices distributed on the segment $[0, h(t)]$ at the flow symmetry axis. In this case, the vortex circulation is equal to a constant of $2\pi K^{1/2}$, while the source power $M = -2\pi R^2F$ is periodic in time.

In the simplest case where $F_0 = k = \text{const}$ and $A_0 = l = \text{const}$, we obtain

$$h(t) = [(\cos t + k\sin t)^2 + (l + 1)\sin^2 t]^{-1}.$$

Moreover, the function M is independent of z and has the form

$$M = -2\pi R^2\frac{k(\cos^2 t - \sin^2 t) + (k^2 + l)\sin t\cos t}{(\cos t + k\sin t)^2 + (l + 1)\sin^2 t}.$$

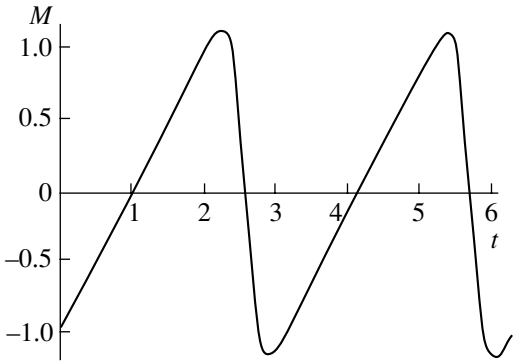

Fig. 2. Function $M(t)$.

For $k = 1$, $l = -0.05$, and $R = (2\pi)^{-1/2}$, the functions $h(t)$ and $M(t)$ are shown in Figs. 1 and 2, respectively.

ACKNOWLEDGMENTS

The work was supported by the Russian Foundation for Basic Research (project nos. 01-01-00782 and 00-15-96162; the latter is for support of Leading Scientific Schools).

REFERENCES

1. A. A. Buchnev, Din. Sploshnoi Sredy, No. 7, 212 (1971).
2. V. K. Andreev, O. V. Kaptsov, V. V. Pukhnachov, and A. A. Rodionov, *Application of Group Theoretical Methods in Hydrodynamics* (Nauka, Novosibirsk, 1994; Kluwer, Dordrecht, 1998).
3. L. V. Ovsiannikov, *Group Analysis of Differential Equations* (Nauka, Moscow, 1968; Academic Press, New York, 1982).
4. L. V. Ovsyannikov, Prikl. Mekh. Tekh. Fiz. **36** (3), 45 (1995).
5. V. V. Pukhnachov, Nonlinear Dyn., No. 22, 101 (2000).
6. E. Yu. Meshcheryakova, in *Mathematical Models and Methods of Their Investigation* (Krasnoyarsk, 2001), Vol. 2, pp. 97–102.
7. L. V. Ovsyannikov, R. M. Garipov, and A. B. Shabat, *Problem on Unsteady Fluid Motion with Free Boundary* (Nauka, Novosibirsk, 1967).
8. V. K. Andreev and A. A. Rodionov, Differen. Uravn. **24**, 1577 (1988).

Translated by V. Chechin

Doklady Physics, Vol. 47, No. 2, 2002, pp. 95–98. Translated from Doklady Akademii Nauk, Vol. 382, No. 4, 2002, pp. 463–466.

PHYSICS

Solid-Phase Reactions, Self-Propagating High-Temperature Synthesis, and Martensitic Transformations in Thin Films

V. G. Myagkov, L. E. Bykova, L. A. Li, I. A. Turpanov, and G. N. Bondarenko

Presented by Academician V.V. Osiko September 18, 2001

Received June 29, 2001

It is widely known that titanium nickelide is one of the most studied alloys exhibiting a shape memory effect. This effect is based on reversible martensitic transformations (see, e.g., [1, 2]). It is somewhat less well known that massive samples of titanium nickelide are prepared by the self-propagating high-temperature synthesis (SHS) of nickel and titanium powders (see, e.g., [3]). The SHS in the powders is considered to be a fairly well-studied process. However, investigation of the SHS in thin films has begun only recently. In [4], it was shown for the first time that in the case of high heating rates, solid-phase reactions between layers of two-layer film samples can occur in the SHS regime. The SHS in thin films represents a surface-combustion wave and is characterized by an initiation temperature T_0 and a front velocity V_f. With increasing substrate temperature T_S, the front velocity V_f increases according to a law close to the Arrhenius law. The value of V_f at T_S slightly exceeding T_0 lies within the range $(0.1–0.5) \times 10^{-2}$ m s^{-1}; therefore, the front propagation can be easily observed by visual means. Thus, in the same two-layer film samples, the solid-phase reactions can be realized in both fast and slow SHS combustion regimes being determined by the reaction diffusion. The choice of regime depends on the control parameter, which is, in fact, the substrate-heating rate $\frac{dT_S}{dt}$.

During the last three decades, solid-phase reactions in thin films were an object of intense study (see, e.g., [5–9]). In two-layer thin films, these reactions occur at temperatures of 400–800 K, which are noticeably lower than in massive samples. Analysis of numerous experimental data has shown that, with increasing temperature of a two-layer thin-film sample, a phase (called the first phase) is initially formed at the interface. Further elevation of the temperature results in the appearance of new phases that form a phase sequence (see, e.g., [6–9]). The prediction of the existence of pairs, i.e., the first phase and the sequence of phases, between which a solid-phase reaction is possible, is extremely important for technological applications. In [6, 7], principles were formulated for the first time that made it possible to predict the first phase and the phase sequence. Furthermore, these principles were extended and modified, which allowed the new experimental data of [8, 9] to be explained. However, even until now, no general rules for predicting the first phase and the phase sequence exist.

Under the sequential deposition of films as a result of chemisorption, the interface can represent a two-dimensional reaction product. At the temperature of the solid-phase transformation, a redistribution of atoms takes place, accompanied by breakage and formation of new bonds. Therefore, it is natural to associate the initiation temperature of the solid-phase reactions and the formation of the first phase in two-layer films with temperatures of solid-phase transformations of reaction products. For example, as was shown in [10], the initiation temperature for the SHS in a two-layer Fe/S-film system coincides with the metal–dielectric phase-transition temperature in the FeS iron monosulfide formed among reaction products. For the classical (from the standpoint of the ordering phenomenon) Cu/Au system, it was shown that the SHS initiation temperature in the Cu/Au two-layer film system is determined by the temperature of the order–disorder transition in the CuAu superstructure formed among reaction products [11]. The class of film pairs for which the initiation temperature coincides with the Kurnakov temperature and of phases precipitating together with reaction products is extended in [13]. Therefore, a following novel rule is proposed in [13]:

The first phase formed at the film interface is a phase being the first in the phase-equilibrium diagram, which has a minimum temperature of structural phase transformations. Further phase formation accompanied by an increase in the annealing temperature for

Kirenskiĭ Physics Institute, Siberian Division, Russian Academy of Sciences, Akademgorodok, Krasnoyarsk, 660036 Russia

1028-3358/02/4702-0095$22.00

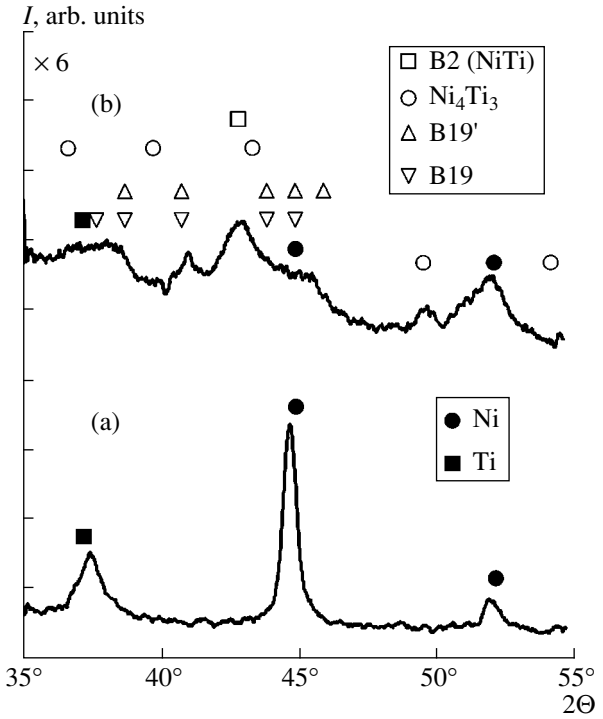

Fig. 1. X-ray diffraction patterns for a two-layer (90 nm)Ti/(75 nm)Ni film sample after the sequential deposition of a titanium layer onto a nickel layer at different substrate temperatures: (a) prior to the reaction, T_S = 300 K; (b) after the reaction, T_S = 420 K.

the solid-phase reactions in thin films is determined by structural transformations in a given binary system. The initiation temperature of solid-phase reactions coincides with temperatures of structural phase transformations.

In this paper, the results of studies of a solid-phase reaction in an Ni/Ti-two-layer film system is presented. The main goal of this study is to extend the first-phase rule to the martensitic transformations and to show that, at the nickel-layer and titanium-layer interface, a solid-phase reaction arises and martensitic phases among reaction products are formed. In this case, the initiation temperature T_0 coincides with the onset temperature A_S of the reverse martensitic transformation.

We sequentially deposited nickel and titanium layers onto glass substrates by employing the ion-plasma sputtering method. The basis pressure and the pressure of argon in the sputtering chamber were 6.5×10^{-3} and 7.5×10^{-2} Pa. The sputtering rates were ~0.02 and ~0.01 nm/s for nickel and titanium layers so that the thicknesses of nickel and titanium films lay within the range 50–100 and 80–150 nm, respectively. It was shown in [4] that the SHS in thin films can be initiated by two methods: either by heating a two-layer film sample at a rate not lower than 20 K/s up to the temperature above the initiation temperature ($T_S > T_0$), or by depositing the second layer at the substrate temperature T_S exceeding the initiation temperature T_0.

The martensitic transitions in the titanium nickelide reveal a temperature hysteresis, and for the stoichiometric composition the temperatures of the onset and the end of the direct and reverse transformation are equal: M_S ~ 360 K, M_f ~ 340 K, A_S ~ 390 K, and A_f ~ 400 K [2]. In our experiments, Ni/Ti films were deposited at the substrate temperatures T_S = 300 K (series 1) and T_S = 420 K (series 2), which are, respectively, lower and higher than the temperatures M_f and A_f. We should also note that in accordance with the phase-equilibrium diagram within the temperature range 300–420 K there exist no other structural phase transformations in the Ni–Ti system except the martensitic one. At the substrate temperature T_S = 300 K, the X-ray patterns for the series 1 (Fig. 1a) contain reflections only from the nickel and titanium layers. This fact implies that only a two-layer nickel–titanium film system is formed. However, if the substrate temperature T_S = 420 K, the formation of compounds at the nickel–titanium interface begins. X-ray diffraction patterns (Fig. 1b) show that reaction products contain the reflections of unreacted nickel and reflections that can be related to the B2(NiTi) high-temperature austenitic phase, the B19 and B19' martensitic phases, and a metastable form of the Ni_3Ti_4 phase with the shape-memory effect. Formation of Ni_3Ti and Ti_2Ni is also possible as a result of the reaction. As a whole, those phases are formed among the reaction products, which are contained in powders after the SHS [3]. The measurement of the magnetic moment of the samples, which is proportional to the thickness of unreacted nickel, shows that the reaction does not occupy the entire depth of the sample but penetrates to a thickness not exceeding 40 nm. The dependences of the electrical resistance $R(T_S)$ on the substrate temperature T_S manifest a large variety, all of them exhibiting a nonmonotone behavior in the region of the martensitic transition. A typical plot for $R(T_S)$ is shown in Fig. 2, which has a nonmetallic behavior. The presence of oxygen atoms and nitrogen atoms that absorb the titanium layer can strongly affect the dependence $R(T_S)$. The nonmonotonic behavior of this dependence shown in Fig. 2 coincides with the dependence $R(T_S)$ in NiTi films [13] and confirms the fact that, basically, martensitic phases are formed among reaction products.

Ni/Ti two-layer film samples obtained at a temperature T_S = 300 K (series 1) were heated up to the temperature of 800 K at a rate of ~20 K/s, which is necessary for initiating an SHS wave. However, the propagation of the SHS front was not visually observed. Therefore, these samples were subjected to rapid temperature annealing. This consisted in heating at a rate of ~20 K/s up to the temperature required, holding at this temperature for 30 s, and cooling at a rate of ~10 K/s. The dependence of the thickness d(Ni) of reacted nickel on the substrate temperature T_S for rapid temperature

annealing is shown in Fig. 3. This dependence is of the Arrhenius type. Since the quantity d(Ni) is proportional to the reaction rate, the activation energy $E_a = 20$ kJ/mol was determined from the dependence of d(Ni) on T_S. This value is close to that of the activation energy for the martensitic transformation in steels (~5 kJ/mol) and strongly differs from the average activation energy of the solid-phase reaction in Ni/Ti-multilayer samples (~150 kJ/mol), which was determined in [14]. It is seen from Fig. 3 that the formation of compounds at the nickel–titanium interface begins from the temperature $T_S < 420$ K and proceeds in a regime of the reaction diffusion. The dependence of the thickness d(Ni) of the reacted nickel on the annealing time t at a substrate temperature $T_S = 420$ K is close to the parabolic law $d^2(\text{Ni}) \sim D_t$. Determination of the diffusivity D yields the value of D on the order of $\sim 0.5 \times 10^{-18}$ m^2/s. This value is by a factor of 10^3–10^5 higher than that for the bulk diffusivity of metals at a temperature of 420 K and is close to the diffusivity related to grain boundaries. The diffusion along grain boundaries is assumed to be a predominant mechanism in the formation of compounds in thin films. However, the martensitic transformations, in which the austenitic phase transforms into a martensitic one by the cooperative displacement of lattice atoms are diffusion-free. As is shown above, the mass transfer to depths attaining 40 nm to both sides occurs from the interface between the layers of nickel and titanium at the temperature somewhat higher than A_f. This implies a mechanism of mass transfer in thin films that is alternative to the diffusion. Such a mechanism consists in the fact that the transfer of reagent atoms (possibly, the transfer of their complete planes) to each other is accompanied by the formation of reaction products by cooperative displacement. This mechanism is analyzed in [15].

It was shown previously in [14] that in Ni/Ti multilayers the solid-phase reaction occurs at temperatures between 420 and 600 K. This reaction is accompanied by the formation of an amorphous phase among the reaction products. However, the X-ray diffraction patterns obtained in this study exhibit an amorphous halo for the reflection angles 2θ belonging to the range {36°, 44°}, which is characteristic of reflections from the martensitic phase of titanium nickelide.

The closeness of the initiation temperature T_0 for the solid-phase reaction between layers of nickel and titanium to the temperatures of martensitic transformation in the titanium nickelide suggests that T_0 must coincide with the temperature of the martensitic transition into the austenitic phase, i.e., with the temperature A_S of the onset of the reverse martensitic transformation.

At the present time, it is generally accepted that, in the martensitic transitions, atoms cooperatively shift to distances not exceeding the lattice parameter without affecting the nearest environment. The results of this study show that, at the onset temperature of the reverse

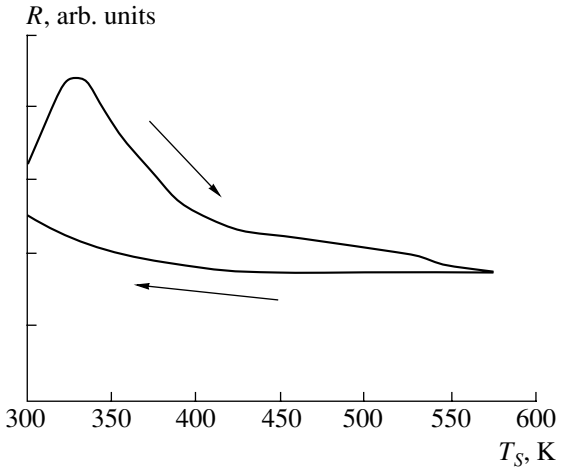

Fig. 2. Dependence of the relative electrical resistance $R(T_S)$ of the two-layer (90 nm)Ti/(75 nm)Ni film sample in which 40 nm of Ni layer has reacted.

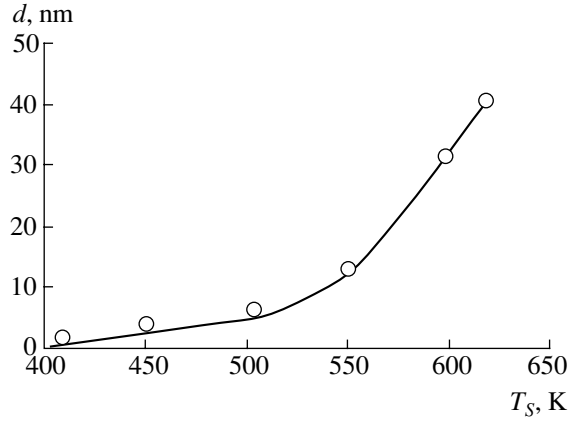

Fig. 3. Dependence of the thickness d(Ni) of nickel reacted in the two-layer (110 nm)Ti/(50 nm)Ni film sample on the substrate temperature T_S in the regime of rapid temperature annealing.

martensitic transformation, a significant mass transfer (up to distances of ~80 nm) accompanied by the formation of compounds in two-layer film condensates takes place. At this temperature, the process of the martensitic transformation is actually a secondary result. This assumes similar chemical mechanisms of martensitic transformations, as well as synthesis that has a long-range nature. The long-range mechanism of the synthesis determines the processes of martensitic transitions by which the breakage and formation of new bonds can arise (possibly with a change of their types). It is well known that the martensitic transformations can occur at very low temperatures. Therefore, on this basis, we can assume that even at these temperatures, compounds can be formed at the interfaces of film condensates. Mechanical stresses also strongly affect the kinetics of martensitic transitions. Thin films are practically always under the action of large mechanical stresses

capable of affecting the kinetics and the character of solid-phase transformations of two-layer systems, provided that martensitic phases are formed among the reaction products. In numerous studies of solid-phase reactions in thin films, the formation of martensitic phases was not found. The results of this study imply that the martensitic phases not only can be formed in the reaction products but also determine the pairs of reagents and temperatures of solid-phase reactions in thin films.

ACKNOWLEDGMENTS

This work was supported by the Russian Foundation for Basic Research, project no. 99-03–32184.

REFERENCES

1. V. N. Khachin, V. G. Pushin, and V. V. Kondrat'ev, *Titanium Nickelide: Structure and Properties* (Nauka, Moscow, 1992).
2. I. I. Kornilov, O. K. Belousov, and E. V. Kachur, *Titanium Nickelide and Other Alloys with the Shape Memory Effect* (Nauka, Moscow, 1977).
3. B. Y. Li, L. J. Wrong, Y. Y. Li, and V. E. Gjunter, Acta Mater. **48**, 3895 (2000).
4. V. G. Myagkov and L. E. Bykova, Dokl. Akad. Nauk **354**, 777 (1997).
5. *Thin Films: Interdiffusion and Reactions*, Ed. by J. Poate, K. Tu, and J. Mayer (Wiley, New York, 1978; Mir, Moscow, 1982).
6. R. W. Bene, Appl. Phys. Lett. **41**, 529 (1982).
7. U. Gosele and K. N. Tu, J. Appl. Phys. **53**, 3252 (1982).
8. M. Zhang, W. Yu, W. H. Wang, and W. K. Wang, J. Appl. Phys. **80**, 1422 (1996).
9. L. A. Clevenger, B. Arcort, W. Ziegler, *et al.*, J. Appl. Phys. **83**, 90 (1998).
10. V. G. Myagkov, L. E. Bykova, V. S. Zhigalov, *et al.*, Dokl. Akad. Nauk **371**, 763 (2000) [Dokl. Phys. **45**, 157 (2000)].
11. V. G. Myagkov, L. E. Bykova, G. N. Bondarenko, *et al.*, Pis'ma Zh. Éksp. Teor. Fiz. **71**, 268 (2000) [JETP Lett. **71**, 183 (2000)].
12. V. G. Myagkov, L. E. Bykova, G. N. Bondarenko, *et al.*, Zh. Tekh. Fiz. **71**, 104 (2001) [Tech. Phys. **46**, 743 (2001)].
13. D. S. Grummon, Li Hou, Z. Zhau, and T. J. Pence, J. Phys. Colloq. **5**, 665 (1995).
14. B. M. Clements, J. Appl. Phys. **61**, 4525 (1987).
15. Yu. D. Tret'yakov, *Solid-Phase Reactions* (Khimiya, Moscow, 1978).

Translated by T. Galkina

Doklady Physics, Vol. 47, No. 2, 2002, pp. 99–101. Translated from Doklady Akademii Nauk, Vol. 382, No. 4, 2002, pp. 467–469.

PHYSICS

Scale-Invariant Extrapolation of a Solution to the Shafranov Equation

N. D. Naumov

Presented by Academician V.V. Osiko October 9, 2001

Received June 28, 2001

As is well known, the Shafranov equation

$$\mathrm{div}\frac{\nabla\psi}{r^2} = -16\pi^3\frac{dF}{d\psi} - \frac{8\pi^2}{c^2r^2}\frac{dG^2}{d\psi} \quad (1)$$

is used to find the steady-state solution to equations of magnetohydrodynamics for a spatially bounded and axially symmetric plasma configuration [1]. Here, the functions F and G are expressed in terms of the plasma pressure p and the total current J across a circle of radius r perpendicular to the z-axis, respectively:

$$F(\psi) = p(r, z),$$
$$G(\psi) = \int_0^r j_z \times 2\pi r\, dr = J(r, z).$$

The corresponding components of magnetic induction are expressed as

$$B_r = -\frac{1}{2\pi r}\frac{\partial\psi}{\partial z}, \quad B_z = \frac{1}{2\pi r}\frac{\partial\psi}{\partial r}, \quad B_\varphi = \frac{2G}{cr}.$$

In previous studies, it was demonstrated that an approach based on scale invariance makes it possible to obtain solutions that describe transient one-dimensional plasma motions belonging to the class of flows with a velocity proportional to the distance from the center of symmetry (see [2, 3] and references cited therein).

The method proposed in this paper can be used to find a time-dependent solution to the magnetohydrodynamics equations

$$\mathrm{div}\mathbf{B} = 0, \quad \frac{\partial\mathbf{B}}{\partial t} = \mathrm{curl}[\mathbf{VB}], \quad (2)$$

$$\frac{\partial\rho}{\partial t} + \mathrm{div}\rho\mathbf{V} = 0, \quad (3)$$

$$\frac{d\mathbf{V}}{dt} \equiv \frac{\partial\mathbf{V}}{\partial t} + (\mathbf{V}\nabla)\mathbf{V} = -\frac{1}{4\pi\rho}(\mathbf{B}\mathrm{curl}\mathbf{B}) - \frac{1}{\rho}\nabla p \quad (4)$$

for an axially symmetric plasma configuration when the corresponding steady state is described by a solution to the Shafranov equation. The resulting solution describes the unsteady motion of the class indicated above.

Let R and L be the characteristic radius and axial length of a quiescent plasma, respectively. Replacing r and z by the new variables $\chi = \frac{r}{R}$ and $\zeta = \frac{z}{L}$, we rewrite the magnetic flux density and plasma density as $\psi(r, z) = \Psi(\chi, \zeta)$ and $\rho = \Phi(\chi, \zeta)$, respectively. Here, Φ is a certain function.

This change of variables leads to somewhat different forms of both Eq. (1) and expressions for the radial and axial components of the magnetic induction:

$$\frac{1}{R^2}\left(\frac{\partial^2\Psi}{\partial\chi^2} - \frac{1}{\chi}\frac{\partial\Psi}{\partial\chi}\right) + \frac{1}{L^2}\frac{\partial^2\Psi}{\partial\zeta^2} = -16\pi^3\chi^2R^2\frac{dF}{d\Psi} - \frac{8\pi^2}{c^2}\frac{dG^2}{d\Psi}, \quad (5)$$

$$B_r = -\frac{1}{2\pi RL\chi}\frac{\partial\Psi}{\partial\zeta}, \quad B_z = \frac{1}{2\pi R^2\chi}\frac{\partial\Psi}{\partial\chi}. \quad (6)$$

We now denote by $a = a(t)$ and $b = b(t)$ the characteristic dimensions of a moving plasma, which were introduced above. Suppose that $a(0) = R$ and $b(0) = L$. For a plasma motion of the class under consideration, the velocity components and density are expressed as

$$V_r = \dot{a}\xi, \quad V_\varphi = 0, \quad V_z = \dot{b}\eta, \quad \rho = \frac{LR^2}{ba^2}\Phi(\xi, \eta),$$

where $\xi = \frac{r}{a}$ and $\eta = \frac{z}{b}$ are scale-invariant variables.

The expressions involved in Eq. (6) suggest that the radial and axial components of magnetic induction in a moving plasma should be represented in terms of the function $\psi(r, z, t) = \Psi(\xi, \eta)$ as

1028-3358/02/4702-0099$22.00

$$B_r = -\frac{1}{2\pi ab\xi}\frac{\partial\Psi}{\partial\eta}, \quad B_z = \frac{1}{2\pi a^2\xi}\frac{\partial\Psi}{\partial\xi}. \tag{7}$$

The applicability of these expressions can be demonstrated by directly substituting expression (7) into Eqs. (2). However, we propose here a simpler method based on a corollary to these equations.

The frozen-in condition for the magnetic-field lines described by Eqs. (2) implies that

$$\frac{d}{dt}\left(\frac{\mathbf{B}\nabla S}{\rho}\right) = 0, \tag{8}$$

where the quantity S is preserved $\left(\frac{dS}{dt} = 0\right)$ in a moving plasma. Since ξ and η are scale-invariant variables, it can be readily shown that expressions (7) are consistent with condition (8). Furthermore, setting $S = \varphi$, we find an expression for the azimuth component of the magnetic induction: $B_\varphi = \frac{2LG(\psi)}{abc\xi}$.

The results obtained above can be used to calculate the components of current density $\mathbf{j} = \frac{c}{4\pi}\mathrm{curl}\mathbf{B}$:

$$j_r = -\frac{L}{2\pi br}\frac{\partial I}{\partial z}, \quad j_\varphi = -\frac{cr}{8\pi^2}\mathrm{div}\frac{\nabla\psi}{r^2}, \quad j_z = \frac{L}{2\pi br}\frac{\partial I}{\partial r}, \tag{9}$$

where $I(r, z, t) = G\psi$. As in the case of a quiescent plasma, the function ψ represents the magnetic flux density for a circle of radius r perpendicular to the z-axis. According to Eqs. (9), the function I corresponding to an unsteady motion differs from the total current across above-indicated circle: $I = \frac{bJ}{L}$. We also consider that the same dependence $p = F(\psi)$ is applicable for the moving-plasma pressure.

As a result, we find from Euler equation (4) that

$$\ddot{a}\xi = -\frac{A}{a\rho}\frac{\partial\Psi}{\partial\xi}, \quad \ddot{b}\eta = -\frac{A}{b\rho}\frac{\partial\Psi}{\partial\eta}. \tag{10}$$

Here, for brevity, the notation is used:

$$A = \frac{dF}{d\Psi} + \frac{1}{2\pi}\left(\frac{L}{abc\xi}\right)^2\frac{dG^2}{d\Psi} + \frac{1}{16\pi^3a^2\xi^2}\left[\frac{1}{a^2}\left(\frac{\partial^2\Psi}{\partial\xi^2} - \frac{1}{\xi}\frac{\partial\Psi}{\partial\xi}\right) + \frac{1}{b^2}\frac{\partial^2\Psi}{\partial\eta^2}\right].$$

As is easy to understand, if the function $\Psi(\chi, \zeta)$ satisfies Eq. (5), then the solution to ordinary differential equations (10) takes the form

$$a = R(1 + ut), \quad b = L.$$

In the case when the flow density is distributed in the azimuth direction in the steady configuration under study, i.e., $G = 0$, the solution is possible with a plasmoid dependent on time and having a longitudinal dimension

$$a = R(1 + ut), \quad b = L(1 + wt).$$

Here, u and w are certain constants.

Thus, using the solutions to the Shafranov equations, we can construct the unsteady solution to the magnetohydrodynamics equations, which describes the variation of the dimensions of an axially symmetric plasma configuration. The unsteady motion of plasma is determined by both the time dependence of the electric current flowing in the plasma and the magnitude of the external confining field.

As an illustration of the applicability of the method proposed here, we consider a spherical configuration with an azimuth current density [1]. This configuration is described by a time-independent solution analogous to Hill's vortex in fluid dynamics:

$$\psi = \frac{3}{2}\pi B_0 r^2\left(\frac{r^2 + z^2}{R^2} - 1\right), \tag{11}$$

where B_0 represents the external confining magnetic field and R is the radius of the plasma ball. This configuration is characterized by $F = -\frac{15B_0\psi}{16\pi^2R^2}$ and $G = 0$. Since $L = R$ in this case, expression (11) is equivalent to

$$\Psi(\chi, \zeta) = \frac{3}{2}\pi B_0 R^2\chi^2(\chi^2 + \zeta^2 - 1).$$

In accordance with the scheme developed above, we obtain the following results for unsteady motion of the plasma ball:

$$\psi(r, z) = \Psi(\xi, \eta) = \frac{3}{2}\pi B_0\frac{R^2}{a^2}r^2\left(\frac{r^2 + z^2}{a^2} - 1\right), \tag{12}$$

$$V_r = r\frac{\dot{a}}{a}, \quad V_\varphi = 0, \quad V_z = z\frac{\dot{a}}{a}, \quad \rho = \left(\frac{R}{a}\right)^3\Phi\left(\frac{r}{a}\right),$$

$$B_r = -B_0\frac{3R^2}{2a^4}rz, \quad B_z = -B_0\frac{3R^2}{2a^2}\left(\frac{2r^2 + z^2}{a^2} - 1\right).$$

Comparing expressions (11) and (12), we can see that the obtained solution to the magnetohydrodynamics equations describes a spherical plasma configuration placed in an unsteady external magnetic field with the induction $B_{ext} = B_0\left(\frac{R}{a}\right)^2$. The distribution of the current density is also a function of time: $j_\varphi = -\frac{15cB_0R^2r}{8\pi a^4}$. A solution describing a plasmoid that has the shape of a prolate or oblate spheroid can be obtained in a similar manner by using the corresponding solution to the time-independent problem [4].

REFERENCES

1. V. D. Shafranov, Zh. Éksp. Teor. Fiz. **33**, 710 (1957) [Sov. Phys. JETP **6**, 545 (1957)].
2. L. I. Sedov, *Similarity and Dimensional Methods in Mechanics* (Academic, New York, 1959; Nauka, Moscow, 1981, 2nd ed.).
3. A. G. Kulikovskiĭ and G. A. Lyubimov, *Magnetohydrodynamics* (Addison-Wesley, Reading, Mass., 1965; Fizmatgiz, Moscow, 1962).
4. L. Zakharov and V. Shafranov, in *Problems of Plasma Theory*, Ed. by M. A. Leontovich and B. B. Kadomtsev (Énergoizdat, Moscow, 1982), No. 11, pp. 118–235.

Translated by A. Betev